NONLINEAR DYNAMICS AND SYSTEMS THEORY
An International Journal of Research and Surveys

Volume 20   Number 2   2020

CONTENTS

NONLINEAR DYNAMICS & SYSTEMS THEORY

Volume 20, No. 2, 2020

Nonlinear Dynamics and Systems Theory

An International Journal of Research and Surveys

INSTRUCTIONS FOR CONTRIBUTORS

(1) General. Nonlinear Dynamics and Systems Theory (ND&ST) is an international journal devoted to publishing peer-refereed, high quality, original papers, brief notes and review articles focusing on nonlinear dynamics and systems theory and their practical applications in engineering, physical and life sciences. Submission of a manuscript is a representation that the submission has been approved by all of the authors and by the institution where the work was carried out. It also represents that the manuscript has not been previously published, has not been copyrighted, is not being submitted for publication elsewhere, and that the authors have agreed that the copyright in the article shall be assigned exclusively to InforMath Publishing Group by signing a transfer of copyright form. Before submission, the authors should visit the website:

http://www.e-ndst.kiev.ua

for information on the preparation of accepted manuscripts. Please download the archive Sample_NDST.zip containing example of article file (you can edit only the file Samplefilename.tex).

(2) Manuscript and Correspondence. Manuscripts should be in English and must meet common standards of usage and grammar. To submit a paper, send by e-mail a file in PDF format directly to

Professor A.A. Martynyuk, Institute of Mechanics,
Nesterov str.3, 03057, MSP 680, Kiev-57, Ukraine
e-mail: journalndst@gmail.com

or to one of the Regional Editors or to a member of the Editorial Board. Final version of the manuscript must typeset using LaTex program which is prepared in accordance with the style file of the Journal. Manuscript texts should contain the title of the article, name(s) of the author(s) and complete affiliations. Each article requires an abstract not exceeding 150 words. Formulas and citations should not be included in the abstract. AMS subject classifications and key words must be included in all accepted papers. Each article requires a running head (abbreviated form of the title) of no more than 30 characters. The sizes for regular papers, survey articles, brief notes, letters to editors and book reviews are: (i) 10-14 pages for regular papers, (ii) up to 24 pages for survey articles, and (iii) 2-3 pages for brief notes, letters to the editor and book reviews.

(3) Tables, Graphs and Illustrations. Each figure must be of a quality suitable for direct reproduction and must include a caption. Drawings should include all relevant details and should be drawn professionally in black ink on plain white drawing paper. In addition to a hard copy of the artwork, it is necessary to attach the electronic file of the artwork (preferably in PCX format).

(4) References. Each entry must be cited in the text by author(s) and number or by number alone. All references should be listed in their alphabetic order. Use please the following style:

Journal: [1] H. Poincare, Title of the article. *Title of the Journal* **volume**
(issue) (year) pages. [Language]

Book: [2] A.M. Lyapunov, *Title of the Book.* Name of the Publishers, Town, year.

Proceeding: [3] R. Bellman, Title of the article. In: *Title of the Book.* (Eds.).
Name of the Publishers, Town, year, pages. [Language]

(5) Proofs and Sample Copy. Proofs sent to authors should be returned to the Editorial Office with corrections within three days after receipt. The corresponding author will receive a sample copy of the issue of the Journal for which his/her paper is published.

(6) Editorial Policy. Every submission will undergo a stringent peer review process. An editor will be assigned to handle the review process of the paper. He/she will secure at least two reviewers' reports. The decision on acceptance, rejection or acceptance subject to revision will be made based on these reviewers' reports and the editor's own reading of the paper.

NONLINEAR DYNAMICS AND SYSTEMS THEORY

An International Journal of Research and Surveys
Published by InforMath Publishing Group since 2001

CONTENTS

NONLINEAR DYNAMICS AND SYSTEMS THEORY

An International Journal of Research and Surveys

Nonlinear Dynamics and Systems Theory (ISSN 1562–8353 (Print), ISSN 1813–7385 (Online)) is an international journal published under the auspices of the S.P. Timoshenko Institute of Mechanics of National Academy of Sciences of Ukraine and Curtin University of Technology (Perth, Australia). It aims to publish high quality original scientific papers and surveys in areas of nonlinear dynamics and systems theory and their real world applications.

AIMS AND SCOPE

Nonlinear Dynamics and Systems Theory is a multidisciplinary journal. It publishes papers focusing on proofs of important theorems as well as papers presenting new ideas and new theory, conjectures, numerical algorithms and physical experiments in areas related to nonlinear dynamics and systems theory. Papers that deal with theoretical aspects of nonlinear dynamics and/or systems theory should contain significant mathematical results with an indication of their possible applications. Papers that emphasize applications should contain new mathematical models of real world phenomena and/or description of engineering problems. They should include rigorous analysis of data used and results obtained. Papers that integrate and interrelate ideas and methods of nonlinear dynamics and systems theory will be particularly welcomed. This journal and the individual contributions published therein are protected under the copyright by International InforMath Publishing Group.

PUBLICATION AND SUBSCRIPTION INFORMATION

Nonlinear Dynamics and Systems Theory will have 4 issues in 2020, printed in hard copy (ISSN 1562–8353) and available online (ISSN 1813–7385), by InforMath Publishing Group, Nesterov str., 3, Institute of Mechanics, Kiev, MSP 680, Ukraine, 03057. Subscription prices are available upon request from the Publisher, EBSCO Information Services (`mailto:journals@ebsco.com`), or website of the Journal: `http://e-ndst.kiev.ua`. Subscriptions are accepted on a calendar year basis. Issues are sent by airmail to all countries of the world. Claims for missing issues should be made within six months of the date of dispatch.

ABSTRACTING AND INDEXING SERVICES

Papers published in this journal are indexed or abstracted in: Mathematical Reviews / MathSciNet, Zentralblatt MATH / Mathematics Abstracts, PASCAL database (INIST–CNRS) and SCOPUS.

Solving a System of Nonlinear Fractional Partial Differential Equations Using the Sinc-Muntz Collocation Method

Mahmood Shareef Ajeel, Morteza Gachpazan * and Ali Reza Soheili

Department of Applied Mathematics, Faculty of Mathematical Sciences,
Ferdowsi University of Mashhad, Mashhad, Iran.

Abstract: We present a new numerical method for solving a system of nonlinear fractional partial differential equations (SNFPDEs). This technique is based on the Sinc functions and the fractional Muntz-Legendre polynomials together with the collocation method. The proposed approximation reduces the solution of the SNFPDEs to the solution of a system of nonlinear algebraic equations. In some numerical examples, we show that approximate solutions also agree with exact solutions.

Keywords: *Sinc functions; fractional Muntz-Legendre polynomials; fractional partial differential equations; collocation method; Caputo fractional derivative.*

Mathematics Subject Classification (2010): 26A33, 34A08.

1 Introduction

Fractional partial differential equations (FPDEs) are used in many physical models and engineering research, see [1–3]. Recently, several numerical techniques have been proposed by researchers for solving the FPDEs. For example, Chen, Sun, and Liu [4] used the generalized fractional-order Legendre function for solving FPDEs. Al-Khaled [5] used the Sinc–Legendre collocation method for the non-linear Burger's fractional equation. Abbasbandy et al. [6] applied an operational matrix of fractional-order Legendre functions for solving the time-fractional convection-diffusion equation. Other numerical methods can be found in [7–11].

   In this paper, we apply a numerical method for solving a system of nonlinear fractional partial differential equations (SNFPDEs) of the following form:

---

* Corresponding author: mailto:gachpazan@um.ac.ir

$$\begin{cases} \dfrac{\partial^\alpha u(x,t)}{\partial t^\alpha} + a\dfrac{\partial v(x,t)}{\partial x} + bv^p(x,t) + cu(x,t) = g(x,t), \\ \dfrac{\partial^\beta v(x,t)}{\partial t^\beta} + d\dfrac{\partial u(x,t)}{\partial x} + eu^q(x,t) + fv(x,t) = h(x,t), \end{cases} \quad (1)$$

with the conditions

$$u(x,0) = u_0(x), \qquad v(x,0) = v_0(x), \qquad u(0,t) = u_1(t), \qquad v(0,t) = v_1(t), \quad (2)$$

where $p, q \in \mathbb{N}$, $(x,t) \in \Omega = (0,1) \times (0,1)$, and $0 < \alpha, \beta \le 1$ are the order of the fractional derivatives in the Caputo sense, the continuous functions g and h are known, and the functions $u(x,t)$ and $v(x,t)$ are unknown and should be determined.

The aim of this paper is to apply the Sinc functions and Muntz–Legendre polynomials to achieve the numerical solution of system (1).

This paper is organized as follows. The review of the Caputo fractional derivative and review of the fractional Muntz–Legendre polynomials are presented in Section 2. In Section 3, we recall the notation of the Sinc functions and their properties. In Sections 4 and 5, we discuss the convergence analysis and the approximate solution of the SNF-PDEs based on the Sinc functions and Muntz–Legendre polynomials using the collocation method. In Section 6, we present some examples of the SNFPDEs to show efficiency and accuracy of the proposed method. Finally, a conclusion is expressed in Section 7.

2 Preliminaries and Notation

In this section, we give the definition and some properties of the Caputo fractional derivative and fractional-order Muntz–Legendre polynomials.

2.1 Review of the Caputo fractional derivative

Definition 2.1 The fractional derivative of $y(t)$ in the Caputo sense is defined as

$$D_*^\alpha y(t) = \frac{1}{\Gamma(m-\alpha)} \int_0^t (t-\tau)^{m-\alpha-1} y^{(m)}(\tau) d\tau$$

for $m-1 < \alpha < m$, $m \in \mathbb{N}$ and $t > 0$.

Definition 2.2 Let $\alpha > 0$. The Riemann–Liouville fractional integral operator J_t^α is defined on $L_1[a,b]$ by

$$J_t^\alpha y(t) = \frac{1}{\Gamma(\alpha)} \int_a^t (t-\tau)^{\alpha-1} y(\tau) d\tau.$$

Some properties of the Riemann–Liouville fractional integral operator J_t^α and the Caputo fractional derivative operator D_*^α, which will be used later, are as follows:

1) $D_*^\alpha C = 0$, where C is a constant.

2)
$$D_*^\alpha t^v = \begin{cases} \dfrac{\Gamma(v+1)}{\Gamma(v+1-\alpha)} t^{v-\alpha}, & v \in \mathbb{N}_0, \ v \ge \lceil \alpha \rceil, \ \ or \ \ v \in \mathbb{N}, \ v > \lfloor \alpha \rfloor, \\ 0, & v \in \mathbb{N}_0, \ v < \lceil \alpha \rceil, \end{cases} \quad (3)$$

where $\lceil \alpha \rceil$ is the smallest integer greater than or equal to α, and $\lfloor \alpha \rfloor$ is the largest integer less than or equal to α. Also $\mathbb{N}_0 = \{0, 1, \dots\}$.

3) The Caputo fractional derivative is a linear operation,

$$D_*^\alpha \Big(\sum_{i=1}^n a_i y_i(t) \Big) = \sum_{i=1}^n a_i D_*^\alpha y_i(t).$$

4)

$$J_t^\alpha (J_t^\beta y(t)) = J_t^\beta (J_t^\alpha y(t)) = J_t^{\alpha+\beta} y(t), \qquad \alpha, \beta > 0.$$

5)

$$J_t^\alpha t^v = \frac{\Gamma(v+1)}{\Gamma(\alpha+v+1)} t^{\alpha+v}.$$

6)

$$D_*^\alpha (J_t^\alpha y(t)) = y(t).$$

7)

$$J_t^\alpha (D_*^\alpha y(t)) = y(t) - \sum_{i=0}^{n-1} y^{(i)}(0) \frac{t^i}{i!}, \qquad n-1 < \alpha \le n, \ \ t > 0.$$

For more details about the properties of the Caputo fractional derivative operator and Riemann–Liouville fractional integral operator see [2].

2.2   Review of the fractional-order Muntz polynomials

Definition 2.3 (see [6]) The fractional-order Muntz–Legendre polynomials on the interval $[0, T]$ are represented by the formula

$$L_n(t; \alpha) = \sum_{k=0}^n C_{n,k} \Big(\frac{t}{T} \Big)^{k\alpha}, \tag{4}$$

where

$$C_{n,k} = \frac{(-1)^{n-k}}{\alpha^n k! (n-k)!} \prod_{v=0}^{n-1} \big((k+v)\alpha + 1 \big).$$

The function $L_k(t; \alpha)$, $k = 0, 1, \ldots, n$, forms an orthogonal basis for $M_{n,\alpha} = \text{Span}\{1, t^\alpha, \ldots, t^{n\alpha}\}$, $t \in [0, T]$. Also it satisfies

$$L_0(t; \alpha) = 1,$$
$$L_1(t; \alpha) = \Big(\frac{1}{\alpha} + 1 \Big) \Big(\frac{t}{T} \Big)^\alpha - \frac{1}{\alpha},$$
$$b_{1,n} L_{n+1}(t; \alpha) = b_{2,n}(t) L_n(t; \alpha) - b_{3,n} L_{n-1}(t; \alpha),$$

where

$$b_{1,n} = a_{1,n}^{0, \frac{1}{\alpha}-1}, \ b_{2,n}(t) = a_{2,n}^{0, \frac{1}{\alpha}-1} \Big(2 \big(\frac{t}{T} \big)^\alpha - 1 \Big), \ b_{3,n} = a_{3,n}^{0, \frac{1}{\alpha}-1},$$
$$a_{1,n}^{\alpha,\beta} = 2(n+1)(n+\alpha+\beta+1)(2n+\alpha+\beta),$$
$$a_{2,n}^{\alpha,\beta}(x) = (2n+\alpha+\beta+1)[(2n+\alpha+\beta)(2n+\alpha+\beta+2)x + \alpha^2 - \beta^2],$$
$$a_{3,n}^{\alpha,\beta} = 2(n+\alpha)(n+\beta)(2n+\alpha+\beta+2).$$

Theorem 2.1 *Let $L_n(t; \alpha)$ be the fractional-order Muntz–Legendre polynomials; then we have the following Caputo fractional derivative of the functions $L_n(t; \alpha)$:*

$$D_*^\alpha L_n(t; \alpha) = \sum_{k=1}^n D_{n,k} \left(\frac{t}{T}\right)^{(k-1)\alpha}, \tag{5}$$

where

$$D_{n,k} = \frac{\Gamma(1 + k\alpha)}{\Gamma(1 + k\alpha - \alpha)T^\alpha} C_{n,k},$$

and $C_{n,k}$ is defined in $L_n(t; \alpha)$.

Proof. It is a result of equations (3) and (4).

Theorem 2.2 *Let $\alpha > 0$ be a real number and let $t \in [0, 1]$. Then*

$$L_n(t; \alpha) = P_n^{(0, \frac{1}{\alpha} - 1)}(2t^\alpha - 1),$$

where $P_n^{(\alpha, \beta)}$ are the Jacobi polynomials with parameters $\alpha, \beta > -1$, see [12, 13].

Proof. See [14].

3   Sinc Function and its Properties

In this section, we recall the notation and properties of the Sinc function and derive useful formulas that will be used in this paper. The Sinc function is defined on $\mathbb{R}$ as (see [15])

$$\text{Sinc}(x) = \begin{cases} \dfrac{\sin(\pi x)}{\pi x}, & x \neq 0, \\ 1, & x = 0. \end{cases}$$

Let $g(x)$ be a function defined on $\mathbb{R}$, and let $h > 0$ be a step size. Consider the Whittaker cardinal function of g defined by the series

$$C(g, h)(x) = \sum_{k=-\infty}^\infty g(kh) \, \text{Sinc}\left(\frac{x - kh}{h}\right).$$

This series converges (see [15]), and the kth Sinc function is defined on $\mathbb{R}$ as

$$S(k, h)(x) = \text{Sinc}\left(\frac{x - kh}{h}\right).$$

Now, for the positive integer N, the function g can be approximated by truncating as follows:

$$C_N(g, h)(x) = \sum_{k=-N}^N g(kh) \, \text{Sinc}\left(\frac{x - kh}{h}\right).$$

The properties of the Whittaker cardinal expansion have been extensively studied in [15]. These properties are derived in the infinite strip D_S-plane of the complex ω-plane, where, for $d > 0$,

$$D_S = \{w = u + iv : |v| < d \leq \pi/2\}.$$

To construct approximations on the interval $[a, b]$, which are used in this paper, the eye-shaped domain in the z-plane (see [15]),

$$D_E = \{z = u + iv : |arg(\frac{x - a}{b - x})| < d \le \pi/2\},$$

is mapped conformally onto the infinite strip D_S via

$$\omega = \psi(z) = ln(\frac{x - a}{b - x}).$$

The basic functions on $[a, b]$ are taken to be the translated Sinc functions

$$S_k(x) \equiv S(k, h) \circ \psi(x) = \text{Sinc}(\frac{\psi(x) - kh}{h}), \tag{6}$$

where $S(k, h) \circ \psi(x)$ is defined by $S(k, h)(\psi(x))$. The inverse map of $\omega = \psi(z)$ is

$$z = \psi^{-1}(\omega) = \frac{a + be^\omega}{1 + e^\omega}.$$

Thus we may define the inverse images of the real line and of the evenly spaced nodes

$$x_k = \psi^{-1}(kh) = \frac{a + be^{kh}}{1 + e^{kh}}, \quad k = 0, \pm 1, \pm 2, \ldots.$$

Definition 3.1 (see [16]) Let $B(D_E)$ be the class of functions g that are analytic in D_E and satisfy

$$\int_{\psi^{-1}(x+L)} |g(z)|dz \to 0, \quad x \to \pm\infty,$$

where

$$L = \{iy : |y| < d \le \pi/2\},$$

and those on the boundary of D_E satisfy

$$\int_{\partial D_E} |g(z)|dz < \infty.$$

4 Convergence Analysis

The following expressions show that the Sinc interpolation on $B(D_E)$ converges exponentially.

Theorem 4.1 (see [15, 16]) *Assume that $g\psi' \in B(D_E)$; then, for all x in $[a, b]$,*

$$|g(x) - \sum_{k=-\infty}^{\infty} g(kh)S(k, h) \circ \psi(x)| \le \frac{2N(g\psi')}{\pi d}e^{-\pi d/h}.$$

Moreover, if $|g(x)| = Ce^{-\gamma|\psi(x)|}, x \in \Gamma$, for some positive constants C and γ and the selection $h = \sqrt{\pi d/\gamma N} \le 2\pi d/ln(2)$, then

$$|\frac{d^n g(x)}{dx^n} - \sum_{k=-N}^{N} g(kh)\frac{d^n}{dx^n}S(k, h) \circ \psi(x)| \le kN^{(n+1)/2}e^{-\sqrt{\pi d\gamma N}}$$

for all $n = 0, 1, 2, \ldots, m$.

Also, the nth derivative of the function g at some points x_k can be approximated (see [17]) as follows:

$$\delta_{k,j}^{(0)} = [S(k,h) \circ \psi(x)]|_{x=x_j} = \delta_{k,j},$$

where

$$\delta_{k,j} = \begin{cases} 1, & j = k, \\ 0, & j \neq k. \end{cases}$$

It has been shown that

$$\delta_{k,j}^{(1)} = \frac{d}{d\psi}[S(k,h) \circ \psi(x)]|_{x=x_j} = \frac{1}{h}\begin{cases} 0, & j = k, \\ \frac{(-1)^{(j-k)}}{j-k}, & j \neq k. \end{cases}$$

So the approximate of a function $u(x)$ by the Sinc expansion is

$$u_N(x,t) \simeq \sum_{i=-N}^{N} c_i S_i(x), \tag{7}$$

where $S_i(x)$ is defined in equation (6). Now, for arbitrary fixed $t_j \in (0,1)$, we define $u(x_k) = u(x_k, t_j)$. Then, to approximate the first derivative at the Sinc nodes x_k, we have

$$\frac{\partial u_{N,n}(x_k, t_j)}{\partial x} = \frac{du(x_k)}{dx} = \frac{du_N(x_k)}{dx} + E_1 = \sum_{i=-N}^{N} c_i \Big(\frac{d}{dx}[S_i(x)]\Big)_{x=x_k} + E_1 \tag{8}$$

$$= \sum_{i=-N}^{N} c_i \Big(\frac{d}{d\psi}[S(i,h) \circ \psi(x)]\frac{d\psi}{dx}\Big)_{x=x_k} + E_1$$

$$= \sum_{i=-N}^{N} c_i \delta_{i,k}^{(1)} \frac{d\psi(x_k)}{dx} + E_1,$$

where

$$E_1 = O(Ne^{-\sqrt{\pi d\gamma N}}).$$

5   Approximate Solution to the S-N-FPDEs

In this section, we approximate the solution of equation (1) by applying the Sinc function and fractional Muntz–Legendre polynomials, which are discussed in the previous sections.

First, we approximate the unknown functions $u(x,t)$ and $v(x,t)$ as follows:

$$u_{N,n}(x,t) \simeq \sum_{i=-N}^{N} \sum_{j=0}^{n} a_{ij} S_i(x) L_j(t; \lambda), \tag{9}$$

$$v_{N,n}(x,t) \simeq \sum_{i=-N}^{N} \sum_{j=0}^{n} b_{ij} S_i(x) L_j(t; \lambda), \tag{10}$$

where $S_i(x)$ and $L_j(t; \lambda)$ are defined in equations (6) and (4), respectively. Also, λ is the parameter such that $\alpha = k_1 \lambda, \beta = k_2 \lambda$, and k_1, k_2 are the smallest natural numbers.

Moreover, let x_k be the Sinc collocation points. Then we approximate the differential $\dfrac{\partial u(x,t)}{\partial x}$, $\dfrac{\partial v(x,t)}{\partial x}$, $\dfrac{\partial^\alpha u(x,t)}{\partial t^\alpha}$, and $\dfrac{\partial^\alpha v(x,t)}{\partial t^\alpha}$ as follows:

$$\frac{\partial u_{N,n}(x_k,t)}{\partial x} = \sum_{i=-N}^{N}\sum_{j=0}^{n} a_{ij}\big(\frac{d}{dx}[S_i(x)]\big)_{x=x_k} L_j(t;\lambda) \tag{11}$$

$$= \sum_{i=-N}^{N}\sum_{j=0}^{n} a_{ij}\big(\frac{d}{d\psi}[S(i,h)\circ\psi(x)]\frac{d\psi}{dx}\big)_{x=x_k} L_j(t;\lambda)$$

$$= \sum_{i=-N}^{N}\sum_{j=0}^{n} a_{ij}\delta_{i,k}^{(1)}\frac{d\psi(x_k)}{dx} L_j(t;\lambda),$$

$$\frac{\partial v_{N,n}(x_k,t)}{\partial x} = \sum_{i=-N}^{N}\sum_{j=0}^{n} b_{ij}\big(\frac{d}{dx}[S_i(x)]\big)_{x=x_k} L_j(t;\lambda) \tag{12}$$

$$= \sum_{i=-N}^{N}\sum_{j=0}^{n} b_{ij}\big(\frac{d}{d\psi}[S(i,h)\circ\psi(x)]\frac{d\psi}{dx}\big)_{x=x_k} L_j(t;\lambda)$$

$$= \sum_{i=-N}^{N}\sum_{j=0}^{n} b_{ij}\delta_{i,k}^{(1)}\frac{d\psi(x_k)}{dx} L_j(t;\lambda),$$

and

$$\frac{\partial^\alpha u_{N,n}(x_k,t)}{\partial t^\alpha} = \sum_{i=-N}^{N}\sum_{j=0}^{n} a_{ij} S_i(x) D_*^\alpha L_j(t;\lambda), \tag{13}$$

$$\frac{\partial^\beta v_{N,n}(x_k,t)}{\partial t^\beta} = \sum_{i=-N}^{N}\sum_{j=0}^{n} b_{ij} S_i(x) D_*^\beta L_j(t;\lambda), \tag{14}$$

where D_*^α and D_*^β are defined in Theorem 2.1.

Substituting equations (9)–(14) into equation (1) and the condition (2), we get

$$\begin{cases} \dfrac{\partial^\alpha u_{N,n}(x_k,t)}{\partial t^\alpha} + a\dfrac{\partial v_{N,n}(x_k,t)}{\partial x} + bv_{N,n}^p(x_k,t) + cu_{N,n}(x_k,t) = g(x,t), \\[2mm] \dfrac{\partial^\beta v_{N,n}(x_k,t)}{\partial t^\beta} + d\dfrac{\partial u_{N,n}(x_k,t)}{\partial x} + eu_{N,n}^q(x_k,t) + fv_{N,n}(x_k,t) = h(x,t), \end{cases} \tag{15}$$

with the conditions

$$u_{N,n}(x,0) = u_0(x), \quad v_{N,n}(x,0) = v_0(x), \quad u_{N,n}(0,t) = u_1(t), \quad v_{N,n}(0,t) = v_1(t). \tag{16}$$

Now, to find the unknown coefficients a_{ij} and b_{ij} in equations (15) and (16), we use the collocation method with suitable collocation points (x_k, t_r), where $x_k = e^{kh}/(1+e^{kh})$, $h = \sqrt{\pi d/N}$, and $d = \pi/2$ for $k = -N,\ldots,N$, (see [15]) and t_r are the Chebyshev–Gauss–Lobatto points with the following relation:

$$t_r = \frac{1}{2} - \frac{1}{2}\cos\frac{\pi r}{n}, \quad r = 1,\ldots,n.$$

Substituting these points into equations (15) and (16), we get

$$
\begin{cases}
\sum_{i=-N}^{N} \sum_{j=0}^{n} a_{ij} S_i(x_k) D_*^{\alpha} L_j(t_r; \lambda) + a \sum_{i=-N}^{N} \sum_{j=0}^{n} b_{ij} \delta_{i,k}^{(1)} \frac{d\psi(x_k)}{dx} L_j(t_r; \lambda) \\
+ b \Big(\sum_{i=-N}^{N} \sum_{j=0}^{n} b_{ij} S_i(x_k) L_j(t_r; \lambda) \Big)^p + c \sum_{i=-N}^{N} \sum_{j=0}^{n} a_{ij} S_i(x_k) L_j(t_r; \lambda) = g(x_k, t_r), \\
\sum_{i=-N}^{N} \sum_{j=0}^{n} b_{ij} S_i(x_k) D_*^{\beta} L_j(t_r; \lambda) + d \sum_{i=-N}^{N} \sum_{j=0}^{n} a_{ij} \delta_{i,k}^{(1)} \frac{d\psi(x_k)}{dx} L_j(t_r; \lambda) \\
+ e \Big(\sum_{i=-N}^{N} \sum_{j=0}^{n} a_{ij} S_i(x_k) L_j(t_r; \lambda) \Big)^q + f \sum_{i=-N}^{N} \sum_{j=0}^{n} b_{ij} S_i(x_k) L_j(t_r; \lambda) = h(x_k, t_r),
\end{cases}
$$

$$
\sum_{i=-N}^{N} \sum_{j=0}^{n} a_{ij} S_i(x_k) L_j(0; \lambda)) = u_0(x_k),
$$

$$
\sum_{i=-N}^{N} \sum_{j=0}^{n} b_{ij} S_i(x_k) L_j(0; \lambda) = v_0(x_k),
$$

$$
\sum_{i=-N}^{N} \sum_{j=0}^{n} a_{ij} S_i(0) L_j(t_r; \lambda) = u_1(t_r),
$$

$$
\sum_{i=-N}^{N} \sum_{j=0}^{n} b_{ij} S_i(0) L_j(t_r; \lambda) = v_1(t_r).
$$

Now, we have a system of nonlinear algebraic equations with unknown coefficients a_{ij} and b_{ij}. By using well-known Newtons method, we can find the approximate solutions given in (9) and (10).

6   Numerical Illustration

In this section, we present some examples of SNFPDEs to show the efficiency of the proposed method. The results will be compared with the exact solutions. The accuracy of the present method is estimated by the absolute errors $E_{N,n}^1$ and $E_{N,n}^2$, which are given as follows:

$$
E_{N,n}^1(\alpha, \beta) = |u(x_i, t_j) - u_{N,n}(x_i, t_j)|, \quad E_{N,n}^2(\alpha, \beta) = |v(x_i, t_j) - v_{N,n}(x_i, t_j)|.
$$

If $\alpha = \beta = \lambda$, we put $E_{N,n}^i(\alpha, \beta) = E_{N,n}^i(\lambda), i = 1, 2$.

Example 6.1 Consider the SNFPDEs

$$
\begin{cases}
\dfrac{\partial^{\alpha} u(x,t)}{\partial t^{\alpha}} + v^2(x,t) + u(x,t) = g(x,t), \\
\dfrac{\partial^{\alpha} v(x,t)}{\partial t^{\alpha}} + u^2(x,t) + v(x,t) = h(x,t),
\end{cases}
$$

with the conditions $u(x,0) = x$, $v(x,0) = x^2$, $u(0,t) = t^{\alpha}$ and $v(0,t) = t^{\beta}$.

Table 1: The maximum absolute errors $\max\{E_{N,n}^1(\lambda)\}$ and $\max\{E_{N,n}^2(\lambda)\}$ for Example 6.1.

$\{N,n\}$	$\max\{E_{N,n}^1(\frac{1}{2})\}$	$\max\{E_{N,n}^2(\frac{1}{2})\}$	$\max\{E_{N,n}^1(\frac{1}{3})\}$	$\max\{E_{N,n}^2(\frac{1}{3})\}$	$\max\{E_{N,n}^1(\frac{3}{5})\}$	$\max\{E_{N,n}^2(\frac{3}{5})\}$
$\{2,4\}$	$1.11e-10$	$1.63e-10$	$3.85e-02$	$5.10e-02$	$1.03e-02$	$1.04e-02$
$\{3,6\}$	$1.06e-10$	$4.51e-10$	$3.99e-15$	$3.33e-15$	$3.30e-03$	$3.36e-03$
$\{4,8\}$	$1.81e-11$	$7.02e-11$	$4.66e-15$	$6.88e-15$	$1.29e-03$	$1.31e-03$
$\{5,10\}$	$1.33e-15$	$1.55e-15$	$4.88e-15$	$5.32e-15$	$6.15e-04$	$6.25e-04$

The exact solutions are $u(x,t) = x + t^\alpha$ and $v(x,t) = x^2 + t^\beta$. For various values of N, n, α, and β, we obtain an approximate solution of this equation. Table 1 shows the maximum absolute errors for the various values of N, n and $\alpha = \beta = \frac{1}{2}, \frac{1}{3}, \frac{3}{5}$. From Table 1, we see that the error can be reduced by increasing the number of collocation points. Also, the absolute errors are shown in Figure 1.
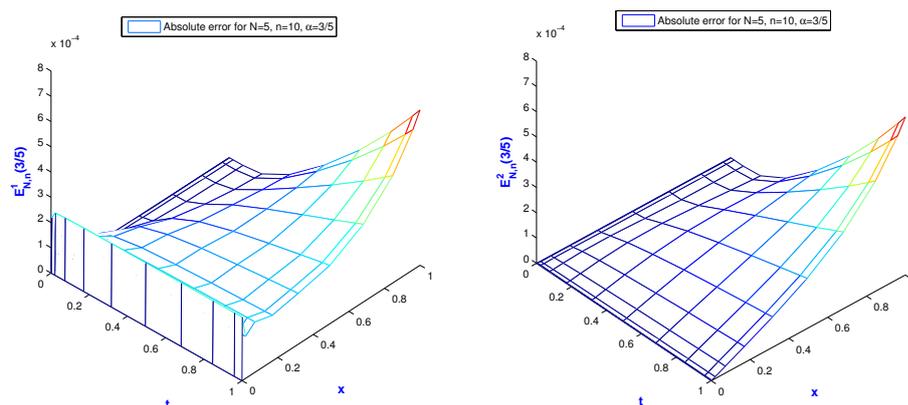
Figure 1: The absolute error functions with $\alpha = \beta = 3/5$ for Example 6.1.

Example 6.2 Consider the SNFPDEs

$$\begin{cases} \dfrac{\partial^\alpha u(x,t)}{\partial t^\alpha} + \dfrac{\partial v(x,t)}{\partial x} + v^3(x,t) = g(x,t), \\ \dfrac{\partial^\beta v(x,t)}{\partial t^\beta} + \dfrac{\partial u(x,t)}{\partial x} + u^3(x,t) = h(x,t), \end{cases}$$

with the conditions

$$u(x,0) = v(x,0) = u(0,t) = v(0,t) = 0.$$

Table 2: The maximum absolute errors $\max\{E^1_{N,n}(\lambda)\}$ and $\max\{E^2_{N,n}(\lambda)\}$ for Example 6.2.

$\{N,n\}$	$\max\{E^1_{N,n}(\frac{1}{2})\}$	$\max\{E^2_{N,n}(\frac{1}{2})\}$	$\max\{E^1_{N,n}(\frac{1}{3})\}$	$\max\{E^2_{N,n}(\frac{1}{3})\}$
$\{2,4\}$	$3.9767e-02$	$3.5755e-02$	$5.0258e-02$	$3.7833e-02$
$\{3,6\}$	$2.4553e-02$	$2.1419e-02$	$2.2845e-02$	$2.0500e-02$
$\{4,8\}$	$5.8731e-03$	$6.0509e-03$	$5.5623e-03$	$6.3847e-03$
$\{5,10\}$	$6.1088e-03$	$5.9381e-03$	$6.1866e-03$	$5.8873e-03$
$\{6,12\}$	$1.9400e-03$	$1.9239e-03$	$1.8999e-03$	$1.9470e-03$
$\{7,14\}$	$2.1785e-03$	$2.1212e-03$	$2.1709e-03$	$2.1308e-03$
$\{8,16\}$	$9.8963e-04$	$8.4617e-04$	$1.3835e-03$	$1.4523e-04$
$\{9,18\}$	$9.1436e-04$	$8.9726e-04$	$9.0637e-04$	$8.9827e-04$
$\{10,20\}$	$5.1216e-04$	$4.8690e-04$	$5.0375e-04$	$4.9526e-04$
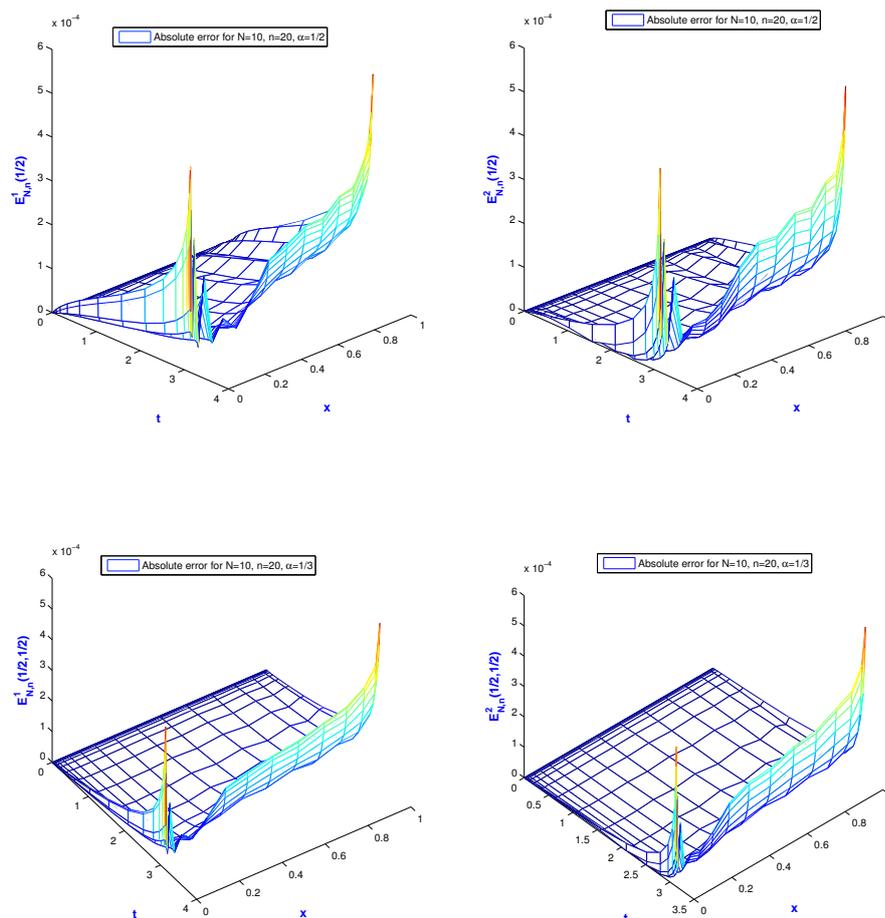
Figure 2: The absolute error functions with $\alpha = \beta = 1/2$ and $\alpha = \beta = 1/3$ for Example 6.2.

Table 3:   The computational convergence order for for Example 6.2.

$\{N,n\}_{new}$	$\{N,n\}_{old}$	$\text{Order}^1_{(\frac{1}{2})}$	$\text{Order}^2_{(\frac{1}{2})}$	$\text{Order}^1_{(\frac{1}{3})}$	$\text{Order}^2_{(\frac{1}{3})}$
$\{3,6\}$	$\{2,4\}$	2.3785	2.5275	3.8891	3.0225
$\{4,8\}$	$\{3,6\}$	9.9447	8.7880	9.8214	8.1098
$\{10,20\}$	$\{9,18\}$	11.0020	11.6037	11.1497	11.3019
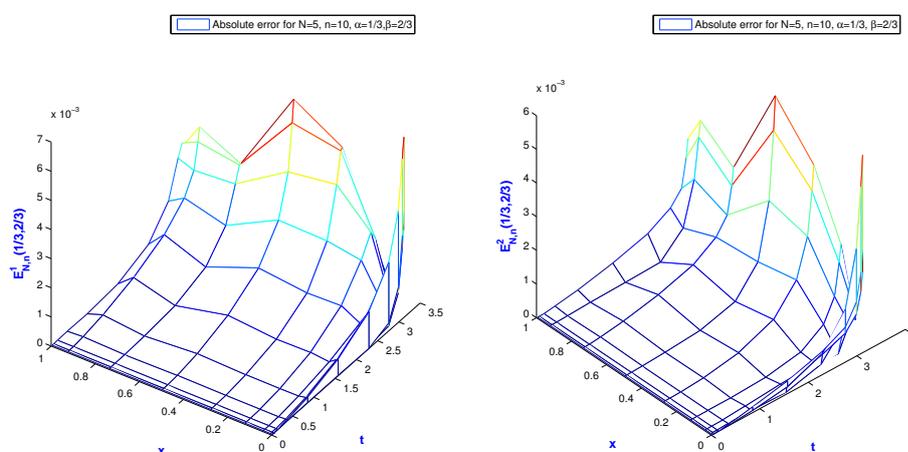
Figure 3: The absolute error functions with $\alpha = 1/3, \beta = 2/3$ for Example 6.2.

The exact solutions are $u(x,t) = t\sin x$ and $v(x,t) = t^2 \sin x$. For various values of N, n, α, and β, we obtain an approximate solution of this equation. The absolute error is shown in Figure 2. Figure 3 shows the maximum absolute error for $\alpha = \frac{1}{3}, \beta = \frac{2}{3}$. Also, Figure 4 and Table 2 show the maximum absolute error for the various values of N, n and $\alpha = \beta = \frac{1}{2}, \frac{1}{3}$. We see that the error can be reduced by increasing the number of collocation points. Also, Table 3 shows the computational convergence orders of the proposed method. We compute the practical orders of convergence as follows:

$$\text{Order}^i_{(\alpha)} = \frac{\log\left(\frac{\max\{E^i_{N,n_{new}}(\lambda)\}}{\max\{E^i_{N,n_{old}}(\lambda)\}}\right)}{\log\left(\frac{h_{new}}{h_{old}}\right)}, \quad i = 1, 2,$$

where

$$h_{new} = \frac{\pi}{\sqrt{2N_{new}}}, \qquad h_{old} = \frac{\pi}{\sqrt{2N_{old}}}.$$

7   Conclusion

In this paper, we applied a basis of the Sinc function and fractional Muntz–Legendre polynomials to obtain the numerical solution of a system of nonlinear fractional partial
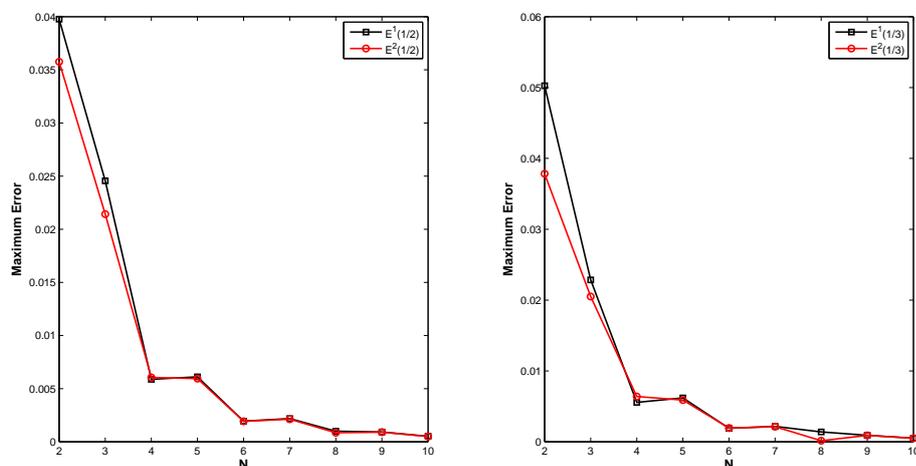
Figure 4: The maximum absolute error convergence of Example 6.2.

differential equations. To get the unknown coefficients of the fractional Muntz–Legendre polynomials, we used the collocation method. The results of the numerical examples showed the efficiency and accuracy of the proposed method.

References

[1] R. Hilfer. *Applications of Fractional Calculus in Physics*. World Scientific Publishing Company, Singapore, 2000.

[2] I. Podlubny. *Fractional Differential Equations*. Academic Press, Inc., San Diego, SA, 1999.

[3] I. Podlubny and M. Kacenak. MATLAB implementation of the Mittag-Leffler function, 2005–2009. http://www.mathworks.com.

[4] Y. Chen, Y. Sun and L. Liu. Numerical solution of fractional partial differential equations with variable coefficients using generalized fractional-order Legendre functions. *Appl. Math. Comput.* **244** (2014) 847–858.

[5] K. AL-Khaled. Sinc–Legendre collocation method for the non-linear Burger's fractional equation. *Annals of the University of Craiova*, Mathematics and Computer Science Serics **41** (2) (2014) 234–250.

[6] S. Abbasbandy, S. Kazem, M. S. Alhuthali and H. Alsulami. Application of the operational matrix of fractional-order Legendre functions for solving the time-fractional convection-diffusion equation. *Appl. Math. Comput.* **266** (2015) 31–40.

[7] Darani, A. M. and M. Nasiri. A fractional type of the Chebyshev polynomials for approximation of solution of linear fractional differential equations. *Computational Methods for Differential Equations* (CMDE) **1** (2) (2013) 96–107.

[8] N. Liu and E. B. Lin. Legendre wavelet method for numerical solutions of partial differential equations. *Numer. Methods Partial Differential Equations* **26** (1) (2010) 81–94.

[9] A. Saadatmandi and M. Dehghan. A new operational matrix for solving fractional-order differential equations. *Comput. math. Appl.* **59** (3) (2010) 1326–1336.

[10] S. Kazem, S. Abbasbandy and S. Kumar. Fractional-order Legendre functions for solving fractional-order differential equations. *Appl. Math. Model.* **37** (7) (2013) 5498–5510.

[11] M. M. Rodrigues. Study of solutions of a nonlinear fractional partial differential equations. In: *Proceedings of the world congress on Engineering*, WCE, 1, 2011.

[12] W. Gautschi. *Orthogonal Polynomials: Computation and Approximation.* Oxford University Press, New York, 2004.

[13] G. Szego. *Orthogonal Polynomials*, 4th ed. AMS Colloq. Publ, 1975.

[14] S. Esmaeili, M. Shamsi and Y. Luchko. Numerical solution of fractional differential equations with a collocation method based on Mntz polynomials. *Comput. Math. Appl.* **62** (3) (2011) 918–929.

[15] F. Stenger. *Handbook of Sinc Numerical Methods, Chapman & Hall/CRC Numerical Analysis and Scientific Computing.* CRC Press, Boca Raton, FL, 2011.

[16] F. Stenger. *Numerical Methods Based on Sinc and Analytic Functions.* Springer, Series in Computational Mathematics, 20. Springer-Verlag, New York, 1993.

[17] M. El-Gamel, S.H. Behiry and H. Hashish. Numerical method for the solution of special nonlinear fourth-order boundary value problems. *Appl. Math. Comput.* **145** (2-3) (2003) 717–734.

Some Problems of Attitude Dynamics and Control of a Rigid Body

to the 90th Birthday of Professor V. I. Zubov

A. Yu. Aleksandrov [1*], A. A. Martynyuk [2] and A. A. Tikhonov [1]

[1] *Saint Petersburg State University, 7-9 Universitetskaya Nab., St. Petersburg, 199034, Russia*
[2] *S. P. Timoshenko Institute of Mechanics, National Academy of Sciences of Ukraine, 3 Nesterov Str., 03057, Kyiv-57, Ukraine*

Abstract: In the present paper, Vladimir Zubov's results on the problems of analysis and control of rotation motion of a rigid body are surveyed together with their developments and extensions.

Keywords: *rigid body; dynamics; Lyapunov function; asymptotic stability; attitude stabilization.*

Mathematics Subject Classification (2010): 70E17, 70E50, 70Q05.

1 Introduction

The outstanding Russian mathematician and mechanical engineer Vladimir Ivanovich Zubov (1930–2000) made an invaluable contribution to the development of Stability Theory and Control Theory.

V. I. Zubov was born on April 14, 1930 in Kashira town, Moscow region, Russia. In 1945, he finished secondary school. At the age of 14, Vladimir was wounded by a hand grenade exploded accidentally and soon failed eyesight. In 1949, he finished the Leningrad special school for blind and visually impaired children and entered the Mathematical and Mechanical Faculty of the Leningrad State University. In 1953, after graduating with honors, he joined the University faculty and since then his career was inseparably associated with the Leningrad (now, Saint Petersburg) State University.

In 1955, V. I. Zubov defended his PhD thesis "Boundaries of the Asymptotic Stability Domain" in which he proved the theorem on the asymptotic stability domain. This result is now known as *Zubov's theorem.*

---

* Corresponding author: `mailto:a.u.aleksandrov@spbu.ru`

Further Zubov's activities involved both pure fundamental investigations and solution of applied real-life problems in several fields — from spacecraft to ship control.

In 1969, the Faculty of Applied Mathematics and Control Processes was founded at the Leningrad State University with Vladimir Zubov's appointment as its first dean. Two years later, a Research Institute of Computational Mathematics and Control Processes was set up by the USSR Government. Zubov became its brains-and-heart. In particular, he headed the projects on the design, development and operation of systems of self-guided winged missiles, and tactical schemes construction for the USSR Navy to oppose aircraft carriers of the potential enemy.

Zubov's scientific activities were surveyed in the paper [1] dedicated to the 80th anniversary of his birth. Zubov's works on the problem of stability by nonlinear approximation are surveyed in [2]. In the present contribution, we focus on Zubov's results on the problems of analysis and control of rotation motion of a rigid body together with their development and extensions in the works of his disciples and followers.

2 A Survey of Zubov's Results

2.1 Investigation of rotation motion of a rigid body

V. I. Zubov succeeded to make essential contributions to the domains of analytical mechanics that had been exhaustively investigated by predecessors, and where it was hard to expect an original result. In the monographs [3–5], he examined the dynamics of the rotational motion of a rigid body around a fixed point in the following three directions:

(i) The complete theory of the motion of a rigid body in the Euler-Poinsot case.

(ii) The complete theory of the motion of a rigid body in the case of Lagrange-Poisson.

(iii) The theory of motion of a heavy solid in the general case in a constant uniform field of gravity.

These problems are considered fundamental in theoretical mechanics. Just a few problems of nonlinear dynamics admit a solution by quadratures; nevertheless, any of such a solution always attracts the interest of researchers. Until now, works devoted to the search for integrable particular cases in the dynamics of a rigid body continue to appear. Most of them discuss purely speculative constructions, the practical significance of which, as a rule, is not discussed. Unlike the background of these works, the works of V. I. Zubov on classical solid mechanics are theoretically elegant but, on the other hand, application-oriented. It should be noted that V.I. Zubov did not concern much about the problems of existence and uniqueness of solutions to the Euler equations of the rigid body motion; his interests were focused on the practical questions relevant to the control of the body's attitude. In particular, he is interested in the qualitative behavior of the spin axis of the body. V.I. Zubov introduced the notion of stability of a rigid body with respect to orientation (see [4]).

Definition 2.1 A body with a fixed point O is stable with respect to orientation if its main axis Oz remains all the time in the half-space bounded by the plane orthogonal to the momentum vector and passing through the point O.

In the Euler-Poinsot case, the equations of motion of a rigid body have the form

$$A\dot{p} + (C - B)qr = 0, \quad B\dot{q} + (A - C)pr = 0, \quad C\dot{r} + (B - A)pq = 0. \qquad (1)$$

Here A, B, C are the principal central moments of inertia of the body, p, q, r are the projections of the body angular velocity on the principal axes of inertia Ox, Oy, Oz.

V. I. Zubov proved that the functions $v_1 = \gamma r2 - \alpha r2$, $v_2 = \gamma q2 - \beta r2$ with $\alpha = (C - B)/A$, $\beta = (A - C)/B$, $\gamma = (B - A)/C$ are the first integrals for the system (1). In terms of v_1 and v_2, he has formulated the following theorem [4].

Theorem 2.1 *A body is stable with respect to orientation if and only if the inequalities $\alpha\beta < 0$, $v_1 v_2 \leqslant 0$ hold.*

In the Lagrange case, the motions of a dynamically symmetric ($A = B$) rigid body with the mass m in a constant uniform field of gravity with the intensity g are described by the equations

$$A\dot{p} + (C - B)qr = -mgly, \quad B\dot{q} + (A - C)pr = mglx, \quad C\dot{r} = 0, \tag{2}$$

$$\dot{x} = ry - qz, \quad \dot{y} = -rx + pz, \quad \dot{z} = qx - py, \tag{3}$$

where x, y, z are the projections of the unit vector directed opposite to the gravity force on the axes Ox, Oy, Oz, and the mass centre (point G) has the coordinates $(0, 0, l)$ in the same reference frame. For this case, necessary and sufficient conditions for the stability of a body with respect to orientation were found as well [4].

V. I. Zubov has established that in the Euler and Lagrange cases, all the motions of a rigid body around a fixed point are periodic or almost periodic with the exception of the motions lying in a special integral manifold. He has determined the precise bounds of the nutational oscillations for the spin axis of a dynamically asymmetric rigid body freely rotating about a fixed point. Furthermore, he has determined stability and instability conditions of the rigid body motions with respect to the spatial orientation of axes [4, 5].

For the problem of the attitude motion of a heavy rigid body in a constant uniform field of gravity, the following equations were studied:

$$\begin{aligned} A\dot{p} + (C - B)qr &= mg(y_G z - z_G y), \\ B\dot{q} + (A - C)pr &= mg(z_G x - x_G z), \\ C\dot{r} + (B - A)pq &= mg(x_G y - y_G x), \end{aligned} \tag{4}$$

where x_G, y_G, z_G are the coordinates of the body mass centre in the coordinate system $Oxyz$. V. I. Zubov proved that any real solution of the Euler-Poinsot differential equations (3), (4) exists and is holomorphic in the strip of the complex plane that is symmetric with respect to the real axis. This solution can be converted into the series converging for all t [4].

The solution to the Darboux problem (the problem of determination of a rigid body attitude motion via given initial orientation and initial angular velocity) was also presented by V. I. Zubov in the form of a series converging for all t [3, 4]. The coefficients of this series are determined by recurrent formulas, which allows them to be found numerically.

In the works of Zubov and his scientific group (see [6]), a complete analysis of free motions of a gyrostat and motions of a gyrostat with a constant external torque was provided. A classification of types of gyrostat motions was given, and the domains of values of constructive parameters and domains of initial conditions are divided into subdomains corresponding to the motions of only one type.

In addition, V. I. Zubov has developed special approaches to constructing conservative numerical methods for integration of equations of motion of a rigid body [6, 7]. These approaches are based on the introduction of controls in the computational process to provide preservation of qualitative characteristics (integrals, integral invariants, stability, etc.) when passing from the differential equations to the corresponding difference ones.

2.2   Attitude control of a rigid body

V. I. Zubov has considered the problem of active attitude control of a rigid body in the general nonlinear statement [6, 8–16]. He has proposed new approaches to the synthesis of control torques providing stabilization of prescribed orientations of a body. Moreover, he has fulfilled complete investigation of qualitative behavior of solutions for the corresponding closed-loop systems.

In particular, consider Zubov's approach to the problem of monoaxial stabilization of a body (see [16]). Let a rigid body rotating around its mass center O with angular velocity $\boldsymbol{\omega}$ be given. Denote by $Oxyz$ the principal central axes of inertia of the body. The attitude motion of the body under a control torque $\mathbf{M}$ is described by the Euler equations

$$\boldsymbol{\Theta}\dot{\boldsymbol{\omega}} + \boldsymbol{\omega} \times \boldsymbol{\Theta}\boldsymbol{\omega} = \mathbf{M}. \tag{5}$$

Here $\boldsymbol{\Theta}$ is the inertia tensor of the body on the axes $Oxyz$.

Let the unit vectors $\mathbf{s}$ and $\mathbf{r}$ be given, and the vector $\mathbf{s}$ be constant in the inertial space and the vector $\mathbf{r}$ be constant in the body-fixed frame. Then the vector $\mathbf{s}$ rotates with respect to the coordinate system $Oxyz$ with the angular velocity $-\boldsymbol{\omega}$. Hence,

$$\dot{\mathbf{s}} = -\boldsymbol{\omega} \times \mathbf{s}. \tag{6}$$

Thus, we consider the differential system consisting of the Euler dynamic equations (5) and the Poisson kinematic equations (6). It is required to design a control torque $\mathbf{M}$ providing monoaxial stabilization of the body: the corresponding closed-loop system should admit the asymptotically stable equilibrium position

$$\boldsymbol{\omega} = \mathbf{0}, \qquad \mathbf{s} = \mathbf{r}. \tag{7}$$

V. I. Zubov has proposed to choose a control torque in the form

$$\mathbf{M} = -\boldsymbol{\omega} + k\mathbf{r} \times \mathbf{s}. \tag{8}$$

Here k is a positive constant. It should be noted that, for such a control, the system (5), (6), along with (7), has the equilibrium position

$$\boldsymbol{\omega} = \mathbf{0}, \qquad \mathbf{s} = -\mathbf{r}. \tag{9}$$

With the aid of the Lyapunov function

$$V = \left(\boldsymbol{\omega}^{\top}\boldsymbol{\Theta}\boldsymbol{\omega} + k\|\mathbf{s} - \mathbf{r}\|^2\right)/2 \tag{10}$$

the following theorem was proved (see [16]).

Theorem 2.2 *Let a control torque be defined by the formula* (8). *Then the equilibrium position* (7) *is asymptotically stable, whereas the equilibrium position* (9) *is unstable. In addition, any motion of the closed-loop system different from the equilibrium position* (9), *for an appropriate choice of the coefficient k, possesses the property $\boldsymbol{\omega} \to \mathbf{0}$, $\mathbf{r} \to \mathbf{s}$ as $t \to +\infty$.*

V. I. Zubov has considered also the problem of scanning a body axis in accordance with the prespecified program [13, 16]. It was assumed that a unit vector $\mathbf{s}_0(t)$ rotates in the inertial space with a given angular velocity $\boldsymbol{\omega_0}(t)$. A control torque should provide the fulfilment of the conditions $\boldsymbol{\omega}(t) \to \boldsymbol{\omega_0}(t)$, $\mathbf{r}(t) \to \mathbf{s}_0(t)$ as $t \to +\infty$.

It was proved (see [13, 16]) that the required control can be chosen in the form

$$\mathbf{M} = \boldsymbol{\omega}_0(t) - \boldsymbol{\omega} + \boldsymbol{\Theta}\dot{\boldsymbol{\omega}}_0(t) + \boldsymbol{\omega}_0(t) \times \boldsymbol{\Theta}\boldsymbol{\omega} + k\mathbf{r} \times \mathbf{s}_0(t), \quad k = \text{const} > 0.$$

Similar approaches were developed for the problem of triaxial stabilization of a rigid body [8, 11, 13, 14].

To construct the control laws ensuring scanning body axes in accordance with the prespecified program, it is necessary to detect first the required elements of body motions. In [3, 6, 13], the problems of determination of orientation of a satellite and localization of motions were solved. New approaches to detect orientation of a satellite via two known physical vectors (for example, direction to the Earth or to the Sun, magnetic field vector, etc.) were proposed.

In addition, V. I. Zubov has developed new methods for the attitude control of a rigid body with the aid of flywheels and rotors connected with the body [6, 11–13, 16]. These methods are based on finding the motions of the carried bodies which create the Coriolis force moments and the moments of relative forces of inertia providing the prescribed motions of the carrying body. For a set of such problems, stationary motions were determined, and stability of these motions was investigated.

Furthermore, for the bodies with liquid-filled cavities and for the bodies with flexible constructions, original mathematical models based on the ordinary differential equations were suggested. For such models, the analytical constructions of controls providing given rotational motions of the carrier were obtained (see [6]).

2.3   Applications

Zubov's investigations were always aimed at applications. He has efficiently exploited the developed methods for the solution of the following practical problems:

(i) the design of precision control systems of spacecraft positions for the "Proton" system;

(ii) the design of control systems for the rotational motion of spacecrafts for the precision orientation of sensitive axes of devices on the base of magneto-hydrodynamic control systems with the use of conducting fluids in feedback contours.

3   Some Extensions of Zubov's Results

The present paper does not claim to provide a comprehensive review of all the numerous publications exploring and developing Zubov's ideas and results. Here we confine ourselves to just a few developments of Zubov's heritage.

3.1   Construction of strict Lyapunov functions

It is worth mentioning that Zubov's results on attitude control of a rigid body are based on the constructing weak Lyapunov functions. Derivatives of these functions with respect to the systems under study are only nonnegative. It is known, that such Lyapunov functions are not well suited to the robustness analysis since their negative semidefinite derivatives along the trajectories could become positive under arbitrarily small perturbations of the dynamics. This has motivated the development of the methods for constructing strict Lyapunov functions, i.e., the functions with negative definite derivatives.

E. Ya. Smirnov has proposed an approach for transforming the weak Lyapunov functions constructed by Zubov into the strict ones (see [17]).

For instance, for the problem of monoaxial stabilization of a rigid body, he has suggested the following modification of the Lyapunov function (10):

$$\widetilde{V} = \left(\boldsymbol{\omega}^\top \boldsymbol{\Theta} \boldsymbol{\omega} + k \|\mathbf{s} - \mathbf{r}\|^2 \right)/2 - \gamma \boldsymbol{\omega}^\top \boldsymbol{\Theta} \mathbf{P}(\mathbf{r} \times \mathbf{s}), \qquad (11)$$

where γ is a positive parameter, $\mathbf{P}$ is a constant matrix [17]. It was proved that, if the matrix $\mathbf{P}^\top + \mathbf{P}$ is positive definite, then, for sufficiently small values of γ, the derivative of (11) along the solutions of the system (5), (6) closed by the control (8) is negative definite with respect to the variables $\boldsymbol{\omega}$ and $\mathbf{r} - \mathbf{s}$.

On the basis of Smirnov's approach, in his works and the works of his scientific group (see [17–20]), various extensions of Zubov's results were obtained. In particular, the methods of robust attitude control were developed for the cases where the inertia tensor of a body and the torques acting on the body are given with some errors [18].

Moreover, in [21–24], strict Lyapunov functions were constructed in the problems of monoaxial and triaxial stabilization of rigid bodies with essentially nonlinear control torques.

3.2 Stabilization with respect to a part of variables

It is known [25, 26], that the perturbations resulting in the attitude deviations of a rigid body from a given position can be treated as the uncontrolled variables when solving the problem of partial stabilization of stationary motions of the body via the flywheels (rotors). It was shown (see [26]) that a flywheel may also be used for the partial stabilization of the permanent rotation of a solid.

Another interesting partial control problem is the problem of "passage" of a solid through a given angular position in the three-dimensional inertial space. This problem is encountered, for example, in a quickly reorienting spacecraft for implementing instant actions (photographing, firing, data transmission, etc.) when the body reaches the desired angular position. For an asymmetric solid, this problem was solved in [27].

Nonlinear game problem of monoaxial reorientation for an asymmetric rigid body with the internal torques applied to the flywheels connected with the body was considered in [28]. The estimates for admissible levels of noise depending on the control constraints were found based on the method proposed in [29], where the control is carried out via the moments of external forces realized by the engines.

Some sufficient conditions of the partial stability and partial asymptotic stability of programmed motions of a rigid body were derived in [22, 23] with the aid of the comparison method.

3.3 Nonstationary moments of inertia and control torques

In the papers [21, 30], the problems of the monoaxial and triaxial stabilization of a rigid body with time-varying moments of inertia were considered, and sufficient conditions of the asymptotic stability of prescribed orientations are found. It is worth noting that, in [30], weak Lyapunov functions and the method of limiting equations were used, whereas the results of [21] are based on the application of special constructions of strict Lyapunov functions and the theory of differential inequalities.

Furthermore, in [21–23, 31], some problems of attitude stabilization of a rigid body with the use of restoring and dissipative torques were studied for the case where control torques evolve with time. In particular, the possibility of implementing the control

systems in which the restoring or dissipative torques tend to zero as time increases was investigated. It is well known that such an evolution could result in new dynamic effects and difficulties of substantiation. Both cases of linear and essentially nonlinear controls were considered. With the aid of the Lyapunov direct method and the comparison method, the conditions were derived under which we can guarantee stability of given equilibrium positions of a body despite the evolution of control torques.

3.4   Application of the averaging technique

In [24, 32], some problems of attitude dynamics of a rigid body influenced by the linear dissipative torque, homogeneous (linear or nonlinear) restoring torque and nonstationary perturbations with zero mean values were studied. It was assumed that the orders of homogeneity of perturbations coincide with those of the components of the restoring torque. The averaging technique was applied and developed for the problems. Original constructions of nonstationary Lyapunov functions taking into account the structure of perturbations acting on the body were proposed. With the aid of these functions, sufficient conditions for the asymptotic stability of the body equilibrium positions were derived. It was proved that, in the case of linear restoring and perturbing torques, the destabilizing effect of nonstationary perturbations can be compensated via introducing a sufficiently large multiplier at the vector of dissipative torque, whereas, for the nonlinear case, to guarantee the asymptotic stability of the equilibrium positions, it is not necessary to use such a parameter.

3.5   Control problems with incomplete feedback

Consider the problem of synthesis of the controls ensuring the asymptotic stability of rotation motion of a body around one of the principal central axes of inertia with a given angular velocity $\boldsymbol{\omega} = \boldsymbol{\omega}_0$. In the presence of complete feedback, when there are three angular velocity sensors measuring its projections onto the selected axes, this problem was solved in [8]. At the same time, A.M. Letov posed the problem of constructing such a control using a smaller number of sensors [33]. Letov's problem, continuing and developing the results of V.I. Zubov, was treated in a number of works. Some of them are mentioned below:

(1) For $\boldsymbol{\omega}_0 = \mathbf{0}$, this problem was solved in [34], and for the case of monoaxial stabilization, in [35].

(2) For $\boldsymbol{\omega}_0 \neq \mathbf{0}$, the monoaxial stabilization problem was solved in a local setting in [36] and [37] for the case where the vector $\boldsymbol{\omega}_0$ is directed along the main axis of inertia of a body.

(3) In the case of two sensors, the problem is solved in [38] for almost all inertia tensors.

(4) In the case of one sensor, the problem is solved in [39] in the linear approximation using a dynamical controller.

(5) The case of one sensor was investigated nonlocally in [40] taking into account nonlinear terms. The investigation is based on the Lyapunov functions method.

(6) In [41], the case of monoaxial stabilization was investigated. It was suggested to choose the required controls as linear functions with respect to the deviations of the projections of the angular velocity vectors from the prescribed values. Conditions were obtained under which such a control provides the asymptotic stability of rotation around the large, small or medium axis of inertia.

3.6   Equilibria of a gyrostat satellite

Permanent Zubov's interest in gyroscopic systems was inspired by their applications in shipbuilding, air- and spacecraft industry [4]. One of the gyroscopic objects is a gyrostat-satellite, the analysis of the dynamics of which attracted the attention of V. I. Zubov and his followers.

Bifurcations of the relative equilibria of a gyrostat satellite moving in a circular Keplerian orbit was investigated in [42] for a special case of the alignment of its gyrostatic moment. The whole set of equilibria with respect to the orbital system of coordinates of the gyrostat satellite was determined using the given moments of inertia, the value of the gyroscopic moment and the direction cosines of the axis of rotation of the flywheel and the changes in this set are investigated as a function of the bifurcation parameter, i.e., the magnitude of the gyrostatic moment of the system. A parametric analysis of the relative equilibria of the three possible classes of equilibria for a system in a circular orbit in a central Newtonian force field is carried out using computer algebra facilities.

The usage of LinModel software package and the symbolic-numerical modeling functions of the Mathematica Computer Algebra System has also proved to be fruitful in the stability investigations of the orbital gyrostat equilibria [43]. By means of Lyapunov's approach, the regions in the space of input parameters are determined, where the stability, instability, or gyroscopic stabilization of relative equilibria of a prolate axisymmetric orbital gyrostat with a constant gyrostatic moment vector are ensured.

A new geometric approach to the analysis of the set of relative gyrostat equilibria is developed in [44]. It is proposed to determine the relative gyrostat equilibria in the corresponding three-dimensional Euclidean space using special aggregated parameters of the system by the coordinates of the intersection points of two pairs of corresponding hyperbolic cylinders with the sphere of unit radius. It is shown that, for the arbitrary values of the gyrostatic moment and other parameters of the system, there are at least eight different relative equilibria.

3.7   A gyrostat satellite in the gravitational and magnetic fields

The attitude motion of a gyrostat satellite is considered in [45] taking into account its interaction with the Earth's magnetic field through its own magnetic moment. The existence of a relative equilibrium of the gyrostat satellite in a special coordinate system associated with the geomagnetic induction vector is proved. The implementation of one particular case of such motion is given. Based on the numerical integration of the differential equations of the perturbed motion, the obtained stability conditions for the gyrostat satellite are analyzed.

A gyrostat satellite moving in a circular Keplerian orbit in the plane of geomagnetic equator is considered in [46]. The gyrostat is equipped with a flywheel, has an electrostatic charge and its own magnetic moment. The attitude motion of the gyrostat under the action of the Lorentz and magnetic torques is studied. It is shown that in the case of dynamic and electromagnetic symmetry of the gyrostat, the problem reduces to quadratures by constructing four first integrals. The motion of the gyrostat axis of symmetry is studied, and its geometric interpretation is given. The same gyrostat in a weakly elliptic orbit is considered in [47]. The reversibility of the differential system with three fixed sets is established. The properties of the symmetric periodic oscillations are analyzed. It is proved that during the transition from a circular orbit to a weakly elliptical one, a bifurcation of the family of symmetric oscillations of the circular problem occurs and

two isolated symmetric oscillations are generated.

A gyrostat satellite with a triaxial inertia ellipsoid in a weakly elliptic orbit with small inclination is considered in [48]. The attitude motion of the gyrostat under the influence of the Lorentz, magnetic and gravitational torques is studied. It is shown that the problem is reversible with two fixed sets. In the case of an isoinertial gyrostat, a third fixed set appears. Two of these three sets correspond to the sets of the degenerate problem [46]. It was found out which sets of symmetric oscillations of the degenerate problem bifurcate and generate isolated oscillations.

3.8   Attitude control of a rigid body using powered gyroscopes

In addition, the development of Zubov's ideas is contained in a series of works by E.Ya. Smirnov and his scientific group devoted to the attitude control of a rigid body using powered gyroscopes [17,18]. For instance, in [18], the problem of triaxial attitude control of a rigid body (carrier) using three pairs of two-degree-of-freedom powered gyroscopes is considered. The errors are taken into account in the construction of the carrier and gyroscopes, as well as the errors in the installation of gyroscopes relative to the carrier. The controls are found that solve the problem of the triaxial orientation of a solid.

3.9   An extension of the classes of stabilizing controls

When solving spacecraft control problems, in numerous cases it is necessary to take into account such effects as the discrete nature of the receipt of information about the state of control objects and its transfer to control devices, the specifics of the functioning of executive devices and the delay in feedback laws. This results in an extension of the classes of applied controls. In particular, in [17, 18], the discrete-time and relay-type control torques providing monoaxial and triaxial stabilization of a rigid body were proposed; in [18, 49], the impulse controls were applied; some problems of the attitude control for the case of delay in feedback laws were solved in [26, 49, 50].

3.10   Development of conservative numerical methods

Among the developments of Zubov's results on the theory of conservative methods for the numerical integration of differential systems, it is worth mentioning the method of numerical continuation with respect to parameters for constructing periodic motions. For an autonomous Hamiltonian system, this method is described in [51]. It has wide applications to the problems of rigid body attitude dynamics in which the numerical construction of the families of periodic motions generated from the regular precessions of a dynamically symmetric satellite is of practical interest. A modification of this method was proposed in [52]. This modification allowed to significantly increase the speed of calculations as well as the accuracy of numerical calculations.

4   Conclusion

Vladimir Zubov was a prominent scholar, engineer and university lecturer. In the previous sections we have reviewed just only one area of scientific activity of him and his successors.

Zubov is the author of about 200 publications including 31 monographs and text books. He was an advisor for 20 DSc and about 100 PhD dissertations. Under Zubov's supervision, a worldwide famous school in control theory was developed in St. Petersburg.

In 1968, V. I. Zubov became the USSR State Prize winner for his pioneer works in control theory. In 1981, he was elected a corresponding member of the Soviet Union Academy of Sciences, and in 1998, he was awarded the title of the Honored Scholar of the Russian Federation. In 1996, the Zubov scientific school "Processes of control and stability" was the winner of the competition for the State support of leading scientific schools of Russia. In 2001, the Research Institute of Computational Mathematics and Control Processes of St. Petersburg State University was named after him.

For outstanding merits to the world science, Zubov's name was perpetuated as the name of the minor planet 'ZUBOV 10022'. This asteroid has a size of 6 km, a brightness of 13.8 magnitude, and the greatest orbit's semiaxis of 2.369 astronomical units.

Acknowledgment

References

[1] A. Yu. Aleksandrov, A. A. Martynyuk and A. P. Zhabko. Professor V. I. Zubov. To the 80th Birthday Anniversary. *Nonlinear Dynamics and Systems Theory* **10** (1) (2010) 1–10.

[2] A. Yu. Aleksandrov, A. A. Martynyuk and A. P. Zhabko. The problem of stability by non-linear approximation. To the 85th Birthday of Professor V.I. Zubov. *Nonlinear Dynamics and Systems Theory* **15** (3) (2015) 221–230.

[3] V. I. Zubov et al. *Dynamics of Free Rigid Body and Determination of its Orientation in the Space.* Leningrad: Leningrad State University, 1968. [Russian]

[4] V. I. Zubov. *Analytical Dynamics of Gyroscopic Systems.* Leningrad: Sudostroenie, 1970. [Russian]

[5] V. I. Zubov. *Analytical Dynamics of Systems of Bodies.* Leningrad: Leningrad State University, 1983. [Russian]

[6] V. I. Zubov et al. *Control of Rotational Motion of a Rigid Body.* Leningrad: Leningrad State University, 1978. [Russian]

[7] V. I. Zubov. Conservative numerical methods for differential equations integration in non-linear mechanics. *Doklady Akademii Nauk Rossii* **354** (4) (1997) 446–448. [Russian]

[8] V. I. Zubov. On the active control of rigid body rotation. *Differencial'nye Uravnenija* **6** (11) (1970) 2086–2087. [Russian]

[9] V. I. Zubov. The control of rotational motion. *Differencial'nye Uravnenija* **7** (7) (1971) 1320–1322. [Russian]

[10] V. I. Zubov. An analytic construction of the guidance law that controls the rotational motion of a rigid body under indirect guidance. *Differencial'nye Uravnenija* **10** (10) (1974) 1898–1899. [Russian]

[11] V. I. Zubov. Controlled rotation and the dynamics of relative motion. *Doklady Akademii Nauk USSR* **219** (3) (1974) 565–566. [Russian]

[12] V. I. Zubov. Using of dynamics of relative motion under control of rotational motion. In: *Selected Problems of Applied Mechanics.* VINITI, Moscow, 1974, pp. 333–339. [Russian]

[13] V. I. Zubov. *Lectures on Control Theory.* Moscow: Nauka, 1975. [Russian]

[14] V. I. Zubov. *Theorie de la Commande.* Moscow: Mir, 1978. [French]

[15] V. I. Zubov. Optimal damping of the rotation motion. *Appl. Mechanics* **16** (5) (1980) 113–121. [Russian]

[16] V. I. Zubov. *Dynamics of Controlled Systems.* Moscow: Vysshaya Shkola, 1982. [Russian]

[17] E. Ya. Smirnov. *Some Problems of Mathematical Control Theory.* Leningrad: Leningrad State University, 1981. [Russian]

[18] E. Ya. Smirnov et al. *Control of Mechanical System Motion.* Leningrad: Leningrad State University, 1985. [Russian]

[19] E. Ya. Smirnov. Control of the rotational motion of a rigid body under conditions of indeterminacy. *Differencial'nye Uravnenija* **11** (5) (1975) 928–929. [Russian]

[20] E. Ya. Smirnov. Control of rotational motion of a free solid by means of pendulums. *Mechanics of Solids* **15** (3) (1980) 1–5.

[21] A. Yu. Aleksandrov. The stability of the equilibrium positions of non-linear non-autonomous mechanical systems. *J. of Appl. Mathematics and Mechanics* **71** (3) (2007) 324–338.

[22] A. Yu. Aleksandrov, E. B. Aleksandrova and A. A. Tikhonov. Monoaxial attitude stabilization of a rigid body under vanishing restoring torque. *Nonlinear Dynamics and Systems Theory* **18** (1) (2018) 12–21.

[23] A. Yu. Aleksandrov and A. A. Tikhonov. Attitude stabilization of a rigid body under the action of a vanishing control torque. *Nonlinear Dynamics* **93** (2) (2018) 285–293.

[24] A. Yu. Aleksandrov and A. A. Tikhonov. Rigid body stabilization under time-varying perturbations with zero mean values. *Cybernetics and Physics* **7** (1) (2018) 5–10.

[25] V. I. Vorotnikov. Partial Stability and control: The state-of-the-art and development prospects. *Automation and Remote Control* **66** (4) (2005) 511–561.

[26] V. I. Vorotnikov and V. V. Rumyantsev. Stability and Control with Respect to a Part of the Variables of a State Vector of Dynamical Systems: Theory, Methods, Applications. Moscow: Nauchnyi Mir, 2001. [Russian]

[27] V. I. Vorotnikov. On the zero-stabilization of nonlinear controllable systems in part of arguments. *Automation and Remote Control* **58** (6) (1997) 924–934.

[28] V. I. Vorotnikov and Yu. G. Martyshenko. On the nonlinear uniaxial reorientation problem for a three-rotor gyrostat in the game noise model. *Automation and Remote Control* **73** (9) (2012) 1469–1480.

[29] A. S. Andreyev. The stability of the equilibrium position of a non-autonomous mechanical system. *J. of Appl. Mathematics and Mechanics* **60** (3) (1996) 388–396.

[30] A. S. Andreev. On the asymptotic stability and instability of the zero solution of a non-autonomous system. *J. of Appl. Mathematics and Mechanics* **48** (2) (1984) 154–160.

[31] A. Yu. Aleksandrov and A. A. Tikhonov. Attitude stabilization of a rigid body in conditions of decreasing dissipation. *Vestnik St. Petersburg University, Mathematics* **50** (4) (2017) 384–391.

[32] A. Yu. Aleksandrov and A. A. Tikhonov. Uniaxial Attitude stabilization of a rigid body under conditions of nonstationary perturbations with zero mean values. *Vestnik St. Petersburg University, Mathematics* **52** (2) (2019) 187–193.

[33] A. M. Letov. *Flight Dynamics and Control.* Moskow, Nauka, 1969. [Russian]

[34] A. M. Meilakhs and G. M. Khitrov. On damping the rotation of a solid. *Differencial'nye Uravnenija* **12** (8) (1976) 1520–1522. [Russian]

[35] A. M. Meilakhs. On the orientation of an inert solid. *Differencial'nye Uravnenija* **12** (11) (1976) 2101. [Russian]

[36] D. V. Lebedev. On controlling the motion of a solid body with data on angular velocity incomplete. *Automation and Remote Control* **39** (12) (1979) 1739–1744.

[37] V. S. Ermolin. Stabilization of the rotational motion of a dynamically symmetric rigid body. In: *Control, Reliability and Navigation.* Mordovian State University, Saransk, 1976, no. 3, pp. 132–137. [Russian]

[38] A. M. Meilakhs. On the stabilization of the rotational motion of a solid. *Differencial'nye Uravnenija* **16** (10) (1980) 1888–1890. [Russian]

[39] D. V. Lebedev. To control the rotational motion of a solid with incomplete information about the angular velocity vector. *Prikl. Matem. and Mech.* **41** (2) (1977) 219–224. [Russian]

[40] A. M. Meilakhs. On the control of the rotational motion of a solid. In: *Mathematical Methods for the Study of Controlled Mechanical Systems.* Leningrad State University, Leningrad, 1982, pp. 121–126. [Russian]

[41] M. B. Dzhumagalieva. On the asymptotic stability of a rigid body rotation motion in the Euler case. In: *Problems of Mechanics of Controlled Motion. Nonlinear Dynamic Systems.* Per'm University, Per'm, 1984, pp. 66–73. [Russian]

[42] S. V. Chaikin. Bifurcations of the relative equilibria of a gyrostat satellite for a special case of the alignment of its gyrostatic moment. *J. of Appl. Mathematics and Mechanics* **77** (5) (2013) 477–485.

[43] A. V. Banshchikov and S. V. Chaikin. Analysis of the stability of relative equilibria of a prolate axisymmetric gyrostat by symbolic-numerical modeling. *Cosmic Res.* **53** (5) (2015) 378–384.

[44] S. V. Chaikin. The set of relative equilibria of a stationary orbital asymmetric gyrostat. *J. of Appl. and Industrial Mathematics* **13** (1) (2019) 30–35.

[45] A. V. Demidov. On the motion of a gyrostat satellite relative to the center of mass. In: *Problems of Mechanics of Controlled Motion.* Leningrad State University, Leningrad, 1974, no. 6, pp. 62–65. [Russian]

[46] A. A. Tikhonov. The integrable case in the gyrostat attitude motion in the gravitational and magnetic Earth's fields. *Vestnik Udmurtgskogo Universiteta. Ser. Mekhanika* (2) (2009) 89–96.

[47] A. A. Tikhonov and V. N. Tkhai. Symmetrical oscillations in the problem of gyrostat attitude motion in a weakly elliptical orbit in gravitational and magnetic fields. *Vestnik St. Petersburg University, Mathematics* **48** (2) (2015) 119–125.

[48] A. A. Tikhonov and V. N. Tkhai. Symmetric oscillations of charged gyrostat in weakly elliptical orbit with small inclination. *Nonlinear Dynamics* **85** (3) (2016) 1919–1927.

[49] A. V. Prasolov. On the triaxial stabilization of a spacecraft using a pulsed system. *Cosmic Res.* **17** (6) (1979) 932–934. [Russian]

[50] A. Yu. Aleksandrov and E. B. Aleksandrova. Monoaxial attitude stabilization of a rigid body under a delay in feedback law. *Mechatronics, Automation, Control* (12) (2014) 18–22. [Russian]

[51] S. R. Karimov and A. G. Sokolsky. Method of continuation with respect to parameters of natural families of periodic motions of Hamiltonian systems. Preprint ITA AN SSSR. No. 9. 1990. [Russian]

[52] E. A. Sukhov and B. S. Bardin. Numerical and analytical construction of a family of periodic motions of a symmetric satellite born from its hyperboloidal precession. *Engineering Journal: Science and Innovation* **53** (5) (2016). DOI: 10.18698/2308-6033-2016-5-1489 [Russian]

Chaos in New 2-d Discrete Mapping and Its Application in Optimization

R. Bououden [1*], M. S. Abdelouahab [1] and F. Jarad [2]

[1] *Laboratory of Mathematics and their Interactions, Abdelhafid Boussouf University Center, Mila, Algeria.*
[2] *Department of Mathematics, Faculty of Arts and Sciences, Cankaya University, Ankara, Turkey.*

Abstract: In this paper, we propose a new map which is a combination of the Hénon and Lozi maps. We analyze the proposed map numerically and with the aid of bifurcation plots. On the other hand, and as an example of application of this new map, we are going to use it in the chaotic optimisation algorithm. To prove the efficiency of this map, we use numerical results thorought the paper.

Keywords: *chaos optimization; test functions; Hénon map; Lozi map.*

Mathematics Subject Classification (2010): 34H05, 34K35.

1 Introduction

Recently, a large number of complex nonlinear optimization problems are solved using chaotic optimization algorithms [2–6]. In such cases, traditional algorithms [7–10] may not often produce the desired outcomes and therefore alternate methods must be employed.

For the last few decades, researchers have focused on developing hybrid algorithms by combining heuristic algorithms with chaos searching techniques to solve a non-linear system of equations and optimization problems such as the chaotic Monte Carlo optimization, chaotic BFGS, chaotic particle swarm optimization, chaotic genetic algorithms, chaotic harmony search algorithm, chaotic simulated annealing, gradient-based methods and so on [11–13]. Due to the non-repetition of chaos, the chaotic optimization algorithm can carry out overall searches at higher speeds than the stochastic ergodic searches that depend on probabilities.

---

* Corresponding author: `mailto:rabouden@yahoo.fr`

Different types of chaotic systems have been considered in literature for applications in optimization methods. The logistic equation and other equations, such as the tent map, Gauss map, Lozi map, Hénon map, sinusoidal iterator, Chua's oscillator, Ikeda map, and others, have been adopted instead of the random ones with very interesting results [14–17].

The most popular map which is used in chaotic optimization algorithm is the Hénon map [18]. M. Hénon has defined a map from the plane to itself. It is one of the most studied examples of dynamical systems that exhibit chaotic behaviour. The Hénon map is defined by

$$H \begin{pmatrix} x \\ y \end{pmatrix} = \begin{pmatrix} 1 - ax^2 + by \\ x \end{pmatrix}. \tag{1}$$

For $a = 1.4$ and $b = 0.3$, the Hénon map (1) is chaotic as in Figure 1 (a). For other values of a and b, the map may be chaotic or converge to a periodic orbit.

(a)   (b)
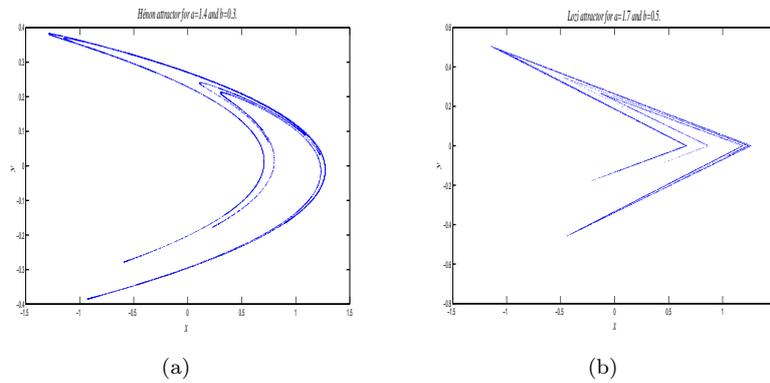
Figure 1: (a) The Hénon attractor obtained for $a = 1.4$ and $b = 0.3$. (b) The Lozi attractor obtained for $a = 1.7$ and $b = 0.5$.

In 1978, Lozi introduced a two-dimensional map (2), see [19], where he replaced the quadratic term in the Hénon map (1) by a piecewise linear one

$$L \begin{pmatrix} x \\ y \end{pmatrix} = \begin{pmatrix} 1 - a \mid x \mid + by \\ x \end{pmatrix}. \tag{2}$$

This map displays a chaotic attractor for $a = 1.7$ and $b = 0.5$ as in Figure 1 (b).

In this paper we propose a new map which is a combination of the Hénon and Lozi maps and we use it to find solutions of complex optimization problems.

2   The New Proposed Map

Because we need a map that has a very complex behaviour to be used in the optimization algorithm as mentioned in the previous section, we suggest the following new map:

$$HL \begin{pmatrix} x \\ y \end{pmatrix} = \begin{pmatrix} 1 - ax^2 + by \\ 1 - a \mid y \mid + bx \end{pmatrix}, \tag{3}$$

where a, b are the bifurcation parameters.

3   Bifurcation and Chaos

In this section, the dynamical behaviour of system (3) will be investigated numerically. We recall that the Lyapunov exponents of an attractive periodic orbit are negative. Also, a periodic point can only bifurcate if at least one of its Lyapunov exponents is zero. Finally, if at least one of the Lyapunov exponents is positive, then the behaviour of the map becomes chaotic.

(a)   (b)
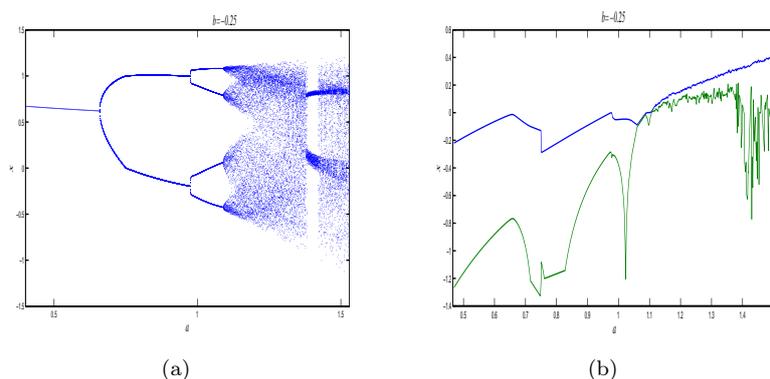
Figure 2: (a) Bifurcation diagram for $b = -0.25$ and $0.4 < a \leqslant 1.5$. (b) Variation of the Lyapunov exponents versus the parameter $0.4 < a \leq 1.5$, with $b = -.025$.

For $b = -0.25$ and $0.4 < a < 1.53$ we can see different bifurcations of map (3) as shown in Figure 2 (a). In the interval $0.4 < a < 0.658$, map (3) converges to a stable fixed point. The first bifurcation occurs at $a = 0.659$ from the fixed point to a period-2 orbit. This period-2 orbit arises out of a period-doubling bifurcation [2]. Then, along the interval $0.659 \leq a < 0.974$, map (3) converges to a stable period-2 orbit. When $a = 0.975$, the second bifurcation (period-doubling bifurcation) occurs from the period-2 orbit to a stable period-4 orbit. The third bifurcation happens when $a = 1.08925$ from period-4 orbit to a full chaotic behaviour. These bifurcations seem very clear in Figure 2 (b), where we notice that the Lyapunov exponents are both negative on the interval $0.4 < a < 1.0892$ except at the bifurcation points $a = 0.659$, $a = 0.975$ and $a = 1.08925$, where one of the Lyapunov exponents is zero. This means that map (3) converges to the periodic orbit on the interval $0.4 < a < 1.0892$. In the interval $1.0893 < a < 1.53$ it converges to a chaotic attractor and this is clear in Figure 2 (b), where one of the Lyapunov exponents is positive. Figure 4 (a) shows an example of the chaotic attractor that appears when $1.0893 < a < 1.53$.

Similarly, as we see in Figure 3 (a), for the fixed $a = 0.95$ and $-0.9487 \leq b \leq 0.4474$, the behaviour of map (3) takes different shapes. On the interval $-0.9487 \leq b < -0.8135$, map (3) converges to the chaotic attractor (one of the Lyapunov exponents is positive as in Figure 3 (b). As an example of the chaotic attractor that appears when $-0.9487 \leq b < -0.8135$, we have Figure 4 (b). In the interval $-0.9488 < b \leqslant 0.177$ we have a series of bifurcations of the types of the period-doubling bifurcation as in Figure 3 (a) and (b). Get back again to a chaotic behaviour when $0.1773 < b \leq 0.2117$. When $b = 0.2118$, we have a new bifurcation from the chaos behaviour to a period-14 orbit. When b exceeds the value $b = 0.253$, map (3) converges to a chaotic attractor (Figure 4 (b)).

The advantage of the proposed map is that it possesses rich dynamical properties such
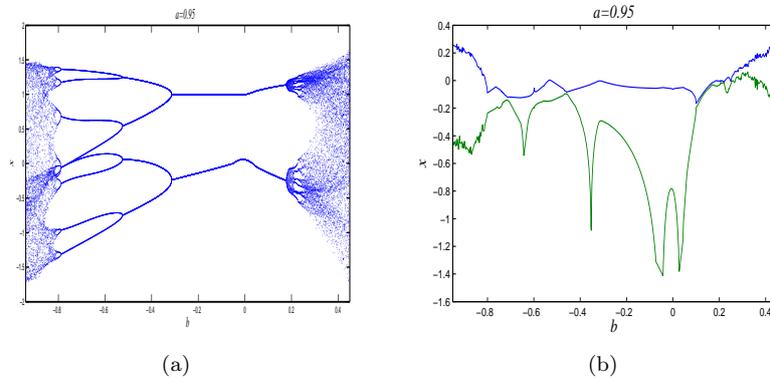
Figure 3: (a) Bifurcation diagram for $a = 0.95$ and $-0.94 < b \leqslant 0.45$. (b) Variation of the Lyapunov exponents versus the parameter $-0.94 < b \leq 0.45$, with $a = 0.95$.
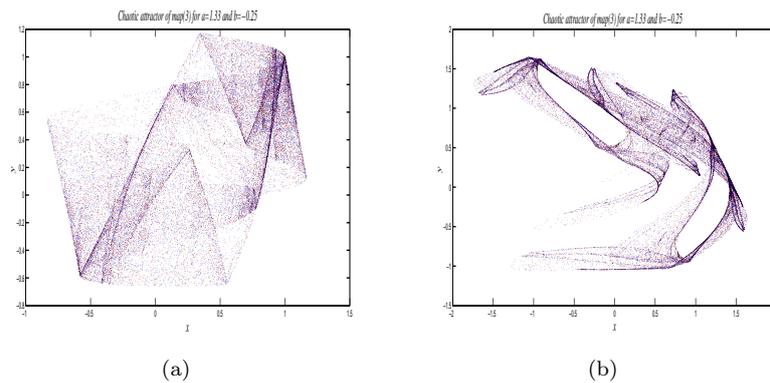
Figure 4: (a) Chaotic attractor of map (3) obtained for $a = 1.33$ and $b = -0.25$. (b) Chaotic attractor of map (3) obtained for $a = 0.95$ and $b = 0.44$.

as fixed points of different types, periodic orbits of different periods and strange attractors which are completely different from all the attractors observed in the behaviour of maps (1) and (2).

4 Pure Chaotic Optimization Algorithm Based on Map (3)

In [2], Bououden R. and Abdelouahab M.S. have used a sampling mechanism to coordinate the research methods based on chaos theory by using the Lozi map. The obtained results show that the $PCOA$ algorithm is fast and converges to a good optimum. In this paper we use map (3) to solve some optimization problems.

In the following we are going to describe the pure chaotic optimization algorithm.

Algorithm 4.1
Inputs:
N**:** max number of iterations of chaotic global search.
N_p**:** max number of packets of global search.

M_g**:** max number of iterations of chaotic global search for any packets.
M_{gl}**:** max number of iterations of chaotic local search in global search.
M_l**:** max number of iterations of chaotic local search.
$Mt = N_p(M_g M_{gl} + M_l)$**:** stopping criterion of chaotic optimization method in iterations.
λ_{gl}**:** the width of the interval in chaotic local search in global search.
λ**:** the width of the interval in chaotic local search.
Outputs:
$\bar{x}$**:** best solution from current run of chaotic search.
$\bar{f}$**:** best objective function (minimization problem).
Step 1: Initialization of the numbers M_g, M_{gl}, M_l of the steps of chaotic search and initialization of the parameters λ_{gl}, λ and initial conditions. The Lozi map (2) is adopted to have a chaotic behaviour in order to use it for generating several sequences of points by using different initial conditions (the number of sequences is equal to the dimension of the objective function) after every sequence $\{y(i), i = 1, 2, ... n\}$ is normalized in the range $[0, 1]$ as follows:

$$z(i) = \frac{y(i) - \alpha}{\beta - \alpha} \tag{4}$$

for all $i = 1, 2, ... n$, where $\alpha = min\{(y(i), i \geq 1\}$, $\beta = max\{(y(i), i \geq 1\}$.
-Step 2-1: Algorithm of chaotic global search:
for $t = 1 : N_p$
Set the initial best objective function $\bar{f}(t) = +\infty$.
while $k \leq M_g$ **do**
$x_i(k) = L_i + z_i(k)(U_i - L_i)$, $i = 1, 2, ..., n$
if $f(x(k)) < \bar{f}$, **then**
$\bar{x} = x(k)$, $\bar{f} = f(x(k))$
- Step 2-2: Sub algorithm of chaotic global-local search:
Transform the points generated by Lozi map in the neighbourhood of the point $\bar{x}$ and we begin the search
while $j \leq M_{gl}$ **do**
if $f(x(j)) < \bar{f}$, **then**
$\bar{x} = x(j)$, $\bar{f} = f(x(j))$
end if
$j = j + 1$
end while
end if
$k = k + 1$
end while
end for
- Step 3: Algorithm of chaotic local search:
Transform the points generated by logistic map in the neighbourhood of the point $\bar{x}$ and we begin the search
while $k \leq M_l$ **do**
if $f(x(k)) < \bar{f}$, **then**
$\bar{x} = x(k)$, $\bar{f} = f(x(k))$
end if
$k = k + 1$
end while

During the chaotic local search, the step size λ (resp λ_{gl}) is an important parameter in convergence behaviour of the optimization method which adjusts small ergodic ranges around X_*. The step sizes λ and λ_{gl} are employed to control the impact of the current best solution on generating a new trial solution. The small λ and λ_{gl} tend to perform exploitation to refine results by local search, while the large ones tend to facilitate a global exploration of search space.

5   Experimental Results and Analysis

5.1   Some test functions

To validate the effectiveness of this new map in solving optimization problems we use it with the PCOA proposed in [2] in order to search for optimal solutions of the following benchmark functions.
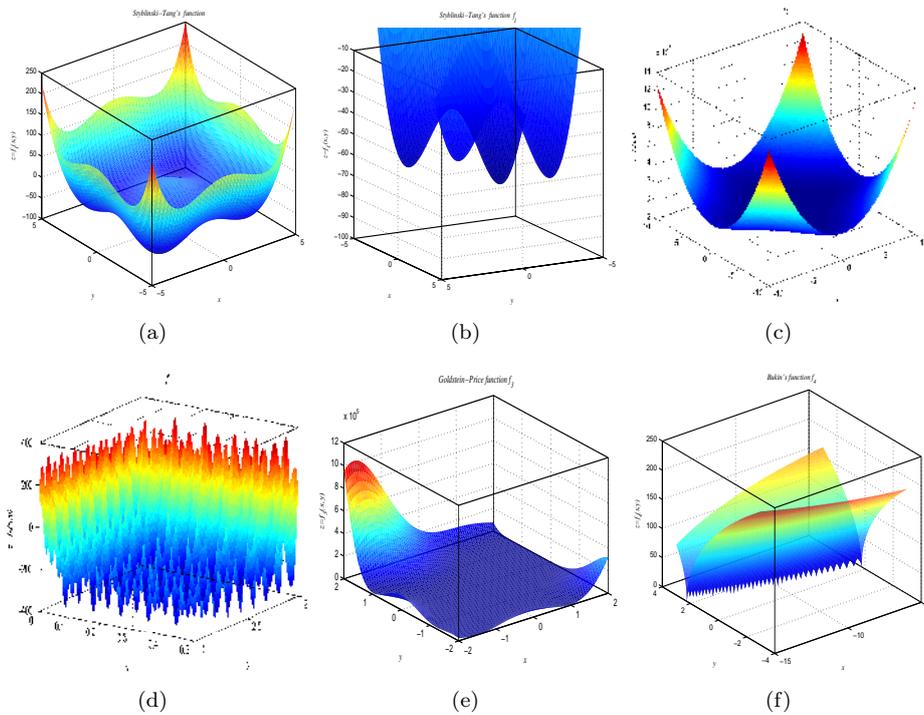
Figure 5: (a) The Styblinski-Tang function f_1. (b) Magnification of the Styblinski-Tang function f_1. (c) Function f_2. (d) Magnification of function f_2. (e) The Goldstein-Price function f_3. (f) The Bukin function f_4.

1.
$$f_1(x_1, x_2, ..., x_n) = \frac{\sum_{i=1}^{n}(x_i^4 - 16x_i^2 + 5x_i)}{2},$$
where $-5 \leq x_i \leq 5$ for $1 \leq i \leq n$.

2.

$$f_2(x_1, x_2) = x_1^4 - 7x_1^2 + x_2^4 - 9x_2^2 - 5x_2 + 11x_1^2 x_2^2 + 99\sin(71x_1)$$
$$+ 137\sin(97x_1 x_2) + 131\sin(51x_2),$$

where $-10 \leq x_1 \leq 10$ and $-10 \leq x_2 \leq 10$.

3.

$$f_3(x_1, x_2) = [1 + (x_1 + x_2 + 1)^2(19 - 14x_1 + 3x_1^2 - 14x_2 + 6x_1 x_2 + 3x_2^2)] \times$$
$$[30 + (2x_1 - 3x_2)^2(18 - 32x_1 + 12x_1^2 + 48x_2 - 36x_1 x_2 + 27x_2^2)],$$

where $-2 \leq x_1 \leq 2$ and $-2 \leq x_2 \leq 2$.

4.
$$f_4(x_1, x_2) = 100\sqrt{|x_2 - 0.01x_1^2|} + 0.01|x_1 + 10|,$$
where $-15 \leq x_1 \leq -5$ and $-3 \leq x_2 \leq 3$.

Figures 5 (a) and (b) show the 3D plots of the Styblinski-Tang function f_1 which is a d-dimensional function, usually evaluated on the hypercube $x_i \in [-5, 5]$, for all $i = 1, ..., d$. It has a global minimum

$$-39.16617 \times d \leq f_4(-2.903534, ..., -2.903534) \leq -39.16616 \times d.$$

Concerning f_2 shown in Figures 5 (c) and (d), it possesses hundreds of local minima [2], but its global minimum is not yet theoretically known.

f_3 is the Goldstein-Price function usually evaluated on the rectangle

$$(x_1, x_2) \in [-2, 2] \times [-2, 2],$$

it has a lot of local minima and one global minimum $f_3(0, -1) = 3$ and the 3D plot of this function is in Figure 5 (e).

f_4 is the Bukin function which is usually evaluated on the rectangle

$$(x_1, x_2) \in [-15, -5] \times [-3, 3],$$

it has a lot of local minima and one global minimum $f_4(-10, 1) = 0$, see Figure 5 (f).

5.2   Numerical experiments

In order to enrich our study, we are going to use different values of the step sizes λ, λ_{gl}, different values of the number of iterations M_g, Mgl and M_l as in Table 1 and different values of the max number of packets of global search N_p presented in Table 1. Each optimization code was implemented in Matlab (MathWorks). All the codes were run on a 2.53 GHz, i3 processor with 4 GB of random access memory.

Table 2 shows the numerical results of the global minima research of the test functions f_1, f_2, f_3 and f_4.

For the Styblinski-Tang function f_1, the best result is -117.4985 and we got it by using the Lozi map and Lozi-Hénon map. Concerning the function f_2, the best result is -395.8756 and we got it by using the Lozi-Hénon map. The Lozi-Hénon map gave the best results for the optimization problem of f_3 in common with the Lozi map. Again, the Lozi-Hénon map gave the best results (0.0049) of the optimization problem of f_4.

	λ	λ_{gl}	N_p	M_g	M_{gl}	M_l
C1	0.001	0.01	100	10	100	100
C2	0.002	0.05	100	100	200	200
C3	0.005	0.08	1000	100	200	200

Table 1: The set of parameter values for every run of the PCOA algorithm.

Function	Cases	$LPCOA$	$HPCOA$	$LHPCOA$	Best map
	$C1$	−117.4772	−116.2624	−117.3158	
f_1	$C2$	−117.4924	−117.1878	−117.4979	Lozi and Lozi-Hénon
	$C3$	−117.4985	−117.4981	−117.4985	
	$C1$	−390.2672	−394.5880	−385.7419	
f_2	$C2$	−395.8622	−395.6099	−395.8374	Lozi-Hénon
	$C3$	−395.8742	−395.8641	−395.8756	
	$C1$	3.0000	3.1689	3.0000	
f_3	$C2$	3.0000	3.0000	3.0000	Lozi and Lozi-Hénon
	$C3$	3.0000	3.0000	3.0000	
	$C1$	0.0322	0.0371	0.0310	
f_4	$C2$	0.0108	0.0096	0.0071	Lozi-Hénon
	$C3$	0.0086	0.0145	0.0049	

Table 2: Optimization results over one run for 3 parameter configurations using the PCA algorithm with three different maps (The Lozi map, Hénon map and Lozi-Hénon map).

6   Conclusion

This paper reported the results of a study of a new 2-d map derived from the Lozi and Hénon maps by mixing between them. The fixed points, periodic orbits and chaotic behaviour of the new 2-d map are analysed by means of the bifurcation diagrams. On the other hand, this paper gives an application of this new map to the optimization problems with a comparison study to the Lozi and Hénon map findings. The results obtained show that the Lozi-Hénon map yields better results than the Lozi and Hénon maps.

Acknowledgment

References

[1] M. F. Hassan and E. K. Boukas. Constrained linear quadratic regulator: continuous-time case. *Nonlinear Dynamics and Systems Theory* **8** (1) (2008) 35–42.

[2] R. Bououden and M. S. Abdelouahab. On Efficient Chaotic Optimization Algorithm Based on Partition of Data Set in Global Research Step. *Nonlinear Dynamics and Systems Theory* **18** (1) (2018) 42–52.

[3] S. F. Woon., V. Rehbock and R. C. Loxton. Global Optimization Method for Continuous-Time Sensor Scheduling. *Nonlinear Dynamics and Systems Theory* **10** (2) (2010) 175–188.

[4] M. Marko., V. Najdan., P. Milica and M. Zoran. Chaotic fruit fly optimization algorithm. *Knowledge-Based Systems* **89** (2015) 446–458.

[5] C. Zhang., L. Xu and H. Shao. Chaos optimization algorithm based on linear search and its application to nonlinear constraint optimization problems. *Chinese Journal of Control and Decision* **16** (1) (2001) 123–128.

[6] R. Bououden and M-S. Abdelouahab. Chaotic Optimization Algorithm Based on the Modified Probability Density Function of Lozi Map. *Boletim da Sociedade Paranaense de Matemática* doi:10.5269/bspm.41668.

[7] V. T. Jovanovic. Chaotic descent method and fractal conjecture. *Internat. J. Numer. Methods Eng* **48** (1) (2000) 137–152.

[8] Z. Povalej. Quasi-Newton's method for multi objective optimization. *J. Comput. Appl. Math* **255** (2014) 765–777.

[9] J. Liu and S.J. Li. New hybrid conjugate gradient method for unconstrained optimization. *Appl. Math. Comput* **245** (2014) 36–43.

[10] T.W.C. Chen and V. S. Vassiliadis . Solution of general nonlinear optimization problems using the penalty/ modified barrier method with the use of exact hessians. *Comput. Chem. Eng* **27** (4) (2003) 501–525.

[11] E. Canale., F. Robledo., P. Romero and P. Sartor. Monte Carlo methods in diameter-constrained reliability. *Opt. Switch. Netw* **14** (2) (2014) 134–148.

[12] J. A.T. Machado. Optimal tuning of fractional controllers using genetic algorithms. *Nonlinear Dyn* **62** (12) (2010) 447–452.

[13] D. Bunnag and M. Sun. Genetic algorithm for constrained global optimization in continuous variables. *Appl. Math. Comput* **171** (1) (2005) 604–636.

[14] B. Li and W. S. Jiang. Chaos optimization method and its application. *Journal of Control Theory and Application* **14** (4) (1997) 613–615.

[15] C. Choi and J. J. Lee. Chaotic local search algorithm. *Artificial Life and Robotics* **2** (1) (1998) 41–47.

[16] C. Jiang., L. Xu and H. Shao. Chaos optimization algorithm based on linear search and its application to nonlinear constraint optimization problems. *Chinese Journal of Control and Decision* **16** (1) (2001) 123–128.

[17] D.Yang., Z.Liu and J. Zhou. Chaos optimization algorithms based on chaotic maps with different probability distribution and search speed for global optimization. *Commun Nonlinear Sci Numer Simulat* **19** (1) (2014) 1229-1246.

[18] M. Hénon. A two dimensional mapping with a strange attractor. *Commun Math Phys* **50** (1) (1976) 69–77.

[19] R. Lozi. Un attracteur étrange du type attracteur de Hénon. *Journal de Physique. Colloque C5, Supplément* **8** (39) (1978) 9–10.

Sensorless Two Series Connected Quasi Six-Phase IM Based Direct Torque Control for Torque Ripples Minimization

Y. Chedni [1], DJ. Boudana [1], A. Moualdia [2*], L. Nezli [1] and P. Wira [3]

[1] *Process Control Laboratory, National Polytechnic School. Algiers, Algeria*
[2] *Laboratory of Electrical Engineering and Automatics (LREA), University of Medea, Algeria*
[3] *IRIMAS, Laboratory of Modeling Intelligence Process Systems (MIPS), University of Haute Alsace, Mulhouse, France.*

Abstract: In this paper, a new direct torque control (DTC) is proposed for a two series connected quasi six-phase induction motor (IM) with sinusoidal distributed windings fed by a single six-phase voltage source inverter (VSI). The developed DTC control is reformulated as a variable structure control strategy characterized by its simplicity, fast response and robustness to motor parameter variations. Indeed, the proposed DTC controller accomplishes two tasks, first it guarantees a decoupled torque/flux control for each machine while imposing separate control loops, the second is to eliminate current circulation that appears in stator windings of each machine through the usage of appropriate vector maps in $(\alpha - \beta)$ and $(x - y)$ plan. The effectiveness and the robustness of the proposed method are shown by computer simulation.

Keywords: *direct torque control; voltage source inverter; two series connected quasi six-phase induction motor drive.*

Mathematics Subject Classification (2010): 03B52, 93C42, 94D05.

---

* Corresponding author: `mailto:amoualdia@gmail.com`

1   Introduction

Technological developments have allowed us to put in place the concept of multiplying the number of phases over three. This is to allow to reach important technical points. Firstly, the distribution of the total power over a large number of arms will allow a better dimensioning of the inverters enabling them to operate with high frequency [1–3]. Secondly, this multiplication of phases allows machines to continue working, even if one or more arms fail operating, till the fault is fixed. Thirdly, the analysis of the stator F.M.M has made it possible to highlight a crucial item, the more the phase multiplication increases, the more interaction between time and space harmonics will be pushed back to its higher ranks [3, 4]. Another important and practical point is the possibility of controlling two or more machines separately fed by a unique single voltage source inverter (VSI), when connected in series with an appropriate phase transposition, something which would always be beyond the reach in the case of three-phase machines; mainly where only parallel structure is allowed under certain strict conditions such as the usage of identical machines possessing equal power ratings when being fed by a single inverter as mentioned in [2]. Moreover, multi-phase systems enhance the series connected topology even when machines in the group are different as it had been demonstrated in the work [5]. The dual star induction motor (DSIM) is an example of this type of machines (two sets of stator windings with 30 deg displacement), it has the property of being easily rebuilt from a simple three-phase machine, but characterized by the fact that it is better than the three-phase machine, when the torque ripples and the rotor losses have to be considered. Despite its reputation, the dual star machine, unfortunately, undergoes a problem characterized by the appearance of stator circulation currents when it is fed through a voltage source inverter as described in [6, 7]. Another challenge is added to the precedent drawback in the case of two series connected dual star machine, therefore, a compromise will be imposed between advantages and the multiplication of the losses generated by the series structure by non-producing torque/flux components if compared with a single machine. Underlying the literature review, a chain of important empirical works have been realized dealing with different types of multi-phase multi-machines such as series connected five-phase, symmetrical six-three phase. In [5], the shortcoming had been resolved in such a way, when one machine in the group operates at low speed with high torque (high current) and the other machine will operate at high speed (high voltage) with low torque, consequently, the total stator copper losses remain less than or equal to the rated value of one machine, however, this solution is still not generalized in the case where the number of machines increases. Direct torque control, or DTC as it is called, is the very latest AC drive technology developed by manufactures in the world consequently after Blaschke and his colleague Depenbrock's research came into sight in 1971. DTC allows the motor torque and stator flux to be used as primary control variables, both of which are obtained directly from the motor itself [8]. The advantages of DTC technology over the traditional AC drive can be summarized as follows. First, a fast torque response can be achieved which will significantly reduce the speed drop time during a load transient, bringing much improved process control and a more consistent product quality, then, it permits torque's control at low frequencies, which is particularly beneficial to cranes or elevators, where the load needs to be started and stopped regularly without any jerking. Moreover, torque linearity, this property is very important in precision application such as winders, where an accurate and consistent level of winding is critical. Another important advantage to be mentioned, is the dynamic speed accuracy

during a sudden load change, helping the drive to quickly recover its stable state. When compared to the other vector control drives, the direct torque control brings the cost saving benefit since no tachometer or feedback is needed. Despite all these advantages, the DTC is still facing considerable drawbacks such as variable switching frequencies and torque ripple because of the use of hysteresis controllers for torque and flux [8–10]. For such reasons, lots of research are being undertaken constantly aiming to develop technical remedy for these disadvantages. In the three phase systems, there exist only eight possible inverter states, while a large number of inverter states depending on the number of phases in the multiphase systems can be found such as 64 states for six phases, 32 states for five phases. This additional degree of freedom allows considerable flexibility in their selection, therefore, finer adjustment of flux and torque could be achieved [11]. Nevertheless, this property requires a special attention and a complex criterion when synthesizing switching lookup tables. Various research have been presented on switching lookup table based direct torque control. In [12], the concept of virtual voltage was introduced to achieve cancellation of low order harmonic currents for a single five-phase induction motor. Another research was presented in [6], where three lookup tables have been implemented for a single split phase induction motor (SPIM) to suppress zero sequence current components. The principle of control decoupling of a two series connected dual star motor drive lies in the fact that the $(\alpha - \beta)$ components of the six-phase VSI control the first motor and the $(x - y)$ components will control the second one. Hence, for the first motor, the $(\alpha - \beta)$ inverter components appear as responsible of producing flux/torque while the $(x - y)$ components appear as non-flux/torque producing and only generate losses. On the contrary, the $(x - y)$ components appear as responsible of producing flux/torque for the second machine while the $(\alpha - \beta)$ only generate losses [3, 5]. In this paper, an extension was made on two series connected dual star induction motor fed by a single six-phase voltage source inverter (VSI) while preserving the technique developed in [6]. Therefore, the proposed DTC controller adopted here aims, on one hand, at ensuring a decoupled flux/torque control for each machine within the group while imposing independent control of the two series connected drive system. On the other hand, it should eliminate the components flowing in each machine, that do not contribute in producing flux/torque but only increase copper losses through a proper selection of virtual voltage vectors. Additionally, to overcome the problems caused by flux/ torque estimators which usually deteriorate the system performances such as those related to signal integration and dc-drift caused by the initial integral condition [12, 13], an adaptive variable observer based on the Lypunov theory was introduced to improve the proposed controller performances. A number of computer simulations are achieved as a comparative study with the conventional DTC controller, where only large vector maps in $(\alpha - \beta)$ and $(x - y)$ plan are used to demonstrate the impact of the proposed controller on torque ripples minimization and current harmonics cancellation.

2 Modelling of the Drive System

This section is devoted to the modelling of two series connected dual-star induction motor (DSIM1) and (DSIM2), respectively, for first and second machine or simply quasi six-phases squirrel cage induction motors where stator winding of each machine is displaced in space by 30 degrees. The two motor drives are connected in series through an appropriate phase transposition and fed by a single six-phase voltage source inverter (VSI) as shown in Fig. 1. The neutral points n1, n2 of the two windings are normally kept isolated to

prevent the stator current harmonics of the order divisible by three from flowing [5]. The
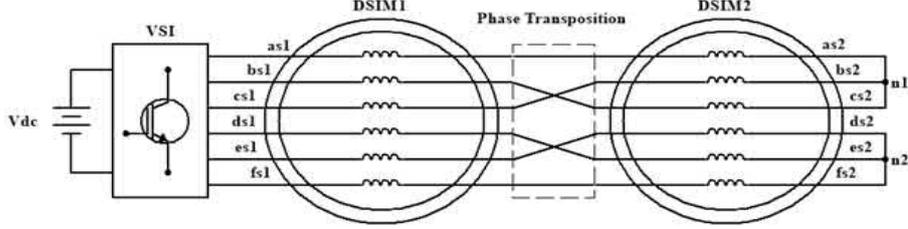
Figure 1: Drive system block diagram.

relation between voltages and currents can be given as

$$
\begin{aligned}
V_A &= v_{as1} + v_{as2}, & i_A &= i_{as1} = i_{as2}, \\
V_B &= v_{bs1} + v_{cs2}, & i_B &= i_{bs1} = i_{cs2}, \\
V_C &= v_{cs1} + v_{bs2}, & i_C &= i_{cs1} = i_{bs2}, \\
V_D &= v_{ds1} + v_{es2}, & i_D &= i_{ds1} = i_{es2}, \\
V_E &= v_{es1} + v_{ds2}, & i_E &= i_{es1} = i_{ds2}, \\
V_F &= v_{fs1} + v_{fs2}, & i_F &= i_{fs1} = i_{fs2},
\end{aligned}
\tag{1}
$$

by using the decoupling power-invariant transformation matrix

$$
C = \frac{1}{\sqrt{3}} \cdot
\begin{bmatrix}
1 & \cos(4\alpha) & \cos(8\alpha) & \cos(\alpha) & \cos(5\alpha) & \cos(9\alpha) \\
0 & \sin(4\alpha) & \sin(8\alpha) & \sin(\alpha) & \sin(5\alpha) & \sin(9\alpha) \\
1 & \cos(8\alpha) & \cos(4\alpha) & \cos(5\alpha) & \cos(\alpha) & cos(9\alpha) \\
0 & \sin(8\alpha) & \sin(4\alpha) & \sin(5\alpha) & \sin(\alpha) & \sin(9\alpha) \\
1 & 1 & 1 & 0 & 0 & 0 \\
0 & 0 & 0 & 1 & 1 & 1
\end{bmatrix},
\tag{2}
$$

where $\alpha = \frac{\pi}{6}$, the original phase variables are transformed to new $(\alpha - \beta)$ and $(x - y)$ variables as

$$
\begin{bmatrix}
v_\alpha^{inv} \\
v_\beta^{inv} \\
v_x^{inv} \\
v_y^{inv} \\
v_{o+}^{inv} \\
v_{o-}^{inv}
\end{bmatrix}
= C
\begin{bmatrix}
v_{as1} + v_{as2} \\
v_{bs1} + v_{cs2} \\
v_{cs1} + v_{bs2} \\
v_{ds1} + v_{es2} \\
v_{es1} + v_{ds2} \\
v_{fs1} + v_{fs2}
\end{bmatrix}
=
\begin{bmatrix}
v_{\alpha s1} + v_{xs2} \\
v_{\beta s1} + v_{ys2} \\
v_{xs1} + v_{\alpha s2} \\
v_{ys1} + v_{\beta s2} \\
0 \\
0
\end{bmatrix},
\tag{3}
$$

$$
\begin{aligned}
i_\alpha^{inv} &= i_{\alpha s1} = i_{xs2}, \\
i_\beta^{inv} &= i_{\beta s1} = i_{ys2}, \\
i_x^{inv} &= i_{xs1} = i_{\alpha s2}, \\
i_y^{inv} &= i_{ys1} = i_{\beta s2}.
\end{aligned}
\tag{4}
$$

Torque equations of two series connected machines are given as follows:

$$
T_{ek} = P_k L_{mk}(i_{\alpha rk} i_{\beta sk} - i_{\beta rk} i_{\alpha sk}),
\tag{5}
$$

where $k = 1, 2$ and P_k is a pole pair. The stator voltage equations of each machine are

$$
\begin{aligned}
v_{\alpha sk} &= R_{sk} i_{\alpha sk} + \frac{d}{dt}(L_{sk} i_{\alpha sk} + L_{mk} i_{\alpha rk}), \\
v_{\beta sk} &= R_{sk} i_{\beta sk} + \frac{d}{dt}(L_{sk} i_{\alpha sk} + L_{mk} i_{\alpha rk}), \\
v_{xsk} &= R_{sk} i_{xsk} + \frac{d}{dt}(L_{lsk} i_{xsk}), \\
v_{ysk} &= R_{sk} i_{ysk} + \frac{d}{dt}(L_{lsk} i_{ysk}).
\end{aligned}
\tag{6}
$$

The rotor voltage equations of each machine are

$$
\begin{aligned}
0 &= R_{rk} i_{\alpha rk} + \omega_{rk}(L_{rk} i_{\beta rk} + + L_{mk} i_{\beta sk}) + \frac{d}{dt}(L_{rk} i_{\alpha rk} + L_{mk} i_{\alpha sk}), \\
0 &= R_{rk} i_{\beta rk} - \omega_{rk}(L_{rk} i_{\alpha rk} + L_{mk} i_{\alpha sk}) + \frac{d}{dt}(L_{rk} i_{\beta rk} + L_{mk} i_{\beta sk}),
\end{aligned}
\tag{7}
$$

where $k = 1, 2$. From (4) and (5) one can see that the currents producing flux/torque for the first machine $(i_{\alpha s1}, i_{\beta s1})$ appear as non producing flux/torque for the second one and vice versa. As a result, the two series connected machine can be controlled independently.

3 Design of Direct Torque Controller

3.1 Conventional DTC controller

For a two level six-phase inverter feeding the two-motor drive system under study there are 64 possible inverter states which are defined as $[s_a, s_b, s_c, s_d, s_e, s_f]$ for the upper switches, while the lower inverter states must operate in a complementary mode with the upper ones in each leg [5].

$$
\underline{v}_{\alpha\beta}^{inv} = \frac{2}{6}(v_a + \underline{a}^4 v_b + \underline{a}^8 v_c + \underline{a} v_d + \underline{a}^5 v_e + \underline{a}^9 v_f),
\tag{8}
$$

$$
\underline{v}_{xy}^{inv} = \frac{2}{6}(v_a + \underline{a}^8 v_b + \underline{a}^4 v_c + \underline{a}^5 v_d + \underline{a} v_e + \underline{a}^9 v_f),
\tag{9}
$$

where $\underline{a} = exp(j\frac{\pi}{6})$.

According to (8) and (9), the six-phase voltages of each inverter state are transformed into two voltage vectors $\underline{v}_{\alpha\beta}^{inv}$ and $\underline{v}_{xy}^{inv}$. Zero-sequence can not be excited because of the star connection, therefore it is omitted. These two voltage vectors are plotted in their associated $(\alpha - \beta)$ and $(x - y)$ sub-space as shown in Figure 2. Each plan comprises four dodecahedrons with magnitude of $\frac{\sqrt{2}(\sqrt{3}+1)}{6}.v_{dc}$, $\frac{\sqrt{2}(\sqrt{3}-1)}{6}.v_{dc}$, $\frac{\sqrt{2}}{3}.v_{dc}$, $\frac{1}{3}.v_{dc}$, and they are classified according to their magnitude into five types: null, smallest, small, largest and large. In total, there exist 64 vectors in each plan. Inverter states which are given in binary form have been coded in octal system for better representation, for example, states (100100) have been coded to (44) and mentioned as v_{44} in Figure 2.

Same technique has been applied for all vectors in each plan. The conventional DTC diagram is shown in Figure 3. Correct inverter states that should be used are based on the stator flux and torque errors. Three-level and two-level hysteresis regulators are used, respectively, for torque and flux. The position information of the stator flux linkage is

required to define sectors for each machine. Voltage lookup tables of conventional DTC for each motor in the group are built using only the largest vector maps in $(\alpha - \beta)$ and $(x - y)$ plan for fully using available DC bus ($\frac{\sqrt{2}(\sqrt{3}+1)}{6}.v_{dc}$) without any compensation. The aim of this sub-section is to show the impact of using only the largest vectors from sub-space $(\alpha - \beta)$ and $(x - y)$ for lookup tables to control, respectively, DSIM1 and DSIM2.

(a)   (b)
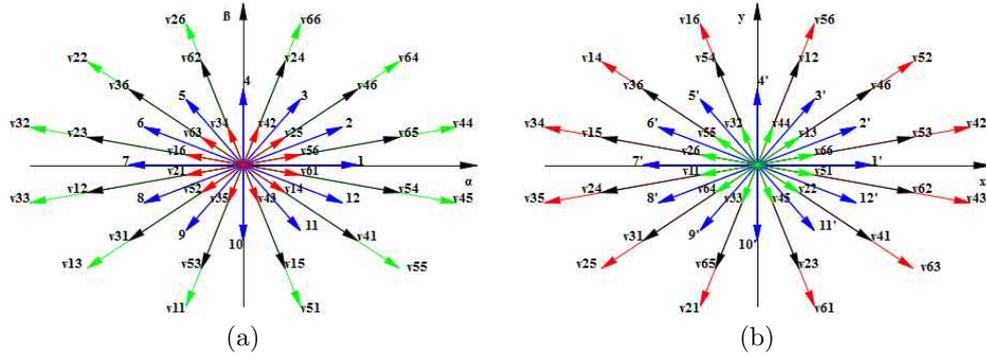
Figure 2: Distribution of basic space vectors: (a) for $(\alpha - \beta)$ plan and (b) for $(x - y)$ plan.
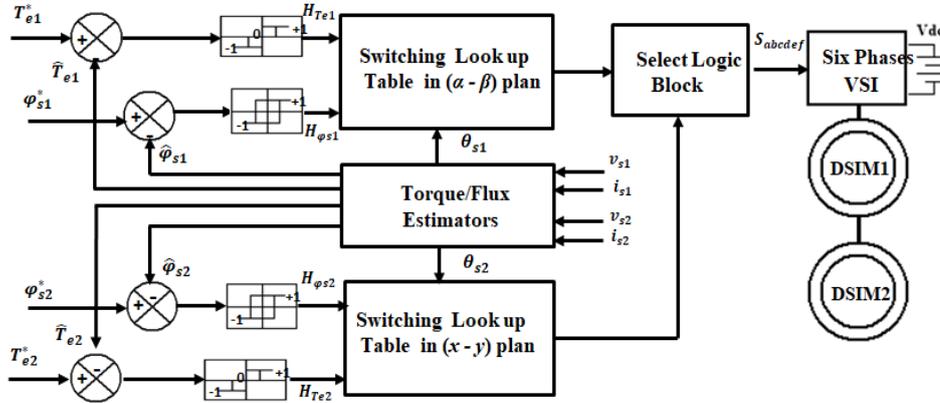
Figure 3: Conventional DTC block diagram.

To confirm our assumptions, a simulation was made first, aiming at the impact of the application of only the largest vectors on the shape of the currents feeding the two motors. An example of phase(a) current is shown in Figure 4, unsatisfactory results were obtained, that is, an amount of distortions can be observed which, consequently, will affects torque and flux variables, as a result, all the system drives efficiency. This is due mainly to the presence of non-producing torque/flux flowing in each machine simultaneously with the producing torque/flux components as explained in Section 1, therefore, to overcome this problem which degrades the performance controller, another strategy will be developed next.
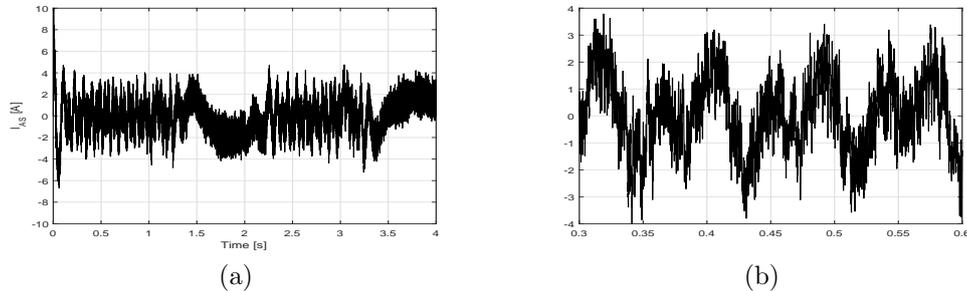
Figure 4: Conventional DTC using only the largest vector : (a) inverter phase (a) current and (b) its zoomed snapshot.

3.2 Proposed DTC controller

The application of a large number of vectors of the subspace $(\alpha - \beta)$ and $(x - y)$ related to the current circulation, does not involve the production of couple / flux, but simply generate losses inside the system. To overcome these drawbacks, a DTC controller has been implemented to these components; benefiting from the possible advantages which ensue from it and which offer polyphase systems in terms of large number of space vectors. The diagram in Figure 5 illustrates the proposed controller.
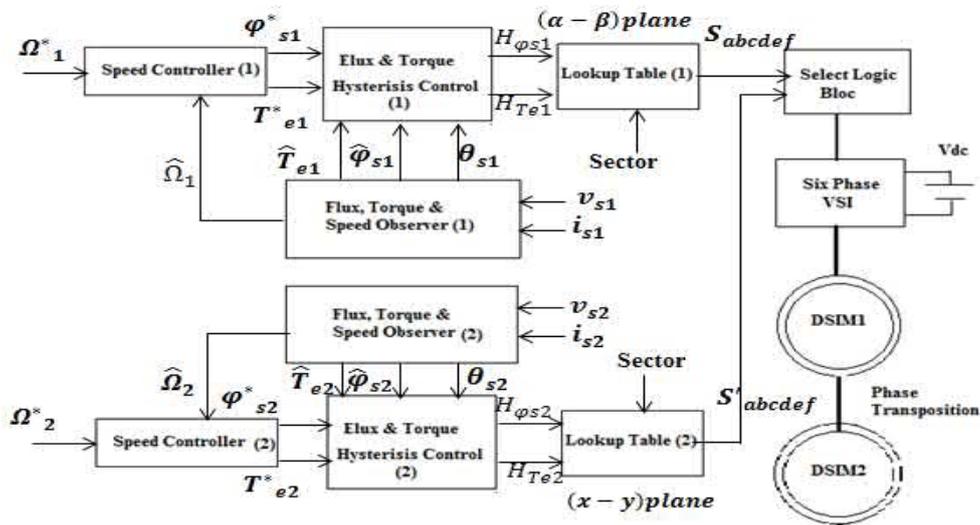
Figure 5: Proposed DTC block diagram.

The reason behind this technique is the vectors distribution, that is, by the help of Figure 2, one can observe the largest vectors in $(\alpha - \beta)$ plan appear as the smallest vectors in $(x - y)$ plan and vice versa, small and large vectors keep their magnitude but are shifted in each sub-space. Let us look, for example, at states 44, 64 and 66, the corresponding vectors v_{44}, v_{64} and v_{66} appear as the largest vectors in $(\alpha - \beta)$ plan while
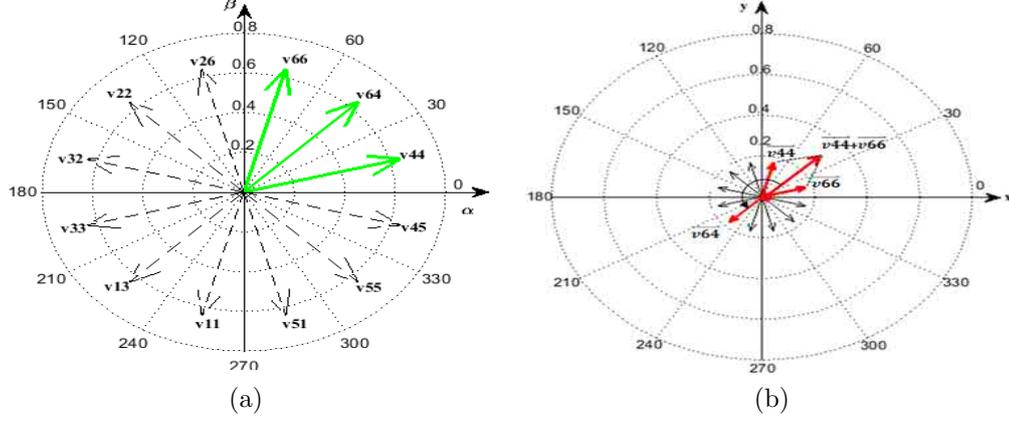
Figure 6: Three largest vectors : (a) in $(\alpha - \beta)$ plan and (b) their projection in $(x - y)$ plan.

they appear as the smallest ones in $(x - y)$ plan where v_{64} is in opposite direction versus the vector sum of v_{44} and v_{66} as shown in Figure 6(b), therefore, to enforce the resultant of these vectors equal to zero mean volt- second product, the switching times should satisfy the following conditions:

$$|v_{44}|.\frac{t_1}{2} + |v_{64}|.\frac{t_1}{2} + |v_{66}|.t_2 = 0, \tag{10}$$

$$\frac{t_1}{2} + \frac{t_1}{2} + t_2 = T_s. \tag{11}$$

From (10) and (11), and taking into account the magnitude of vectors v_{44}, v_{64} and v_{66}, solving for t_1, t_2 (switching time of the applied vectors) gives

$$\frac{t_1}{2} \approx 0.25.T_s, \tag{12}$$

$$t_2 \approx 0.5.T_s. \tag{13}$$

The proposed technique will be extended to all vectors in each sub-space resulting in twelve active virtual vectors, i.e., $V_1 - V_{12}$, in $(\alpha - \beta)$ plan and twelve active virtual vectors from $(x - y)$ plan, i.e., $V_1' - V_{12}'$ as shown, respectively, in Figure 7 to synthesize two lookup tables identified with index '1' for the first motor and index '2' for the second motor in Figure 5. This selection of inverter states and dwell times should cancel current circulation which flows simultaneously with the energy producing components in each motor, as a result, less distortions in wave current forms and high performances of controller could be achieved within the drive system. If we consider the sector (1) indexed S1 in Figure 7(a), for example, to control the torque and flux of the first motor DSIM1, the voltage vector criterion is stated as follows. If the torque and flux have to be increased, i.e., $HT_{e1} = +1$ and $H\varphi_{s1} = +1$, the active virtual voltage V_2 or V_3 is selected; if the torque is to be increased and the flux is to be decreased, i.e., $H_{T_{e1}} = +1$ and $H\varphi_{s1} = -1$, then V_4 or V_5 is selected; if the torque is to be decreased and the flux is to be increased, i.e., $H_{T_{e1}} = -1$ and $H\varphi_{s1} = +1$, then V_{11} or V_{10} is selected; if the torque and flux have to be decreased, i.e., $H_{T_{e1}} = -1$ and $H\varphi_{s1} = -1$, then V_8 or V_9 is
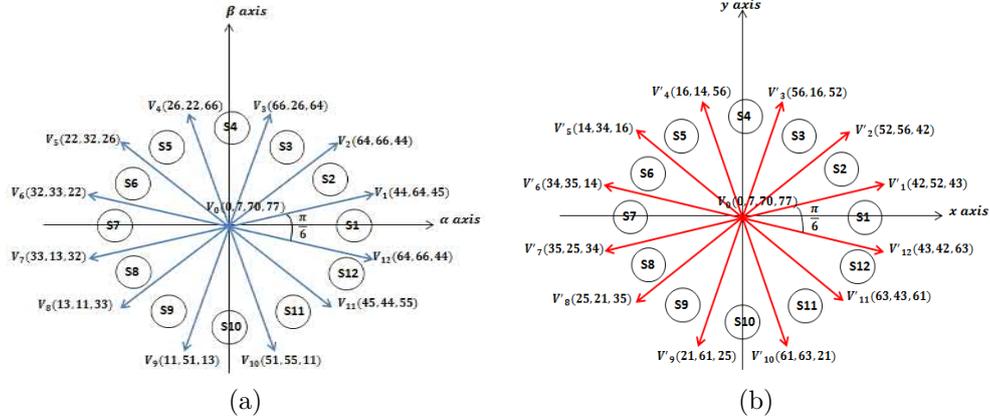
Figure 7: Twelve active virtual voltage vectors and twelve sectors in (a) $(\alpha - \beta)$ plan and (b) $(x - y)$ plan.

selected; if the torque error is within the error band, i.e., $H_{T_{e1}} = 0$, the null voltage V_0 or V_{77} is selected regardless of the flux control loop. All cases are summarized in Table 1. The second voltage lookup table (not shown in this paper) will use $V_1' - V_{12}'$ from $(x - y)$ plan shown in Figure 7(b) to control the second motor DSIM2

$H_{\varphi_{s1}}$	$H_{T_{e1}}$	Sector number in $(\alpha - \beta)$ plan											
		I	*II*	*III*	*IV*	*V*	*VI*	*VII*	*VIII*	*IX*	*X*	*XI*	*XII*
+1	+1	V_2	V_3	V_4	V_5	V_6	V_7	V_8	V_9	V_{10}	V_{11}	V_{12}	V_1
		V_3	V_4	V_5	V_6	V_7	V_8	V_9	V_{10}	V_{11}	V_{12}	V_1	V_2
	-1	V_{11}	V_{12}	V_1	V_2	V_3	V_4	V_5	V_6	V_7	V_8	V_9	V_{10}
		V_{10}	V_{11}	V_{12}	V_1	V_2	V_3	V_4	V_5	V_6	V_7	V_8	V_9
-1	+1	V_5	V_6	V_7	V_8	V_9	V_{10}	V_{11}	V_{12}	V_1	V_2	V_3	V_4
		V_4	V_{16}	V_6	V_7	V_3	V_{43}	V_{41}	V_{61}	V_{60}	V_{70}	V_{30}	V_{34}
	-1	V_8	V_9	V_{10}	V_{11}	V_{12}	V_1	V_2	V_3	V_4	V_5	V_6	V_7
		V_9	V_{10}	V_{11}	V_{12}	V_1	V_2	V_3	V_4	V_5	V_6	V_7	V_8
+1	0	V_0	V_{77}	V_0	V_{77}	V_0	V_{77}	V_0	V_{77}	V_0	V_{77}	V_0	V_{77}
		V_0	V_{77}	V_0	V_{77}	V_0	V_{77}	V_0	V_{77}	V_0	V_{77}	V_0	V_{77}
-1	0	V_{77}	V_0	V_{77}	V_0	V_{77}	V_0	V_{77}	V_0	V_{77}	V_0	V_{77}	V_0
		V_{77}	V_0	V_{77}	V_0	V_{77}	V_0	V_{77}	V_0	V_{77}	V_0	V_{77}	V_0

Table 1: Voltage lookup table for DTC controller: shadowed part for low speed and unshaded part for high speed.

3.2.1   Derivation of flux and speed adaptive variable structure observer.

To provide motor's information for such control purposes, a derivative speed and flux observer is developed for DSIM1 based on the state-space model of the first motor DSIM1 given in (A.1), where

$\sigma_1 = 1 - \frac{L_{m1}^2}{L_{s1}L_{r1}}$, $T_{s1} = \frac{\sigma_1 L_{s1} + L_{ls2}}{(R_{s1} + R_{s2})}$ and $T_{r1} = \frac{L_{r1}}{R_{r1}}$,

$$p\underline{i}_{\alpha\beta s1} = \left(-\frac{1}{T_{s1}} - \frac{(1-\sigma_1)L_{s1}}{(\sigma_1 L_{s1} + L_{ls2})T_{r1}}\right) \underline{i}_{\alpha\beta s1} + \left(\frac{L_{m1}}{(\sigma_1 L_{s1} + L_{ls2})L_{r1}}\right)\left(\frac{1}{T_{r1}} - j\omega_{r1}\right)\underline{\phi}_{\alpha\beta r1}$$

$$+\frac{1}{(\sigma_1 L_{s1} + L_{ls2})}\ \underline{v}_{\alpha\beta s1},$$

$$p\hat{\underline{i}}_{\alpha\beta s1} = \left(-\frac{1}{T_{s1}} - \frac{(1-\sigma_1)L_{s1}}{(\sigma_1 L_{s1} + L_{ls2})T_{r1}}\right) \hat{\underline{i}}_{\alpha\beta s1} + \left(\frac{L_{m1}}{(\sigma_1 L_{s1} + L_{ls2})L_{r1}}\right)\left(\frac{1}{T_{r1}} - j\hat{\omega}_{r1}\right)\hat{\underline{\phi}}_{\alpha\beta r1},$$

$$+\frac{1}{(\sigma_1 L_{s1} + L_{ls2})}\ \underline{v}_{\alpha\beta s1} + G_1 sign(\underline{i}_{\alpha\beta s1} - \hat{\underline{i}}_{\alpha\beta s1})$$

(A-1)

$$p\underline{\phi}_{\alpha\beta r1} = \frac{L_{m1}}{T_{r1}}\ \underline{i}_{\alpha\beta s1} + \left(\frac{1}{T_{r1}} - j\omega_{r1}\right)\underline{\phi}_{\alpha\beta r1},$$

$$p\hat{\underline{\phi}}_{\alpha\beta r1} = \frac{L_{m1}}{T_{r1}}\ \hat{\underline{i}}_{\alpha\beta s1} + \left(\frac{1}{T_{r1}} - j\hat{\omega}_{r1}\right)\hat{\underline{\phi}}_{\alpha\beta r1} + ... + \underline{G}_2 G_1 sign(\underline{i}_{\alpha\beta s1} - \hat{\underline{i}}_{\alpha\beta s1}).$$

(A-2)

Subtracting (A.2) from (A.1) gives the error dynamics

$$p\Delta\underline{i}_{\alpha\beta s1} = \left(-\frac{1}{T_{s1}} - \frac{(1-\sigma_1)L_{s1}}{(\sigma_1 L_{s1} + L_{ls2})T_{r1}}\right) \underline{i}_{\alpha\beta s1} + \left(\frac{L_{m1}}{(\sigma_1 L_{s1} + L_{ls2})L_{r1}}\right)\left(\frac{1}{T_{r1}} - j\omega_{r1}\right)\underline{\phi}_{\alpha\beta r1}$$

$$-\left(\frac{L_{m1}}{(\sigma_1 L_{s1} + L_{ls2})L_{r1}}\right)j\Delta\omega_{r1}\hat{\underline{\phi}}_{\alpha\beta r1} - G_1 sign(\Delta\underline{i}_{\alpha\beta s1}),$$

$$p\Delta\underline{\phi}_{\alpha\beta r1} = \frac{L_{m1}}{T_{r1}}\ \Delta\underline{i}_{\alpha\beta s1} - \left(\frac{1}{T_{r1}} - j\omega_{r1}\right)\Delta\underline{\phi}_{\alpha\beta r1} + j\Delta\omega_{r1}\hat{\underline{\phi}}_{\alpha\beta r1} - \underline{G}_2 G_1 sign(\Delta\underline{i}_{\alpha\beta s1}).$$

(A-3)

Provided that the scalar gain G1 is large enough, the equivalent component of the current error will converge to zero, such that $p\Delta\underline{i}_{\alpha\beta s1} = \Delta\underline{i}_{\alpha\beta s1} = 0$. Under this condition, the low frequency flux error dynamics is described by

$$\Delta\underline{\phi}_{\alpha\beta r1} = \left(j\Delta\omega_{r1}\hat{\underline{\phi}}_{\alpha\beta r1} + B\ G_1 sign(\Delta\underline{i}_{\alpha\beta s1})|_{eq}\right)\ \times \left(\frac{1}{T_{r1}} - j\omega_{r1}\right)^{-1}, \qquad \text{(A-4)}$$

$$p\ \Delta\underline{\phi}_{\alpha\beta r1} = (B - \underline{G}_2)\ G_1 sign(\Delta\underline{i}_{\alpha\beta s1})|_{eq}, \qquad \text{(A-5)}$$

where $B = \frac{L_{m1}\sigma_1}{1-\sigma_1}$. The positive definite Lyapunov candidate function V is chosen as in (A.6), with its time derivative $\dot{V}$ shown in (A.7).

$$V = \frac{1}{2}\left(\Delta\phi_{\alpha r1}^2 + \Delta\phi_{\beta r1}^2\right) + \frac{\Delta\omega_{r1}^2}{2\rho}, \quad \rho > 0, \qquad \text{(A-6)}$$

$$\dot{V} = \Delta\underline{\phi}_{\alpha\beta r1} \cdot \frac{d}{dt}\Delta\underline{\phi}_{\alpha\beta r1} + \frac{\Delta\omega_{r1}\frac{d}{dt}\Delta\omega_{r1}}{\rho} < 0. \qquad \text{(A-7)}$$

Substituting (A.4) and (A.5) into (A.7) leads to (A.8). Negative definite $\dot{V} < 0$ is guaranteed if (A.9) is satisfied. The imaginary part in (A.9) is configured as zero to

avoid oscillation during error convergence. By solving (A.9) and replacing real speed with its estimated, the speed-dependent complex gain G2 can be determined as

$$\dot{V} = \underbrace{\left(B\, G_1 sign(\Delta\underline{i}_{\alpha\beta s1})|_{eq} \left(\frac{1}{T_{r1}} - j\omega_{r1} \right)^{-1} \right) . \left((-B - G2)\, G_1 sign(\Delta\underline{i}_{\alpha\beta s1})|_{eq} \right)}_{\dot{V}<0}$$

$$+ \underbrace{\left(\Delta\omega_{r1} j\hat{\underline{\phi}}_{\alpha\beta r1} \left(\frac{1}{T_{r1}} - j\omega_{r1} \right)^{-1} \right) \left((-B - G2)\, G_1 sign(\Delta\underline{i}_{\alpha\beta s1})|_{eq} \right) + \frac{1}{\rho}\Delta\omega_{r1}\frac{d}{dt}\Delta\omega_{r1}}_{\dot{V}=0}$$

$$\text{(A-8)}$$

$$\frac{1}{B}\left(-B - \underline{G}_2 \right)\left(\frac{1}{T_{r1}} - j\omega_{r1} \right) = \mu, \quad \mu < 0. \tag{A-9}$$

By using (A.9) and considering $p\omega_{r1} = \frac{1}{J_1}\left(\hat{T}_{e1} - \hat{T}_{l1} \right)$, the speed adaptation law (A.10) can be determined from $\dot{V} = 0$ in (A.8)

$$\frac{d}{dt}\,\hat{\omega}_{r1} = K_\omega \left(sign(i_{\alpha s1} - \hat{i}_{\alpha s1})\hat{\phi}_{\beta r1} - sign(i_{\beta s1} - \hat{i}_{\beta s1}) \right) \hat{\phi}_{\alpha r1}$$

$$+ \frac{\hat{T}_{e1} - \hat{T}_l}{J_1}, \qquad K_\omega > 0. \tag{A-10}$$

The electromagnetic torque is estimated by the deterministic model (A.8), and the load torque is estimated by an adaptation mechanism [13], as shown in (A.9):

$$\hat{T}_{e1} = 3\frac{P_1}{2}\frac{L_{m1}}{L_{r1}}\left(\hat{\phi}_{\alpha r1}\hat{i}_{\beta s1} - \hat{\phi}_{\beta r1}\hat{i}_{\alpha s1} \right), \tag{A-11}$$

$$\frac{d}{dt}\,\hat{T}_{l1} = -K_t\left(sign(i_{\alpha s1} - \hat{i}_{\alpha s1})\hat{\phi}_{\beta r1} - sign(i_{\beta s1} - \hat{i}_{\beta s1})\hat{\phi}_{\alpha r1} \right), \qquad K_t > 0. \tag{A-12}$$

Same procedure will be applied for DSIM2 to derive the flux and speed observer. The observer and controller parameters for each motor are: $G_1 = G_2 = 2000$, $\mu_1 = \mu_2 = -15$, $k_{w1} = 500$, $k_{w2} = 300$, $k_t = 50$, $F_{bw} = 0.02$, $T_{bw} = 2$.

4 System Synthesis and Simulation Results

In order to demonstrate the proposed DTC controller's performances adopted here in combination with the derived speed and flux observer, various simulations have been implemented as a comparative study to the conventional DTC controller, keeping the same motor and simulation parameters. For the conventional controller, only the largest virtual vectors have been used, while for the proposed one, the synthesized vectors shown in Table 1 are used, enabling the control of the drive system even at a low speed (shadowed part) or at a high speed (unshaded part), therefore, some figures are established, and then being compared to each other to reassert the performance of the proposed controller. In the appendix we show motor's parameters identified by index 1 and index 2 for DSIM1 and DSIM2, respectively. Additional bloc as shown in Figure 5 has been used to synthesize vector application of the proposed method and aims to alternatively keep flowing state signals generated from the lookup tables to inverter switches in each

half switching period. The model is discrete, good simulation results have been obtained with a 5 μs time step. The control system has two different sampling times : the speed controller sampling time has to be a multiple of the DTC sampling time, i.e., 50μs. The latter has to be a multiple of the simulation time step, i.e., 10μs. The following results are obtained for an exponential reference rotor speed from zero to 700 rpm for DSIM1 and from zero to 1400 rpm for DSIM2. Stator flux references for DSIM1 and DSIM2 are set, respectively, to 1Wb and 1.5 Wb and the dc-link voltage Vdc is set to 1000 Volt (2 Pu).

Figures 8 and 9 summarize the results of simulations for the system drive. Figure 8(a)
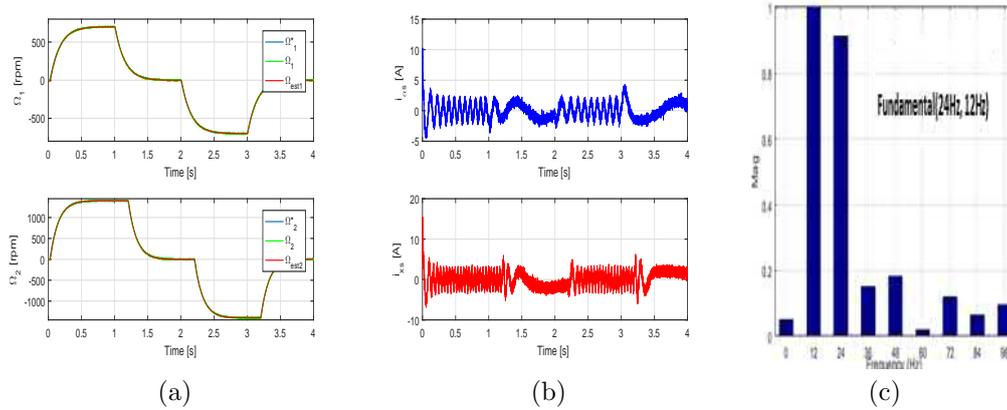
Figure 8: Proposed controller: (a) motor's speed, (b) $i_{\alpha s}$, i_{xs} inverter currents, (c) inverter currents spectrum.

shows both actual, estimated and reference speed under reversal speed transient with mechanical load (4 N.m) applied to DSIM1 and DSIM2 at 0.02s. Actual speeds follow precisely their references, as expected. Figure 8(b) and Figure 8(c) illustrate (α, β), (x, y) inverter currents and their harmonic spectrum, where we observe two different frequencies approximatively (24Hz and 12Hz). In Figure 9 and Figure 10, motor's torque and stator flux are shown, decoupled flux/torque for each machine within the whole system drive can be observed , in addition, less distortions can be seen in motor's torque with the proposed controller in Figure 9(a) if compared with Figure 9(b). Current waveforms of inverter phase (a) and their zoomed responses are shown in Figure 12 and Figure 13, respectively. One can observe a non sinusoidal waveform for both current responses, that is due to two different frequencies which provide the inverter to fed the system drive simultaneously running under different speed (700 and 1400 rpm). In Figure 12(b) an amount of distortions can be observed in the current waveform (without compensation of (x, y) components) if compared with the one obtained with the proposed DTC shown in Figure 12(a).

5 Conclusion

In this paper, the effectiveness and ability of controlling separately a two series connected quasi six-phase induction motor's drive fed by a single six-phase voltage source inverter (VSI), with an appropriate phase transposition based direct torque control (DTC), running under different working modes regardless of the torque and speed references, is
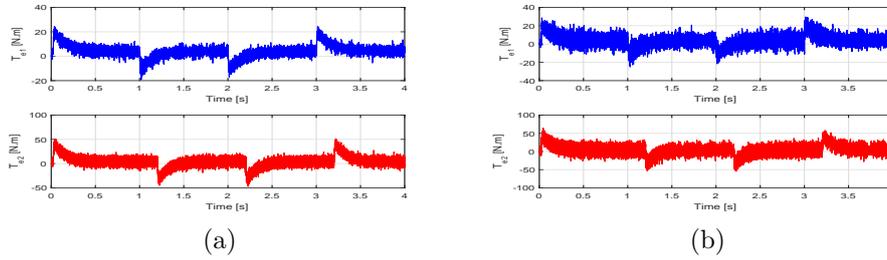
Figure 9: Motor's torque: (a) proposed controller, (b) conventional controller.
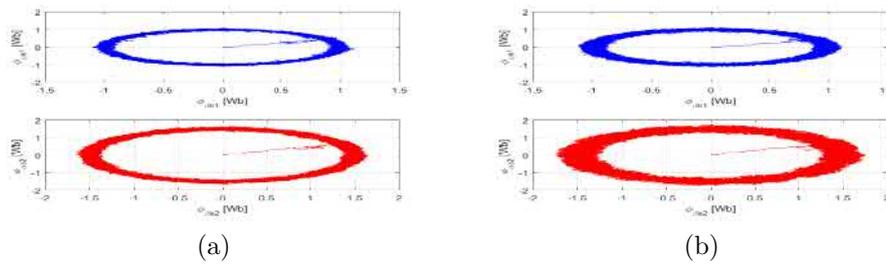
Figure 10: Flux locus versus each other: (a) proposed controller, (b) conventional controller.
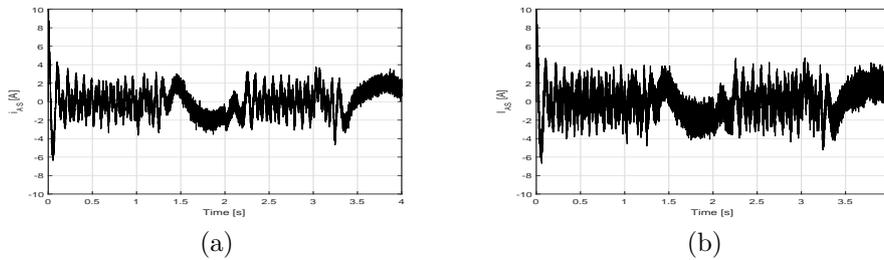
Figure 11: Zoomed phase (a) current: (a) proposed controller, (b) conventional controller.

developed and verified by computer simulation. The technique is adopted under comparative analysis through the conventional controller and is possible via the usage of a large number of vectors that offers a multiphase system, in the minimization of machine's torque ripples and the controller's performance improvement by judicious voltage vectors selection. The cornerstone advantage of the proposed controller is the elimination of the harmonic current's low frequencies that make no contribution in producing of energy, but only generate extra losses within stator windings of the drive system, consequently, its efficiency is being degraded.

(a)   (b)
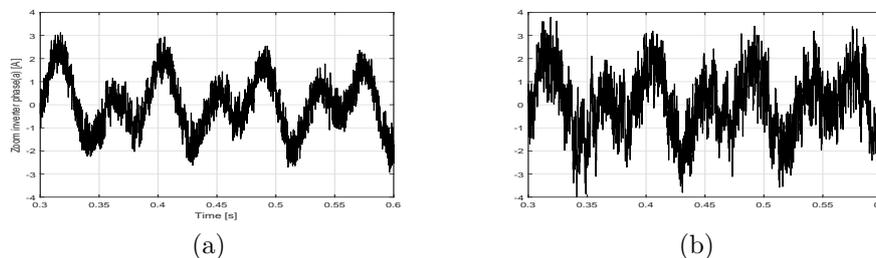
Figure 12: Zoomed phase (a) current: (a) proposed controller, (b) conventional controller.

Acknowledgment

References

[1] E. Levi, M. Jones, S. N. Vukosavic and H. A. Toliyat. *A* novel concept of a multiphase, multi-motor vector controlled drive system supplied from a single voltage source inverter. *IEEE Trans. Power Electron.* **19**(2) (2004) 320–335.

[2] I. Zoric, M. Jones and E. Levi. *A*rbitrary Power Sharing Among Three-Phase Winding Sets of Multiphase Machines. *IEEE Trans. Ind. Electron.* **65**(2) (2018) 1128–1139.

[3] E. Levi. *A*dvances in Converter Control and Innovative Exploitation of Additional Degrees of Freedom for Multiphase Machines. *IEEE Trans. Ind. Electron.* **63**(5) (2016) 433–448.

[4] M.J. Duran and F. Barrero. *R*ecent Advances in the Design, Modeling, and Control of Multiphase Machines: Part II. *IEEE Trans. Ind. Electron.* **63**(3) (2016) 459–468.

[5] E. Levi, A. Iqbal, S. N. Vukosavic and H. A. Toliyat. Modeling and Control of a Five-Phase Series-Connected Two-Motor Drive. In: *The 29th Annual Conference of the IEEE Industrial Electronics Society (IECON)* **1**(1) (2003) 208–213.

[6] N.R. Abadji and D. Ghanbari. Direct torque and flux control of asymmetrical six-phase induction motor with zero sequence components elimination. *Rev. Roum. Sci. Techn. ectrotechn. et nerg.* **62**(1) (2017) 63–41.

[7] E. Daryabeigi, N.R. Abjadi and G.R. Arab Markadeh. Automatic speed control of an asymmetrical six-phase induction motor using emotional controller *Journal of Intelligent Fuzzy Systems* BELBIC **26**(4) (2013) 1879–1892.

[8] A. Azib, D. Ziane, T. Rekioua and A. Tounzi. Robustness of the direct torque control of double star induction motor in falut condition. *Rev. Roum. Sci. Techn. ectrotechn. et nerg.* **61**(2) (2016) 147–152.

[9] E. Benyoussef, A. Meroufel and S. Barkat. Neural network and fuzzy logic direct torque control of sensorless double star synchronous machine. *Rev. Roum. Sci. Techn. ectrotechn. et nerg.* **61**(3) (2016) 239–243.

[10] G. Sheng-wei and C. Yan. *R*esearch on torque ripple minimization strategy for direct control of induction motors. In: *Proc. ICCASM* (2010) 278–281.

[11] Libo Zheng, John E. Fletcher, Barry W. Williams and Xiangning He. A novel direct torque control scheme for a sensorless five-phase induction motor drive. *IEEE Transactions on industrial electronics.* **58**(2) (2011) 503–513.

[12] J. Soltani, N. R. Abjadi, Gh. R. Arab Markadeh and H. W. Ping. Adaptive sliding-mode control of a two five-phase series-connected induction motors drive. *Proceeding of International Conference on Electrical Machines and Systems.* (2007), Oct. 8-11, Seoul, Korea.

[13] Masood Hajian, Jafar Soltani, Gholamreza Arab Markadeh and Saeed Hosseinnia. Adaptive Nonlinear Direct Torque Control of Sensorless IM Drives With Efficiency Optimization. *IEEE Trans. Ind. Electron.* **57**(3) (2010) 975–985.

[14] F. Hamidia, A. Abadi, A. Tlemcani and M. S. Boucherit. Dual star induction motor supplied with double photovoltaic panels based on fuzzy logic type–2. *Nonlinear Dynamics and Systems Theory* **18**(4) (2018) 359–371.

[15] S. Boulkhrachef, A. Moualdia, Dj. Boudana and P. Wira. Higher-order sliding mode control of a wind energy conversion system. *Nonlinear Dynamics and Systems Theory* **19**(4) (2019) 486–496.

[16] A.G. Mazko. Robust output feedback stabilization and optimization of discrete-time control systems. *Nonlinear Dynamics and Systems Theory* **18**(1) (2018) 92–106.

[17] Djamel Boudana, Lazhari Nezli, Mohand Oulhadj Mahmoudi and Mohame Tadjne. Robust dtc based on adaptive fuzzy control of double star synchronous machine drive with fixed switching frequency. *Journal of Electrical Engineering* **63**(3) (2012) 133–143.

[18] A. Moualdia, M. O. Mahmoudi and L. Nezli. *Direct Torque Control of the DFIG and Direct Power Control for Grid Side Converter in wind power generation system. *The Mediterranean Journal of Measurement and Control, MEDJMC* **9**(3) (2013) 101–108.

[19] A. Chalanga, S. Kamal and B. Moreno. *Implementation of super-twisting control: supertwisting and higher Order sliding-mode observer-based approaches. *IEEE Trans. on Industrial Electronics* **63** (6) (2016) 3677–3685.

Appendix

DSIM1 and DSIM2 Parameters

Parameters	DSIM1	DSIM2
Stator resistance	$R_{s1} = 9\Omega$	$R_{s2} = 9\Omega$
Rotor resistance	$R_{r1} = 8.37\Omega$	$R_{r2} = 8.37\Omega$
Stator inductance	$L_{s1} = 740mH$	$L_{s2} = 740mH$
Rotor inductance	$L_{r1} = 740mH$	$L_{r2} = 740mH$
Mutual inductance	$L_{m1} = 712mH$	$L_{m2} = 712mH$
Number of pole	$P_1 = 4$	$P_2 = 4$
Moment of inertia	$J_1 = 0.066Kg.m^2$	$J_2 = 0.066Kg.m^2$
Friction coefficient	$B_1 = 0.001N.m.s/rd$	$B_2 = 0.001N.m.s/rd$

Analysis of the Dynamics of a Two-Degree-of-Freedom Nonlinear Mechanical System under Harmonic Excitation

Akram Khalil Cheib [1,2], V. E. Puzyrov [2] and N. V. Savchenko [3*]

[1] *The International University of Beirut, Beirut, Lebanon*
[2] *Vasyl Stus Donetsk National University, Vinnytsia, Ukraine*
[3] *Zhukovsky National Aerospace University "KhAI", Kharkiv, Ukraine*

Abstract: In this paper the 2-degree-of-freedom mechanical system under the action of external harmonic excitation is considered. The system consists of the rotating elastically mounted frame and attached mass (absorber) with viscous friction and nonlinear stiffness. The stability problem of periodic regimes is investigated based on the averaging method. The influence of nonlinear component is analyzed with respect to responses of the main mass in the vicinity of resonance frequencies.

Keywords: *harmonic excitation; averaging technique; resonance frequency; stability; nonlinear stiffness.*

Mathematics Subject Classification (2010): 34C46, 34D20, 70E50, 70E55, 70K20.

1 Introduction

The problems associated with unwanted vibrations are encountered in many applied tasks in machine-building, construction, aerospace engineering, biomechanics, etc. For a number of reasons, a structure may encounter excitation sources that are not provided for in the design. To improve the reliability of the design, the engineers aim at a simple, low cost and efficient solution. In many cases, dynamic vibration absorbers (DVA) meet these requirements. Dynamic vibration absorbers or tuned mass dampers are small mass-spring-damper elements locally attached to the structure designed to dissipate excessive vibration energy.

---

* Corresponding author: mailto:nina_savchenko@hotmail.com

One of the important goals of the vibration control is to create a frequency zone free from resonance (or a spectral gap around an inconvenient frequency) by connecting a vibration absorber. As a rule, the DVA parameters are determined according to the eigenvector of the unstable vibration mode, which ensures the spatial distribution of the vibration energy within one vibration mode. However, this single-mode approach does not take into account the influence of adjacent oscillation modes which may become important under some circumstances.

In recent decades, the nonlinear absorbers have become widespread in the passive vibration control [1 – 10]. A key feature of such DVAs is the absence of a preferred frequency, that is, they can be functional at almost any frequency. This gives a great advantage over the linear absorbers. At the same time, the nonlinearity leads to the amplitude dependency, because a critical energy threshold exists, and an "inappropriate" nonlinear characteristic of the DVA generates the instability of the working regime.

In the present paper, we study the system which allows the rotation of the main mass in addition to the lateral motion. Such systems may be found in various applications in which a relative rotational motion is presented: rotor dynamics [11], a coupled pitch-roll ship model under harmonic excitation [12, 13], vibration control by rotating masses [14], rotor dampers in bridge structures [15], the use of the Helmholtz resonators for low frequencies in acoustics [16] and many others.

2   Statement of the Problem

Let us consider the following mechanical system: the frame of mass m_1 is mounted on the weightless platform as it is schematically shown in Fig. 1.
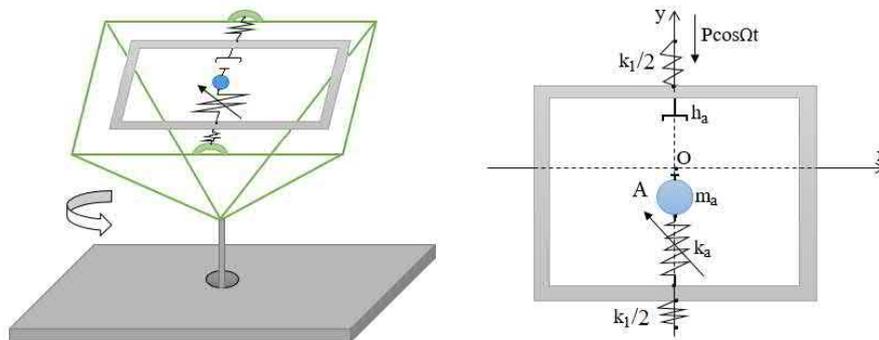
Figure 1: Elastically conjoint rotating frame with the DVA.

The platform is rotating with a constant angular velocity ω around the vertical axis. The frame is subjected to the harmonic excitation $F_e = P\cos\Omega t$. The absorber A is attached to the frame with the aim to prevent the possible resonance.

The motion equations of the mechanical system under consideration are

$$
\begin{aligned}
&(m_1 + m_a)\ddot{y}_1 + m_a\ddot{\tilde{y}} + [k_1 - (m_1 + m_a)\omega^2]y_1 - m_a\omega^2\tilde{y} = P\cos\Omega t, \\
&m_a\ddot{y}_1 + m_a\ddot{\tilde{y}} + h_a\dot{\tilde{y}} - m_a\omega^2 y_1 + (k_a - m_a\omega^2)\tilde{y} - k_3\tilde{y}^3 = 0.
\end{aligned}
\tag{1}
$$

The coordinate y represents the displacement of the main mass m_1 with respect to its frame, while $\tilde{y}$ stands for the relative displacement of the absorber mass m_a with respect

to the mass m_1. The stiffness of the main mass is denoted by k_1, and the restoring force of the absorber is expressed as $k_a\tilde{y} - k_3\tilde{y}^3$; h_a is the coefficient of viscous friction.

Introducing the dimensionless parameters and time by the formulas

$$\mu = \sqrt{\frac{m_a}{m_1}}, \ \kappa_1 = \frac{k_1 - (m_1 + m_a)\omega^2}{m_1\Omega^2}, \ \alpha = \frac{\omega^2}{\Omega^2}, \ p = \frac{P}{m_1\Omega^2}, \ h = \frac{h_a}{m_a\Omega},$$
$$\kappa_2 = \frac{k_a - m_a\omega^2}{m_a\Omega^2}, \ \kappa_3 = \frac{3m_1k_3}{4m_a^2\Omega^2}, \ \tau = \Omega t, \tag{2}$$

and replacing the variable $\tilde{y}$ with μy_1, we can rewrite the motion equations in the following form:

$$My'' + Dy' + Ky = F. \tag{3}$$

Here

$$y = \begin{pmatrix} y_1 \\ y_2 \end{pmatrix}, \ M = \begin{pmatrix} 1 + \mu^2 & \mu \\ \mu & 1 \end{pmatrix}, \ D = diag(0, h), \ K = \begin{pmatrix} \kappa_1 & -\mu\alpha \\ -\mu\alpha & \kappa_2 \end{pmatrix},$$

$$F = \begin{pmatrix} p\cos\tau \\ \frac{4}{3}\kappa_3 y_2^3 \end{pmatrix}$$

and prime means the derivative with respect to time τ.

Let us introduce the complex variables

$$z = \mathrm{col}(z_1, z_2), \ z_j = (y_j + \imath y_j')e^{\imath\tau}, \ j = 1, 2.$$

Taking into account that

$$y = Re(e^{-\imath\tau} z), \ y' = Im(e^{-\imath\tau} z), \ y'' = Im(e^{-\imath\tau} (z' - \imath z)),$$

equations (3) can be rewritten as follows:

$$MIm[e^{-\imath\tau}(z' - \imath z)] + DIm(e^{-\imath\tau}z) + KRe(e^{-\imath\tau}z) = F. \tag{4}$$

In addition to equation (4), the relation

$$Re[e^{-\imath\tau}(z' - \imath z)] - Im(e^{-\imath\tau}z) = 0 \tag{5}$$

holds (because of $y' = \frac{d}{d\tau}y$).

Multiplying both sides of equality (5) by M from the left-hand side and adding the equation (4) with the multiplier $\imath$, we get

$$e^{-\imath\tau}M(z' - \imath z) - (M - \imath D)Im(e^{-\imath\tau}z) + \imath KRe(e^{-\imath\tau}z) = \imath F.$$

Now we assume that z_1, z_2 are the slow functions in time τ. Applying the method of averaging [17], we get

$$2Mz' + (D + \imath C)z = \imath F_1, \ 2M\bar{z}' + (D - \imath C)\bar{z} = -\imath\overline{F}_1,$$
$$C = K - M = \begin{pmatrix} c_{11} & c_{12} \\ c_{12} & c_{22} \end{pmatrix}, \ F_1 = \begin{pmatrix} p \\ \kappa_3 z_2^2\bar{z}_2 \end{pmatrix}. \tag{6}$$

It should be noted that

$$\langle e^{\imath\tau}Im(e^{-\imath\tau}z)\rangle = -\frac{1}{2}\imath z, \ \langle e^{\imath\tau}Re(e^{-\imath\tau}z)\rangle = \frac{1}{2}z, \ \langle e^{\imath\tau}(Re(z)^3)\rangle = \frac{3}{8}z^2\bar{z},$$

where

$$\langle * \rangle \triangleq \frac{1}{2\pi} \int_0^{2\pi} (*) d\tau.$$

The conditions for periodic steady state vibration are determined by stationary points of the system (6), namely,

$$c_{11} z_1 + c_{12} z_2 = p, \ \ c_{12} z_1 + (c_{22} - \imath h) z_2 = \kappa_3 z_2^2 \bar{z}_2, \tag{7}$$

and their conjugate counterparts for $\bar{z}_1, \bar{z}_2$.

Depending on the value of c_{11}, we have two cases.

1) $c_{11} = 0$. This case may be interpreted as a resonant case for the system with "frozen" absorber, i.e., $\tilde{y} = 0, \dot{\tilde{y}} = 0$, and

$$\frac{k_1 - (m_1 + m_a)\omega^2}{m_1 + m_a} = \Omega^2. \tag{8}$$

Then, taking into account that $c_{12} = -\mu(1 + \omega^2/\Omega^2) \neq 0$, from equations (7) it is easy to get

$$z_{20} = \frac{p}{c_{12}}, \ \ z_{10} = \frac{p}{c_{12}^2}(-c_{22} + \imath h + \kappa_3 \frac{p^2}{c_{12}^2}). \tag{9}$$

Hence, the system (6) has a unique constant solution (9).

2) $c_{11} \neq 0$. Then expressing z_1 from the first equation (7) and substituting it into the second one, we get

$$c_{12} p + (\delta - \imath h c_{11}) z_2 = c_{11} \kappa_3 z_2^2 \bar{z}_2, \ \ \ c_{12} p + (\delta + \imath h c_{11}) \bar{z}_2 = c_{11} \kappa_3 z_2 \bar{z}_2^2, \tag{10}$$

where $\delta = \det C$. Subtracting the second equation (10) from the first one, we come to the relation

$$(\delta - c_{11} \kappa_3 z_{20} \bar{z}_{20})(z_{20} - \bar{z}_{20}) - \imath h c_{11}(z_{20} + \bar{z}_{20}) = 0. \tag{11}$$

Also we subtract the second equation (10) with the multiplier z_{20} from the first equation multiplied by $\bar{z}_{20}$. As a result, we have another auxiliary equation

$$p c_{12}(z_{20} - \bar{z}_{20}) + 2\imath h c_{11} z_{20} \bar{z}_{20} = 0. \tag{12}$$

Denoting the real and imaginary parts of z_{20} by u_0 and v_0, respectively, from (11) and (12) we get the following system:

$$[\delta - c_{11} \kappa_3(u_0^2 + v_0^2)]v_0 - h c_{11} u_0 = 0, \ \ \ p c_{12} v_0 + h c_{11}(u_0^2 + v_0^2) = 0, \tag{13}$$

which is equivalent[1] to the system (7). These last equations allow the variable u_0 to be expressed in terms of v_0 : $u_0 = v_0(h\delta + p c_{12} \kappa_3 v_0)/h^2 c_{11}$, which leads to the cubic equation

$$\Phi(v_\star) = v_\star^3 + 2\delta v_\star^2 + (\delta^2 + h^2 c_{11}^2)v_\star + p^2 c_{11} c_{12}^2 \kappa_3 = 0, \ v_\star = \frac{p}{h} c_{12} \kappa_3 v_0.$$

The number of the real roots of this equation is determined by the sign of discriminant of the polynomial $\Phi(v)$. Namely, the latter has three different real roots if the expression

$$D_\Phi = -c_{11}[27 c_{11}(p^2 c_{12}^2 \kappa_3)^2 - 4\delta(\delta^2 + 9h^2 c_{11}^2)p^2 c_{12}^2 \kappa_3 + 4h^2 c_{11}(h^2 + 2\delta^2)^2] \tag{14}$$

---

[1] With the proviso that $z_{20} \neq 0$. As $c_{12} \neq 0$, it is obvious that otherwise the equalities (7) are broken.

is positive, and it has one real root if D_Φ is negative. The expression (14) can be considered as a polynomial of the second order with respect to the parameter κ_3, hence, the necessary and sufficient condition for D_Φ to be positive is the following double inequality:

$$\frac{2}{27} \frac{\delta(\delta^2 + 9h^2 c_{11}^2) - (\delta^2 - 3h^2 c_{11}^2)^{3/2}}{p^2 c_{11} c_{12}^2} < \kappa_3 < \frac{2}{27} \frac{\delta(\delta^2 + 9h^2 c_{11}^2) + (\delta^2 - 3h^2 c_{11}^2)^{3/2}}{p^2 c_{11} c_{12}^2}. \tag{15}$$

Thus, the necessary condition for three real roots of $\Phi(v)$ is $d = \delta^2 - 3h^2 c_{11}^2 > 0$. This condition is not so simple, with respect to formulas (2) it turns to

$$m_1^2 m_a^2 (1+\alpha)^4 \Omega^8 - (1+\alpha)^2 \Omega^6 \{3(m_1 + m_a)^2 h_a^2 + 2m_1 m_a (1+\alpha)[m_a k_1 + (m_1 + m_a)k_a]\} +$$
$$+ (1+\alpha)\Omega^4 \{6k_1(m_1 + m_a)h_a^2 + (1+\alpha)[m_a^2 k_1^2 + 2m_a k_1 k_a(2m_1 + m_a) + k_a^2(m_1 + m_a)^2]\} -$$
$$- k_1 \Omega^2 \{k_1 h_a^2 + k_a(1+\alpha)[m_a k_1 + (m_1 + m_a)k_a]\} + k_1^2 k_a^2 > 0.$$

In the case when the upper limit for the frequency value Ω is unknown, the expression for d may be positive for any linear characteristics of the absorber (k_a, h_a). Then, for the appropriate values of κ_3, which characterizes the nonlinear component of absorber's stiffness, the polynomial $\Phi(v)$ has three real roots, and the system (7) has three stationary points.

Alternatively, if the upper limit for the excitation frequency is bounded from above, then with the condition $h > |\delta/\sqrt{3}c_{11}|$, the system (7) has the unique stationary point. The same result takes place in the vicinity of condition (8), because of $c_{11} \to 0$, $\delta \to -c_{12}^2$, and the right-hand side of double inequality (15) tends to $-\infty$, though $D_\Phi < 0$.

3 Stability Analysis

In order to determine the stability of a periodic solution related to averaged equations (6), the small perturbations of the solutions are introduced in a common way

$$z(\tau) = z_0 + \tilde{z}(\tau),$$

where z_0 is a solution of the system (7). Taking into account that

$$\frac{\partial F_1}{\partial z} = \kappa_3 \begin{pmatrix} 0 & 0 \\ 0 & 2z_2\bar{z}_2 \end{pmatrix}, \quad \frac{\partial F_1}{\partial \bar{z}} = \kappa_3 \begin{pmatrix} 0 & 0 \\ 0 & z_2^2 \end{pmatrix},$$

the $\lambda-$ matrix for linearized system (6) has the following form:

$$\begin{pmatrix} 2\lambda + \imath c_{11} & \imath c_{12} & 0 & 0 \\ \imath c_{12} & 2\lambda + h + \imath(c_{22} - \kappa_3 z_{20}\bar{z}_{20}) & 0 & -\imath\kappa_3 z_{20}^2 \\ 0 & 0 & 2\lambda - \imath c_{11} & -\imath c_{12} \\ 0 & \imath\kappa_3 \bar{z}_{20}^2 & -\imath c_{12} & 2\lambda + h - \imath(c_{22} - \kappa_3 z_{20}\bar{z}_{20}) \end{pmatrix}.$$

Accordingly, the characteristic polynomial is as follows:

$$f(\lambda) = a_4 \lambda^4 + a_3 \lambda^3 + a_2 \lambda^2 + a_1 \lambda + a_0,$$

where

$$a_4 = 16, \ a_3 = 16h(1+\mu^2), \ a_2 = 4\{c_{11}^2 + 2c_{12}^2 + c_{22}^2 - 4\mu c_{12}[c_{11} + c_{22}(1+\mu^2)] +$$
$$+ 2\mu^2(c_{11}c_{22} + c_{22}^2 + 2c_{12}^2) + \mu^4 c_{22}^2 + h^2(1+\mu^2)^2\} - 8a[\mu^2 c_{11} - 2\mu(1+\mu^2)c_{12} +$$
$$+ (1+\mu^2)^2 c_{22}] + 3(1+\mu^2)^2 a^2, a_1 = 4h[(c_{11} - \mu c_{12})^2 + c_{12}^2], \tag{16}$$
$$a_0 = \delta^2 + h^2 c_{11}^2 - 2c_{11}\delta\sigma + \frac{3}{4}c_{11}^2\sigma^2.$$

Here the relation $\sigma = \kappa_3 z_{20} \bar{z}_{20} = \kappa_3 (u_0^2 + v_0^2)$ is introduced. The solution under study is asymptotically stable if all roots of the polynomial $f(\lambda)$ have negative real parts. Such conditions, according to the Lienard–Chipart criterion [18], can be written in the form

$$
a_0 > 0, \ a_2 > 0, \ \Delta_3 = \begin{vmatrix} a_3 & a_1 & 0 \\ a_4 & a_2 & a_0 \\ 0 & a_3 & a_1 \end{vmatrix} > 0. \tag{17}
$$

Note the fact that in our case the condition $a_2 > 0$ is excessive. In fact, because of $h > 0$, $c_{12} \neq 0$, the coefficients a_1, a_3 are positive. But then, if $a_2 \leq 0$, we have $\Delta_3 = -[a_0 a_3^2 + a_4 a_1^2 + a_1 a_3(-a_2)] < 0$. Thus, the inequality $\Delta_3 > 0$ entails the positiveness of a_2.

The boundary cases $a_0 = 0$, $\Delta_3 = 0$ determine the bifurcation surfaces in parameters space. Namely:

A) $a_0 = 0$, $\Delta_3 > 0$. The polynomial $f(\lambda)$ has one zero root and three roots with negative real parts;

B) $a_0 > 0$, $\Delta_3 = 0$. There are two purely imaginary roots

$$
\lambda_{1.2} = \pm \imath \frac{1}{2} \sqrt{\frac{(c_{11} - \mu c_{12})^2 + c_{12}^2}{1 + \mu^2}}
$$

and two roots with negative real parts;

C) $a_0 = 0$, $\Delta_3 = 0$. The polynomial $f(\lambda)$ has one zero root, a pair of purely imaginary roots $\lambda_{1,2}$ and one negative real root.

In Fig. 2 the typical form of bifurcation surface $\Delta_3 = 0$ related to the parameters κ_2, σ, h is presented. After substituting the expressions from (16), we have
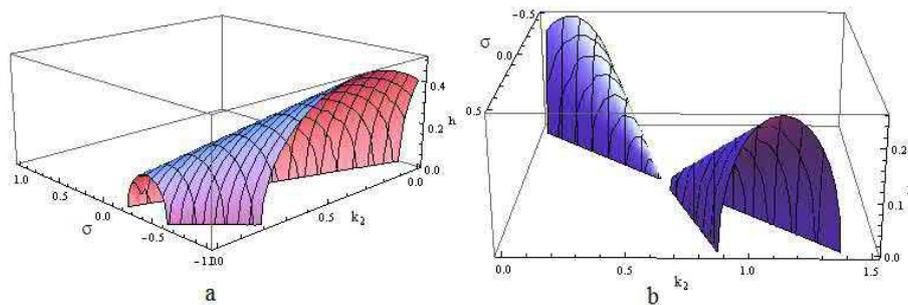
Figure 2: The typical form of bifurcation surface $\delta_3 = 0$. Cases a and b are related to the values of $\kappa_1 = 0.5$ and $\kappa_1 = 1.2$, respectively.

$$
\Delta_3 = 64h^2[c_{11}\mu - c_{12}(1 + \mu^2)]^2 \{3\sigma^2(1 + \mu^2)^2 - 8\sigma(1 + \mu^2)[c_{11} - 2\mu c_{12} + c_{22}(1 + \mu^2)] +
$$
$$
+ 4h^2(1 + \mu^2 + \mu^4 c_{11}^2) + 4[c_{11} - 2\mu c_{12} + c_{22}(1 + \mu^2)]^2\}.
$$

The expression in square brackets can be rewritten as

$$
c_{11}\mu - c_{12}(1 + \mu^2) = \mu(\kappa_1 - 1 - \mu^2) + \mu(1 + \alpha)(1 + \mu^2) = \mu[\kappa_1 + \alpha(1 + \mu^2)].
$$

Due to the assumption $\kappa_1 > 0$, it is positive, therefore the sign of Δ_3 is determined by the sign of the expression in brackets. The latter can be presented in the form

$$\{*\} = 4h^2(1 + \mu^2 + \mu^4 c_{11}^2) + (3O_1 - 2Q_2)(Q_1 - 2Q_2), \ Q_1 = \sigma(1 + \mu^2),$$
$$Q_2 = c_{11} - 2\mu c_{12} + c_{22}(1 + \mu^2).$$

For the linear absorber we have $\kappa_3 = 0$, hence $\sigma = 0$, and $\{*\} > 0$ (as well as $a_2 > 0$, $a_0 > 0$). Then, if the parameter κ_3 is rather small[2], the inequalities (17) are still valid.

4 Numerical Simulations and Discussion

Although it is possible to determine the type of the stationary points of the system in explicit form relatively to the set of parameters $\{m_1, k_1, m_a, k_a, \omega, h, P, \Omega\}$, it is reasonable not to do this. Firstly, due to relations (12), (13) the explicit representation of the expression for σ is too cumbersome and not convenient for analysis. Another reason is that for the purposes of engineering applications, it is much more suitable to use the procedure oriented towards numerical calculations, which allow to do some significant simplifications (for instance, introduce one or several small parameters [3]).

The calculations were carried out as follows: for some given values of μ, α and κ_1, the magnitudes of κ_2 and h were determined as for the linear DVA according to [19, 20]. Then the values found (say, κ_{20}, h_0) were changed, and the responses of the main mass were analyzed. Thereafter, the influence of the nonlinear stiffness k_3 was investigated. The results are presented in Figs. 3-6. The parameter p may be counted as optional, because with the transformation

$$y = py_\star, \quad \tilde{y} = p\tilde{y}_\star, \quad k_3 = \frac{k_{3\star}}{p^2}$$

one can add the subscript "$\star$" to the variables, their derivatives and parameter k_3, and take $p = 1$. The magnitude of P/Ω^2 may be small enough, hence the initial conditions for integrating the motion equations (1) were taken correspondingly. For the reason of simplicity, the subscript "$\star$" is omitted in the figures.

In Fig. 3 the evolution of oscillations of the main mass is presented. For $\mu = 0.2$, $\alpha = 0.1, k_1 = 1.25$ and the fixed value of $k_2 = k_{20} \approx 1.17$, the magnitude of h_a was changed. Based on the obtained calculations, we can conclude the following.

1) If the coefficient h is small ($h < 0.05$ in our example), the amplitude of oscillations is increasing slowly. Although in linear case the motion is asymptotically stable in the Lyapunov sense, in the vicinity of resonant frequencies small denominators in the general solution of system (1) (with $k_3 = 0$) appear, and the damping rate cannot "counteract" successfully to the growth of the amplitude. This growth is not unbounded, but it is big enough (Fig.3a), so such absorber is ineffective.

2) The optimal magnitude of damping coefficient belongs to some "middle" range ($h \in [0.08, 0.12]$). The behaviour of solutions is characterized as follows. After the initial perturbations, there exists a transitional time interval (about $100 - 120$ τ- seconds, see Fig.3) where the amplitude achieves its maximal value, and varying the parameters of

---

[2] Or p is small, which leads to the smallness of v_0, u_0 due to formulas (12), (13).
[3] Depending on the circumstances, it may be $\mu, p, 1 - \frac{k_1}{m_1\Omega^2}, h$ and so on.
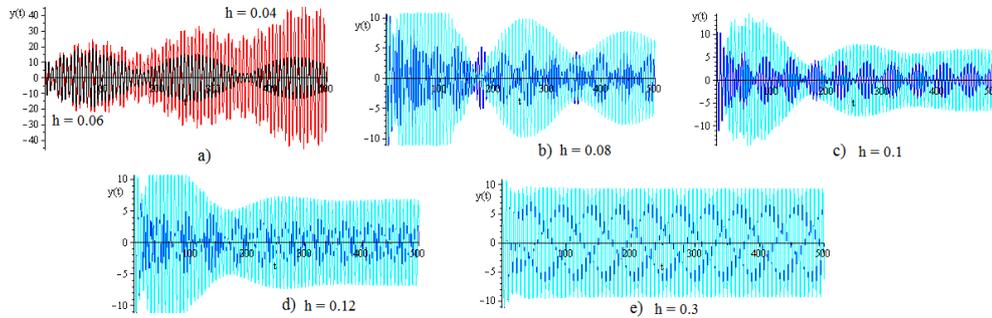
Figure 3: The shape of the oscillations of the main mass depending on the damping coefficient h. The light lines (cyan) correspond to the value $k_3 = 0$, the dark ones (blue) – to the value $k_3 = 0.0002$.

DVA has little effect on reducing this value. However, after this period, we can distinguish two cases:

A) On the left side of this interval the amplitude of oscillations goes down slowly, but finally, the smallest rate of the main mass responses is achieved (Fig. 3b, c).

B) Increasing the value of h over 0.1 leads to more fast mitigation of the oscillation amplitude, but the rate of the main mass responses grows up (Fig. 3d).

3) Finally, with further increase of the parameter h, the shape of the oscillations changes (Fig.3e). In contradiction to the previous cases, this shape becomes of the "stripe" type - like for a simple harmonic oscillation – for both cases $k_3 = 0$ and $k_3 = 0.0002$ (increasing the value of k_3 over 0.0008 leads to instability). The amplitude of oscillations is big enough, and such values of the damping coefficient, as well as too small values in case 1), are unsuitable for mitigation of the responses of the system.

These results were compared with the integration of averaged equations transformed by the substitution $u_j = pr_j cos\varphi_j, v_j = pr_j sin\varphi_j \ (j = 1, 2)$. These equations are

$$2r'_1 - r_2[\mu h cos(\varphi_2 - \varphi_1) + (\tilde{c}_{12} + \mu\kappa_{3\star}r_2^2)sin(\varphi_2 - \varphi_1)] = sin\varphi_1,$$

$$2r_1\varphi'_1 + \tilde{c}_{11}r_1 + r_2[-\mu h sin(\varphi_2 - \varphi_1) + (\tilde{c}_{12} + \mu\kappa_{3\star}r_2^2)cos(\varphi_2 - \varphi_1)] = cos\varphi_1,$$

$$2r'_2 + \tilde{c}_{21}r_1 sin(\varphi_2 - \varphi_1) + h(1 + \mu^2)r_2 = -\mu sin\varphi_2,$$

$$2r_2\varphi'_2 + r_2[\tilde{c}_{22} - \kappa_{3\star}(1 + \mu^2)r_2^2] + \tilde{c}_{21}r_1 cos(\varphi_2 - \varphi_1) = -\mu cos\varphi_2.$$

Here $\tilde{c}_{jk}$ are the elements of the matrix $M^{-1}C$.

The time histories for $r_1(t)$ are presented in Fig. 4.

Also, the influence of the coefficient κ_3 (which relates to nonlinear stiffness) was tested. The results are presented in Fig. 5 for given values $\mu = 0.2, \kappa_1 = 0.95, \kappa_2 = 0.97,$ $\alpha = 0.1, h = 0.25$. Both cases $\kappa_3 > 0$ (softening spring) and $\kappa_3 < 0$ (hardening spring) were considered. The hardening spring (line 1 in Fig. 5) gives the worst result, while the softening spring with $\kappa_3 \approx 0.006$ (line 4) gives the best response. The further increasing of κ_3 (line 5) worsens the state.

Finally, in Fig.6 the mutual influence of the linear and nonlinear characteristics of the restoring force on the responses of the main mass is presented.
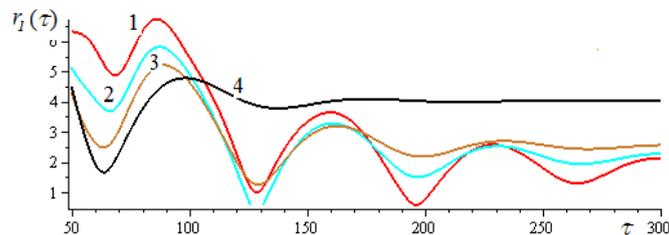
Figure 4: Time history for $r_1(\tau)$. Lines 1 - 4 are related to the values of $h = 0.08, 0.1, 0.12$ and 0.15, respectively.
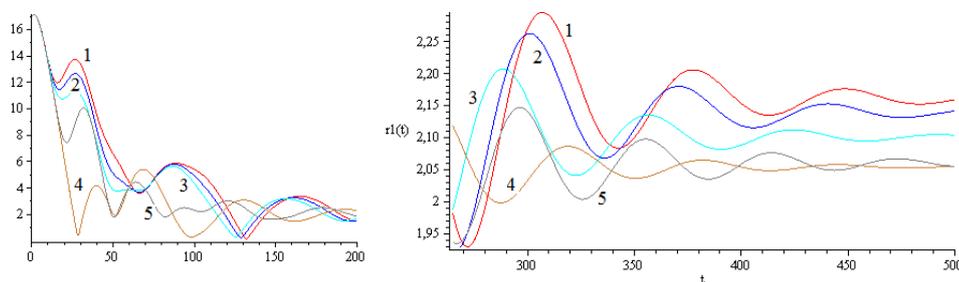
Figure 5: Influence of the nonlinear stiffness on the responses of the main mass. The values of κ_3 for lines $1 - 5$, respectively, are $-0.002, 0.0, 0.002, 0.006, 0.008$.
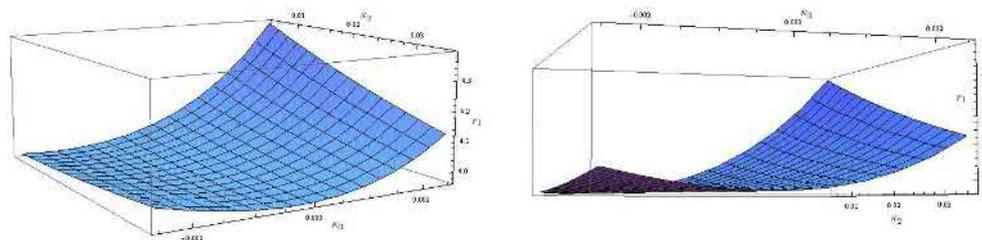
Figure 6: Influence of the absorber's stiffnesses on the responses of the main mass.

5   Conclusion

In this paper we have studied the dynamics of a 2-DOF mechanical system with combined translational and rotational motions under external harmonic excitation. The influence of the dynamical absorber with nonlinear stiffness on the responses of the main mass was investigated. The analytical approach based on the averaging method was used. The stability conditions for periodic solutions are obtained and analyzed. The numerical calculations have shown that the averaged equations correlate well with the motion equations. A suitable choice of the absorber's parameters (linear and nonlinear stiffness, and the damping coefficient) in the vicinity of resonant frequencies was discussed. In particular, it was shown that the nonlinear spring of the absorber may improve essentially the responses of the main mass (counteract to the growth of the amplitude) caused by the external excitation.

References

[1] O. Gendelman, L. Manevitch, A. Vakakis and R. M'Closkey. Energy pumping in nonlinear mechanical oscillators. *Journal of Applied Mechanics* **68** (2001) 34–41.

[2] A. Vakakis and R. Rand. Non-linear dynamics of a system of coupled oscillators with essential stiffness non-linearities. *International Journal of Non-Linear Mechanics* **39** (2004) 1079–1091.

[3] S. J. Zhu, Y. F. Zheng and Y. M. Fu. Analysis of non-linear dynamics of a two-degree-of-freedom vibration system with non-linear damping and non-linear spring. *Journal of Sound and Vibration* **271** (2004) 15–24.

[4] O. Gendelman, Y. Starosvetsky and M. Feldman. Attractors of harmonically forced linear oscillator with attached nonlinear energy sink I: Description of response regimes. *Nonlinear Dynamics* **51** (2008) 31–46.

[5] R. A. Ibrahim. Recent advances in nonlinear passive vibration isolators. *Journal of Sound and Vibration* **314** (2008) 371–452.

[6] L. Kela and P. Vhoja. Recent Studies of Adaptive Tuned Vibration Absorbers/Neutralizers. *Applied Mechanics Reviews* **62** (6) (2009) 060801–060810.

[7] J. C. Ji and N. Zhang. Suppression of the primary resonance vibrations of a forced nonlinear system using a dynamic vibration absorber. *Journal of Sound and Vibration* **329** (2010) 2044–2056.

[8] H. El-Ghareeb Taha, S. Hamed Yaser and S. Abd Elkader Mohamed. Non-Linear Analysis of Vibrations of Non-Linear System Subjected to Multi-Excitation Forces via a Non-Linear Absorber. *Applied Mathematics* **3** (2012) 64–72.

[9] M. Makkar and J.-Y. Dieulot. Passivity Based Control of Continuous Bioreactors. *Nonlinear Dynamics and Systems Theory* **17** (4) (2017) 357–368.

[10] G. I. Melnikov, N. A. Dudarenko, K. S. Malykh, L. N. Ivanova and V. G. Melnikov. Mathematical Models of Nonlinear Oscillations of Mechanical Systems with Several Degrees of Freedom. *Nonlinear Dynamics and Systems Theory* **17** (4) (2017) 369–375.

[11] M. Guskov, J.-J. Sinou and F. Thouverez. Multi-dimensional harmonic balance applied to rotor dynamics. *Mechanics Research Communications* **35** (2008) 537–545.

[12] R. Pan and H. G. Davies. Responses of a non-linearly coupled pitch-roll ship model under harmonic excitation. *Nonlinear Dynamics* **9** (4) (1996) 349–368.

[13] M. Sayed and Y. S. Hamed. Stability and response of a nonlinear coupled pitch-roll ship model under parametric and harmonic excitations. *Nonlinear Dynamics* **64** (3) (2011) 207–220.

[14] R. Baumer and U. Starossek. Active vibration control using centrifugal forces created by eccentrically rotating masses. *J. Vib. Acoust. ASME* **138** (4) (2016) 1–14.

[15] Y. Zhang, L. Li and X. Zhang. Switch Control of Twin Rotor Damper for Bridge Vibration Mitigation under Different Excitations. *X International Conference on Structural Dynamics EURODYN 2017, Procedia Engineering* **199** (2017) 1707–1712.

[16] S. Bellizzi, R. Cote and M. Pachebat. Responses of a two degree-of-freedom system coupled to a nonlinear damper under multi-forcing frequencies. *Journal of Sound and Vibration, Elsevier* **332** (7) (2013) 1639–1653.

[17] Yu. A. Mitropolskii. *Method of Averaging in the Investigations of Resonance Systems.* Moscow: Nauka, 1992. [Russian]

[18] A. Lienard and M. H. Chipart. Sur le signe de la partie reelle des racines d'une equation algebrique. *J. Math. Pures Appl.* **10** (6) (1914) 291–346.

[19] C. P. Den Hartog. *Mechanical Vibrations*. New York: McGraw-Hill, 1956.

[20] A. Thompson. Optimum tuning and damping of a dynamic vibration absorber applied to a force excited and damped primary system. *Journal of Sound and Vibration* **77** (1981) 403–415.

Numerical Approximation of the Exact Control for the Vibrating Rod with Improvement of the Final Error by Particle Swarm Optimization

A. Khernane *

Department of Computing, Faculty of Mathematics and Computing, University of Batna 2, Fesdis, Batna 05078, Algeria

Abstract: The paper studies the numerical approximation of the exact boundary controllability for the vibrating rod by the Hilbert uniqueness method (HUM). This study is based on the knowledge of the asymptotic behavior of the control governing the system at time T. This is the idea developed in this work concerning the Dirichlet boundary case. More precisely, an approximate control shall be found which returns the system under consideration to rest at time T with an estimation of the final state error and the improvement of it by using the particle swarm optimization algorithm (PSO).

Keywords: *exact controllability; vibrating rod; Hilbert uniqueness method; asymptotic behavior; Dirichlet control; particle swarm optimization.*

Mathematics Subject Classification (2010): 93B05, 74K10, 65K10, 65N25, 65M06, 78M32.

1 Introduction

Controllability is a classical problem in control theory. The idea that motivated this work is that control theory is certainly, at present, one of the most interdisciplinary areas of research. It is nowadays a rich crossing point of engineering and mathematics. Many problems of control theory such as optimal control and stabilizability may be solved under assumption that the system is controllable, see [9, 16, 19]. Controllability means that it is possible to drive a dynamic system from an arbitrary initial state to an arbitrary

---

* Corresponding author: mailto:abdelaziz.khernane@gmail.com

final state using the set of admissible controls. There are two basic concepts of controllability in the case of infinite dimensional systems: approximate and exact controllability. Approximate controllability allows to drive the dynamic system to arbitrary small neighbourhood of final state while exact controllability means that the dynamic system can be driven to arbitrary final state.
In the case of finite dimensional systems, these concepts are equivalent, see [18].

Approximate controllability has been studied for different types of semilinear dynamical systems, see, for example, [1, 14] and the references therein.

Regarding the problem of exact controllability of linear systems, great efforts have been devoted to its study both theoretically and numerically.

The theory of solving this problem has been introduced in [17] by the use of the semigroup approach. In [15], a new approach called the Hilbert uniqueness method (HUM) has been proposed to solve this problem for hyperbolic systems. Another approach has been proposed to solve this problem for parabolic systems, see, for instance, [2].

Numerically, the problem has been studied in [6, 10–12] through the numerical implementation of the Hilbert uniqueness method.

This method leads to the resolution of the equation

$$\Lambda\{\psi^0, \psi^1\} = \{u^1, -u^0\}, \tag{1}$$

where u^0 and u^1 are the initial conditions of the system and Λ is an isomorphism between the Hilbert space F and its dual F'.

The conjugate gradient method was introduced in [6], later on this method was developed in [10] in order to solve (1). The approximate solutions obtained do not converge to the exact solutions as the temporal and spatial grid sizes tend to zero. Methods of regularization including the Tikhonov regularization that result in convergent approximations were introduced in the papers on HUM-based methods. This method shows that this technique improves the last results.

In [11, 12], an alternative to the Tikhonov regularization procedure based on spectral analysis is presented. It was shown that this approach improves the method described in [6, 10].

Another computational method for boundary controllability of the wave equation is the one based on the method proposed in [13]. This approach permits to directly solve an optimization problem in which the equations of the linear system act as equality constraints. To resolve this problem, two methods are proposed. The first one is based on the Lagrange multiplier method. The second one transforms the constrained optimization problem to an unconstrained optimization problem and uses the conjugate gradient method for its resolution. The computational results show that this method provides convergent approximations for problems in which existing methods produce divergent approximations unless they are regularized in some manner. Therefore, this method improves the results found in [6].

The numerical methods cited studied the exact controllabilty of hyperbolic systems. For parabolic systems, see [4].

Motivated by the existence in the literature of these numerical studies, we want to feed it by the numerical study of a system which is neither hyperbolic nor parabolic. More precisely, we study numerically the exact Dirichlet boundary controllability of the vibrating rod.

This study goes through the numerical resolution of equation (1), which determines explicit formulas for ψ^0 and ψ^1 and therefore, the approximate control that steers the

system under consideration to rest time T with an estimation of the final state error.

By a particular example, we present the graphics of the approximate control, the cost function, and the final state error when the points are equidistant and improve it by using a stochastic optimization algorithm named the particle swarm optimization (PSO).

The remaining of the paper is organized as follows.
Section 2 defines the exact Dirichlet boundary controllability of the vibrating rod. Section 3 describes the HUM approach. In Section 4, we present the method of solving the problem under consideration. In Section 5, we give explicit formulas. In Section 6, experimental results are presented. In Section 7, a stochastic optimization algorithm is used to improve the final error. The results obtained confirm it. Section 8 concludes the paper.

2 The Problem under Study

Let T be a given positive number, $u^0(x)$ and $u^1(x)$ denote given functions defined on $\Omega =]0, L[$. Let $\Sigma = \{0, L\} \times]0, T[$, $Q =]0, L[\times]0, T[$ and $(u^0, u^1) \in L^2(\Omega) \times H^{-2}(\Omega)$. The exact Dirichlet boundary controllability problem for the vibrating rod is as follows. Find a control function g defined on Σ such that u satisfies the system

$$
\begin{cases}
u_{tt} + u_{xxxx} = 0 & \text{in } Q, \\
u(x,0) = u^0(x), \ \dfrac{\partial u}{\partial t}(x,0) = u^1(x) & \text{in } \Omega, \\
u(x,T) = 0, \ \dfrac{\partial u}{\partial t}(x,T) = 0 & \text{in } \Omega, \\
u(0,t) = 0, \ u(L,t) = 0, & t \in [0,T], \\
\dfrac{\partial u}{\partial x}(0,t) = 0, \ \dfrac{\partial u}{\partial x}(L,t) = g(t), & t \in [0,T].
\end{cases}
\tag{2}
$$

The first equation in (2) represents the vibrations of the rod. It models the vertical motion of a thin, horizontal rod with small displacements from the rest position. It is neither hyperbolic nor parabolic. $u(x,t)$ denotes the displacement of the point x of the rod, at the instant t. $u^0(x)$ and $u^1(x)$ represent, respectively, the initial position and the initial velocity of the rod. The third equation in (2) is the final condition and is called the equilibrium condition. It is well known that when $T > 0$, the exact controllability problem (2) admits at least one state-control solution pair (u,g); furthermore, the exact controller g having minimum boundary L^2 norm is unique, see [15, 20].

Our work consists in solving numerically the exact boundary controllability of the vibrating rod when the control is of the Dirichlet type. For this purpose, we consider the control given by the HUM approach and we develop some techniques which allow computation of the control that steers the system at hand to rest at time T with a final error

$$
\|\xi\|^2 = \|u(x,T)\|_{L^2(\Omega)}^2 + \left\| \frac{\partial u(x,T)}{\partial t} \right\|_{L^2(\Omega)}^2 .
\tag{3}
$$

3 Choice of the Control

We recall briefly how the control which steers the system (2) to rest at time T is found. Let $F = H_0^2(\Omega) \times L^2(\Omega)$ and $F' = H^{-2}(\Omega) \times L^2(\Omega)$. For any $\{\psi^0, \psi^1\} \in F$, solve the

system

$$\begin{cases} \psi_{tt} + \psi_{xxxx} = 0 & \text{in } Q, \\ \psi(x,0) = \psi^0(x), \quad \dfrac{\partial \psi}{\partial t}(x,0) = \psi^1(x) & \text{in } \Omega, \\ \psi = \dfrac{\partial \psi}{\partial x} = 0 & \text{on } \Sigma, \end{cases}$$

and then resolve the reverse system in Θ:

$$\begin{cases} \Theta_{tt} + \Theta_{xxxx} = 0 & \text{in } Q, \\ \Theta(x,T) = \dfrac{\partial \Theta}{\partial t}(x,T) = 0 & \text{in } \Omega, \\ \Theta = \dfrac{\partial^2 \psi}{\partial x^2} & \text{on } \Sigma. \end{cases}$$

This enables us to (implicitly) define a linear operator Λ by

$$\Lambda\{\psi^0, \psi^1\} = \{\frac{\partial \Theta}{\partial t}(x,0), -\Theta(x,0)\}.$$

So, for convenient ψ^0, ψ^1 and T, if one can solve the equation (1), then it is possible to obtain the control g explicitly.

We obtain the corresponding unique minimum L^2-norm control by setting $g = \frac{\partial^2 \psi}{\partial x^2}$. It is proved in [15] that λ is an isomorphism from F to F'. Consequently, for any initial data u^0, u^1, such that $\{u^1, -u^0\} \in F'$, equation (1) has a unique solution $\{\psi^0, \psi^1\} \in F$. The Θ system is, in fact, the u one (reverse) and the state $\{0,0\}$ is reached at time T. See [15] for more details.

4   Presentation of the Resolution Method

In this section, we will show how to solve equation (1) and give expressions for ψ^0 and ψ^1 which can be used for numerical simulations.
Using the techniques of standard optimization, we know that solving (1) is equivalent to solving the minimization problem

$$\underset{\{\psi^0, \psi^1\} \in F}{Inf} J\left(\{\psi^0, \psi^1\}\right), \tag{4}$$

where

$$J(\{\psi^0, \psi^1\}) = \frac{1}{2} \int_0^T \left[\frac{\partial^2 \psi(L,t)}{\partial x^2}\right]^2 dt - \int_\Omega \left[\psi^0 u^1 - \psi^1 u^0\right] dx. \tag{5}$$

In the problems of controllability, the knowledge of the asymptotic behavior of the control governing the system at time T may be used for its calculation. This idea will be used to determine explicit formulas for ψ^0 and ψ^1.

Let $\{\psi_T^0, \psi_T^1\}$ be the solution of (4). We introduce a T factor to transform the functional (5) in the following way:

$$T.J(\{\psi^0, \psi^1\}) = \frac{T}{2} \int_0^T \left[\frac{\partial^2 \psi(L,t)}{\partial x^2}\right]^2 dt - \int_\Omega \left[u^1 T \psi^0 - u^0 T \psi^1\right] dx.$$

Let $\phi = T.\psi$, where ϕ is the solution of the system

$$\begin{cases} \dfrac{\partial^2 \phi}{\partial t^2} + \dfrac{\partial^4 \phi}{\partial x^4} = 0 & \text{in } Q, \\[2mm] \phi(x,0) = \phi^0, \quad \dfrac{\partial \phi}{\partial t}(x,0) = \phi^1 & \text{in } \Omega, \\[2mm] \phi = \dfrac{\partial \phi}{\partial x} = 0 & \text{on } \Sigma. \end{cases}$$

$$T.J(\{\psi^0, \psi^1\}) = \frac{1}{2T} \int_0^T \left[\frac{\partial^2 \phi(L,t)}{\partial x^2}\right]^2 dt - \int_\Omega \left[u^1 \phi^0 - u^0 \phi^1\right] dx = J\left(\{\phi^0, \phi^1\}\right). \qquad (6)$$

The problem (4) becomes

$$Inf \ J\left(\{\phi^0, \phi^1\}\right). \qquad (7)$$

Assume the solution of (7) is $\{\phi_T^0, \phi_T^1\}$, then we have $\phi_T^0 = T.\psi_T^0$ and $\phi_T^1 = T.\psi_T^1$. Consider

$$\phi^0 = \lim_{T \to +\infty} \phi_T^0, \quad \phi^1 = \lim_{T \to +\infty} \phi_T^1,$$

then, according to [3], it is possible to determine explicitly (ϕ^0, ϕ^1). Numerical approximations useful for calculations are determined by this approach. Then, it will be possible to calculate ψ_T^0 and ψ_T^1 by using

$$\psi_T^0 = \frac{1}{T} \phi^0, \quad \psi_T^1 = \frac{1}{T} \phi^1.$$

5 Resolution of the Problem

Denote the orthonormal eigenfunctions by $\omega_j(x)$ and the eigenvalues by λ_j^2 of $\frac{d^4}{dx^4}$ with the homogeneous Dirichlet condition. Consider (6) and look for $\lim\limits_{T \to +\infty} J\left(\{\phi^0, \phi^1\}\right)$.

Let

$$u^0 = \sum_{j=1}^\infty u_j^0 \omega_j \ , \ u^1 = \sum_{j=1}^\infty u_j^1 \omega_j$$

with $u_j^0 = (u^0, \omega_j)$ and $u_j^1 = (u^1, \omega_j)$. Then

$$\int_\Omega u^0 \phi^1 dx = \sum_j (u^0, \omega_j)(\phi^1, \omega_j), \quad \int_\Omega u^1 \phi^0 dx = \sum_j (u^1, \omega_j)(\phi^0, \omega_j).$$

We have, in the same way,

$$\phi(x,t) = \sum_j \phi_j(t) \omega_j(x),$$

where

$$\phi_j(t) = (\phi^0, \omega_j) cos(\lambda_j t) + \frac{1}{\lambda_j}(\phi^1, \omega_j) sin(\lambda_j t).$$

Thus

$$\begin{aligned} \frac{1}{2T} \int_0^T \left[\frac{\partial^2 \phi(L,t)}{\partial x^2}\right]^2 dt &= \frac{1}{2T} \int_0^T \left[\sum_{j,l} \phi_j(t).\phi_l(t) \frac{d^2 \omega_j(L)}{dx^2}.\frac{d^2 \omega_l(L)}{dx^2}\right] dt \\[2mm] &= \frac{1}{2} \sum_{j,l} \frac{d^2 \omega_j(L)}{dx^2}.\frac{d^2 \omega_l(L)}{dx^2} \left[\frac{1}{T} \int_0^T \phi_j(t).\phi_l(t) dt\right]. \end{aligned}$$

By developing, we obtain

$$\frac{1}{T}\int_0^T \phi_j(t).\phi_l(t)dt$$

$$= \frac{1}{T}\int_0^T \left\{(\phi^0,\omega_j)cos(\lambda_j t) + (\phi^1,\omega_j)\frac{sin(\lambda_j t)}{\lambda_j}\right\}\left\{(\phi^0,\omega_l)cos(\lambda_l t) + (\phi^1,\omega_l)\frac{sin(\lambda_l t)}{\lambda_l}\right\}dt$$

$$= \frac{1}{T}\int_0^T \left[(\phi^0,\omega_j)(\phi^0,\omega_l)cos(\lambda_j t)cos(\lambda_l t)\right]dt + \frac{1}{T}\int_0^T \left[(\phi^0,\omega_j)(\phi^1,\omega_l)cos(\lambda_j t)\frac{sin(\lambda_l t)}{\lambda_l}\right]dt$$

$$+ \frac{1}{T}\int_0^T \left[(\phi^1,\omega_j)(\phi^0,\omega_l)cos(\lambda_l t)\frac{sin(\lambda_j t)}{\lambda_j}\right]dt + \frac{1}{T}\int_0^T \left[(\phi^1,\omega_j)(\phi^1,\omega_l)\frac{sin(\lambda_j t).sin(\lambda_l t)}{\lambda_j.\lambda_l}\right]dt$$

For $j \neq l$, the calculation gives

$$\frac{1}{T}\int_0^T \phi_j(t).\phi_l(t)dt \longrightarrow 0 \; as \; T \longrightarrow \infty.$$

and for $j = l$, we have

$$\frac{1}{T}\int_0^T \phi_j(t).\phi_l(t)dt \longrightarrow \left[\frac{1}{2}(\phi^0,\omega_j)^2 + \frac{1}{2\lambda_j^2}(\phi^1,\omega_j)^2\right] as \; T \longrightarrow \infty.$$

Finally,

$$\frac{1}{T}\int_0^T \phi_j(t).\phi_l(t)dt \longrightarrow \delta_j l \left[\frac{1}{2}(\phi^0,\omega_j)^2 + \frac{1}{2\lambda_j^2}(\phi^1,\omega_j)^2\right] as \; T \longrightarrow \infty,$$

where $\delta_j l = 1 \; if \; j = l$ and $\delta_j l = 0 \; if \; j \neq l$, and then

$$\frac{1}{2T}\int_0^T \left[\frac{\partial^2\phi(L,t)}{\partial x^2}\right]^2 dt \longrightarrow \frac{1}{4}\sum_j \left[(\phi^0,\omega_j)^2 + \frac{1}{\lambda_j^2}(\phi^1,\omega_j)^2\right]\left[\frac{d^2\omega_j(L)}{dx^2}\right]^2.$$

The initial problem (7) is transformed to the minimization problem according to ϕ^0 and ϕ^1

$$\frac{1}{4}\sum_j \left[(\phi^0,\omega_j)^2 + \frac{1}{\lambda_j^2}(\phi^1,\omega_j)^2\right]\left[\frac{d^2\omega_j(L)}{dx^2}\right]^2 - \int_\Omega (u^1\phi^0 - u^0\phi^1)dx$$

$$= \sum_j \left[\frac{1}{4}(\phi^0,\omega_j)^2\left[\frac{d^2\omega_j(L)}{dx^2}\right]^2 - u_j^1(\phi^0,\omega_j)\right]$$

$$+ \sum_j \left[\frac{1}{4\lambda_j^2}(\phi^1,\omega_j)^2\left[\frac{d^2\omega_j(L)}{dx^2}\right]^2 + u_j^0(\phi^1,\omega_j)\right] \tag{8}$$

We see that in this equality, the first term does not depend on ϕ^1 and the second does not depend on ϕ^0. Therefore, the minimization of (8) conducts to the minimization of

$$\frac{1}{4}(\phi^0,\omega_j)^2\left[\frac{d^2\omega_j(L)}{dx^2}\right]^2 - u_j^1(\phi^0,\omega_j) \;\; according \; to \;\; \phi^0$$

and

$$\frac{1}{4\lambda_j^2}(\phi^1, \omega_j)^2 \left[\frac{d^2\omega_j(L)}{dx^2}\right]^2 + u_j^0(\phi^1, \omega_j) \ \ according \ to \ \ \phi^1.$$

The minimum is determined by

$$\frac{1}{2}(\phi^0, \omega_j)\left[\frac{d^2\omega_j(L)}{dx^2}\right]^2 - u_j^1 = 0,$$

$$\frac{1}{2\lambda_j^2}(\phi^1, \omega_j)\left[\frac{d^2\omega_j(L)}{dx^2}\right]^2 + u_j^0 = 0.$$

Finally, when $T \longrightarrow \infty$, we obtain

$$\phi^0 = \sum_{j=1}^{\infty} \frac{2.(u^1, \omega_j).\omega_j}{\left[\frac{d^2\omega_j(L)}{dx^2}\right]^2},$$

$$\phi^1 = -\sum_{j=1}^{\infty} \frac{2\lambda_j^2(u^0, \omega_j).\omega_j}{\left[\frac{d^2\omega_j(L)}{dx^2}\right]^2}.$$

We conclude the following approximations:

$$\psi_T^0 = \frac{2}{T}\sum_{j=1}^{n} \frac{(u^1, \omega_j).\omega_j}{\left[\frac{d^2\omega_j(L)}{dx^2}\right]^2}, \tag{9}$$

$$\psi_T^1 = \frac{-2}{T}\sum_{j=1}^{n} \frac{\lambda_j^2(u^0, \omega_j).\omega_j}{\left[\frac{d^2\omega_j(L)}{dx^2}\right]^2}. \tag{10}$$

are explicit formulas.

6 Computational Results

In this section, we determine the graphs of the approximate control, the cost function and the final error (3) at the instant $t = T$ and the initial data
$u^0(x) = Ax(1 + x); \ u^1(x) = (1 + A)u^0(x)$. A is a coefficient chosen by numerical considerations. The control steering the system (2) to rest at time T is given by $g* = \frac{\partial^2 \psi}{\partial x^2}$, where ψ is the solution of the system

$$\begin{cases} \dfrac{\partial^2\psi(x,t)}{\partial t^2} + \dfrac{\partial^4\psi(x,t)}{\partial x^4} = 0 & \text{in Q ,} \\ \psi(x,0) = \psi_T^0, \quad \dfrac{\partial\psi(x,0)}{\partial t} = \psi_T^1 & \text{in } \Omega, \\ \psi = \dfrac{\partial\psi}{\partial x} = 0 & \text{on } \Sigma, \end{cases} \tag{11}$$

and ψ_T^0 , ψ_T^1 are the initial conditions given in (9) and (10).

We use the following algorithm for the implementation.

Algorithm 6.1 1: Choice of the initial data u^0 and u^1.
2: Choice of the order n.
3: Calculation of the explicit formulas ψ_T^0 and ψ_T^1 using (9) and (10).
4: Resolution of the system (11).
5: Calculation of the explicit control $g*$.
6: Calculation of the cost function $\|g*\|^2$.
7: Resolution of the system (2) using the explicit control $g*$.
8: Calculation of the final state error $\|\xi\|^2$.
Return to 2.

Remark 6.1 The numerical method for resolution of systems (2) and (11) is based on a symmetric finite difference scheme, see [7]. This scheme leads to the resolution of a linear system whose matrix is pentadiagonal symmetric positive.

We have introduced a new approach to determine explicitly the control driving the system (2) to rest at time T with an estimation of the final state error. Particular attention is paid to the system which is neither hyperbolic nor parabolic.

Our paper presents a new view for the numerical approximation of the exact boundary controllability.

We have the following graphs with $L = 1$, $n = 4$ and $T = 1$.
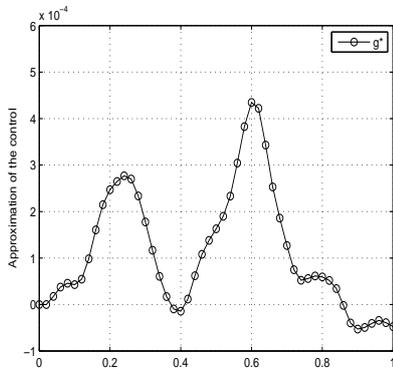
Figure 1: The form of approximate control g^* steering the system (2) to rest at time T.
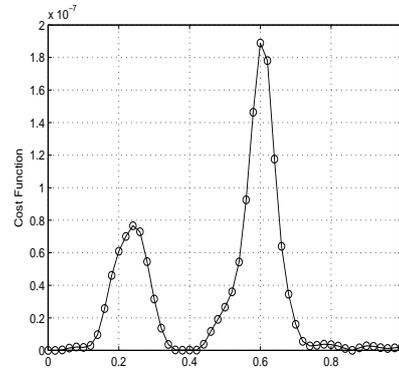
Figure 2: Illustration of the cost function obtained by the corresponding unique minimum L^2-norm control.

Remark 6.2 The results obtained are satisfactory althought many approximations have been made (asymptotic aspect, truncation, etc.). However, we think that increasing the value of n increases the efficiency of formulas (9), (10) and allows to make the final state error close to zero. In this perspective, we are trying in the following section to improve the result of the final state error so that the control steers the considered system (2) to rest at time T.
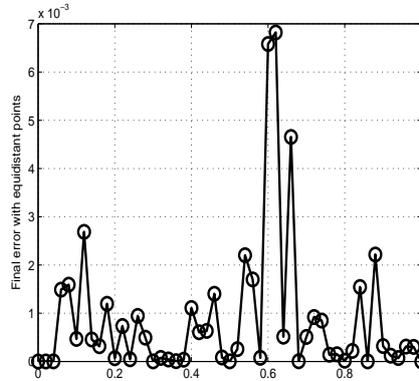
Figure 3: Estimation of the final state error with equidistant points so that the system (2) steers to rest at time T.

7   Improvement of the Final State Error

In this section, the calculation of the final state error is improved to make it as small as possible. The problem that we consider is to minimize (3) using the particle swarm optimization algorithm (PSO) and taking the same example treated in Section 6. For this, we try to determine x_i by the PSO so that the final state error (3) is close to zero. This method is an effective way to improve the final state error.

7.1   Basic particle swarm optimization algorithm

The particle swarm optimization (PSO) is a non deterministic method simulated by social behavior of bird flocking or fish schooling, that can be used to optimize a function objective, and was described in [5, 8]. In the PSO algorithm, each individual is called the "particle", which represents a potential solution in a swarm.

We present in the following, the main steps of the basic PSO algorithm. Three $M-$ dimensional vectors compose each particle: the current position $Y_j = (y_{j1}, y_{j2}, ..., y_{jM})$, the velocity $V_j = (v_{j1}, v_{j2}, ..., v_{jM})$ which represents its direction of searching, and the previous best position that it has individually found $P_j = (p_{j1}, p_{j2}, ..., p_{jM})$, called (pbest), the subscipt j ranges from 1 to s, where s indicates the size of swarm. Habitually, each particle stores its position and its best value so far (pbest), and therefore recognizes the best value in the swarm, called (sbest) between the set of values (pbest).

The following system shows the displacement of each particle j:

$$v_{jl}^{k+1} = w_{jl}v_{jl}^k \quad + \quad c_1 r_1^k[(pbest)_{jl}^k - x_{jl}^k], +c_2 r_2^k[(sbest)_{jl}^k - x_{jl}^k] \tag{12}$$

$$x_{jl}^{k+1} = v_{jl}^{k+1} + x_{jl}^k, \tag{13}$$

where $v_{jl}^{k+1}, x_{jl}^{k+1}$ are the velocity and the position of particle j, respectively, at iteration $k + 1$, w_{jl} is the inertia weight with its value that ranges from 0.9 to 1.2, c_1 and c_2 are two parameters situated in the range of 2 to 4, called the acceleration coefficients and r_1^k, r_2^k are two random numbers uniformly distributed in the range $[0, 1]$. In the double

subscript in the equations (12) and (13) the first subscript stands for the particle j and the second one for the dimension l. The (basic) process for imlementing the PSO is in the algorithm below.

Algorithm 7.1 Particle Swarm Optimisation.
1: Set the dimension M, and the size s of the swarm.
2: Set the iteration number k to zero.
3: Evaluate, for each particle, the velocity vector using its memory and equation (12), where pbest and sbest can be modified.
4: Move each particle to its new position, according to equation (13).
5: Let $k = k + 1$.
6: Go to step 2, and repeat until convergence condition is satisfied.

Remark 7.1 This section was the subject of a personal communication entitled "Particle Swarm Optimization Algorithm to Improve the Final State Error of the Exact Boundary Controllability", presented at the Sixth International Conference on Meta-heuristics and Nature Inspired Computing that was organized in Marrakech (Morocco) in October 2016.

From Figure 4 shown below, it can be seen that the final state error is improved.
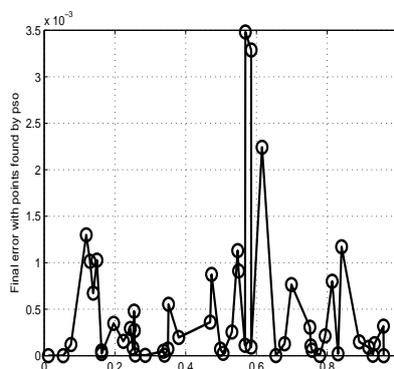
Figure 4: Estimation of the final state error with points chosen by the PSO so that the system (2) steers to rest at time T.

7.2   Discussion

Figure 4 illustrates the decrease of the final state error in comparison with Figure 3 of Section 6. It can be said that the particle swarm optimization (PSO) algorithm has improved the value of the final state error.

The main limitation of the experimental result is the non-comparison of the final error provided by the PSO with other metaheuristics such as the ABC (Artificial Bee Colony), FWA (Fireworks Algorithm), FPA algorithm (Flower Pollination Algorithm).

8   Conclusion

The numerical implementation of the Hilbert uniqueness method allowed us to approximate the exact control for the vibrating rod with an estimation of the final state error. The calculation of this error when the selected points are equidistant is compared with the error when points are chosen by the PSO. The results show the improvement of the final error in the second case compared to the first one. In the future, we intend to study the comparison of the final error provided by the PSO with other metaheuristics and study the case of dimension two of the same system.

Acknowledgment

References

[1] U. Arora and N. Sukavanam. Approximate controllability of non densely defined semilinear control system with non local conditions. *Nonlinear Dynamics and Systems Theory* **17** (1) (2017) 5–18.

[2] A. Benabdallah, F. Boyer, M. G. Burgos and G. Olive. Sharp estimates of the one-dimensional boundary control cost for parabolic systems and application to the N-dimensional boundary null controllability in cylindrical domains. *SIAM J. Control and Optimization* **52** (5) (2014) 2970–3001.

[3] A. Bensoussan. On the general theory of exact controllability for skew symmetric operators. *Acta Applicandae Mathematicae* **20** (3) (1990) 197–229.

[4] C. Carthel, R. Glowinski and J. L. Lions. On exact and approximate boundary controllability for the heat equation: A numerical approach. *Journal of optimization, Theory and Applications* **82** (3) (1994) 429–484.

[5] T. I. Cristian. The particle swarm optimization algorithm: convergence, analysis and parameter selection. *Information Processing Letters* **85** (6) (2003) 317–325.

[6] E. Dean, R. Glowinski and C. H. Li. Supercomputer solutions of partial differential equation problems in computational fluid dynamics and in control. *Computer Physics Communications* **53** (1-3) (1989) 401–439.

[7] P. Duchateau and D. W. Zachmann. *Schaum's of Theory and Problems for Partial Differential Equations*. McGraw Hill, New York, 1986.

[8] R. C. Eberhart and J. Kennedy. A new optimizer using particles swarm theory. In: Sixth international symposium on micro machine and human science. Nagoya, Japan, 1995, 39–43.

[9] A. Feydi, S. Elloumi and B. Braiek. Decentralized stabilization for a class of nonlinear interconnected systems using sdre optimal control approach. *Nonlinear Dynamics and Systems Theory* **19** (1) (2019) 55–67.

[10] R. Glowinski, C. H. Li and J. L. Lions. A numerical approach to the exact boundary controllability of the wave equation(I) Dirichlet controls: Description of the numerical methods. *Japan Journal of Applied Mathematics* **7** (1) (1990) 1–76.

[11] R. Glowinski and C. H. Li. On the numerical implementation of the Hilbert uniqueness method for the exact boundary controllability of the wave equation. *C.R. Acad. Sci. Paris, série I Math.* **311** (2) (1990) 135–142.

[12] R. Glowinski. Ensuring well-posedness by analogy; stockes problem and boundary control for the wave equation. *Journal of Computational Physics* **103** (2) (1992) 189–221.

[13] M. Gunzburger, L. S. Hou and L. A. Ju. Numerical method for exact boundary controllability problems for the wave equation. *Journal Computers and Mathematics with Applications* **51**, (5) (2006) 721–750.

[14] S. Kumar. Approximate controllability of non local impulsive fractional order semilinear time varying delay systems. *Nonlinear Dynamics and Systems Theory* **16** (4) (2016) 420–430.

[15] J. L. Lions. Exact controllability, stabilization and perturbations for distributed systems. *SIAM Review* **30** (1) (1988) 1–68.

[16] A. G. Mazko. Robust output feedback stabilization and optimization of discrete-time control systems. *Nonlinear Dynamics and Systems Theory* **18** (1) (2018) 92–106.

[17] D. L. Russell. Controllability and stabilizability theory for linear partial differential equations. Recent progress and open questions. *SIAM Review* **20** (4) (1978) 639–739.

[18] J. Zabczyk. *Mathematical Control Theory. An Introduction.* Birkhauser, Boston, 2008.

[19] E. Zerrik, A. Ait Aadi and R. Lahrissi. On the stabilization of infinite dimensional bilinear systems with unbounded control operator. *Nonlinear Dynamics and Systems Theory* **18** (4) (2018) 418–425.

[20] E. Zuazua. Contrôlabilité exacte d'un modèle de plaques vibrantes en un temps arbitrairement petit. *C.R. Acad. Sci. Paris, série I Math.* **304** (7) (1987) 173–176. [French]

The Finite Element Method for Nonlinear Nonstandard Volterra Integral Equations

M. Khumalo * and A. Dlamini

University of South Africa, P.O. Box 392, UNISA 0003, Republic of South Africa

Abstract: In this work, we look at the implementation of the finite element method to a nonlinear (nonstandard) Volterra integral equation. We consider the Galerkin approach, where we choose the weight function in such a way that it takes the form of the approximate solution. We work on a uniform mesh and choose the Lagrange polynomials as basis functions. We consider the error analysis of the method. We look at a specific example to illustrate the implementation of the finite element method. Finally, we consider the estimated rate of convergence.

Keywords: *Volterra integral equations; finite element method; Galerkin approach.*

Mathematics Subject Classification (2010): 45D05, 65R20, 65N30.

1 Introduction

In this paper, we consider the nonlinear Volterra integral equation of the second kind

$$u(x) = \sum_{m=1}^{r} b_m \left(g_m(x) + \int_0^x k_m(x,y)u(y)dy \right)^m, \qquad x \in [0, L], \tag{1}$$

where $r \in \mathbb{N}, r \geq 2$, $b \in \mathbb{R}$, $g : [0, L] \to \mathbb{R}$ and $k : [0, L] \times [0, L] \to \mathbb{R}$ are continuous functions. The unknown function $u(x) \in C[0, L]$.

In essence, (1) is nonstandard in that in its simplest form, it has the structure

$$u = \sum_{m=1}^{r} b_m \left(g_m + W_m u \right)^m, \qquad x \in [0, L],$$

---

* Corresponding author: `mailto:khumam@unisa.ac.za`

where W_m is the standard linear Volterra operator, see [9]. Volterra integral equations find applications in many fields of science and engineering, including population dynamics, the spread of epidemics, semi-conductor devices, wave propagation, super-fluidity and traveling wave analysis, see Saveljeva [14], for example. Many authors have used numerical methods to solve Volterra integral equations. The authors in [1, 8, 11, 13] solved linear Volterra integral equations using quadrature rules such as the repeated Simpson's and repeated trapezoidal rule. Other authors, see [3–7], used collocation methods to find approximate solutions for Volterra integral equations.

Sloss and Blyth [15] implemented Corrington's Walsh function method to (1) and also proved the existence and uniqueness of the solution in a Banach space L^2. Malindzisa and Khumalo [9] used the collocation methods and quadrature rules to approximate the solution to (1). They pointed out that the repeated Simpson's rule gives better solutions when a reasonable value of the step size is used. They also provided sufficient conditions for the existence and uniqueness of the solutions for (1) and for the case where $b_1 = 0$ and $r = 2$ in the space $C[0, L]$. A similar study was done by Mamba and Khumalo [10]. They presented convergence analysis for the collocation methods and trapezoidal rule. Benitez and Bolos [2] highlighted that the collocation methods have proven to be appropriate techniques for finding the approximate solutions for nonlinear integral equations because of their accuracy and stability. However, the finite element method has not been used to approximate solutions to (1). In this work, we will consider the implementation of the finite element method to find the approximate solutions for (1). In particular, we will consider the case where $b_1 = 0$ and $r = 2$.

$$u(x) = b\left(g(x) + \int_0^x k(x,y)u(y)dy\right)^2, \tag{2}$$

where $b \in \mathbb{R}$, $g : [0, L] \to \mathbb{R}$ and $k : [0, L] \times [0, L] \to \mathbb{R}$ are continuous functions. The unknown function $u(x) \in C[0, L]$. We will also compare the results obtained from the implementation of the finite element method to the ones obtained in [9, 10] using the collocation method and quadrature rules.

2 Well-Posedness of the Problem

The following theorem shows that when $b_1 = 0$ and $r = 2$, the solution of the VIE of the non-standard type (1) exists in the space $C[0, L]$. In this section, we will prove that the solution exists using a method analogous to the one used by Malindzisa and Khumalo in [9]. The uniqueness of the solution for the case where $b_1 = 0$ and $r = 2$ is presented in [9].

Theorem 2.1 *Consider the VIE (2). There exists a solution $u(x)$, where $u \in C[0, L]$, provided that*

$$2K|b|\big(\|g\|_\infty + KL\big) < 1,$$

$$\tag{3}$$

$$|b|\big(\|g\|_\infty + KL\big)^2 < L,$$

where $K = \sup\limits_{[0,1] \times [0,1]} |k(x,y)|$.

Proof.   We use Banach's fixed point theorem.   Define $Tz(x) = b\Big(g(x) +$ $\int_0^x k(x,y)z(y)dy\Big)^2$ for each $z \in C[0,L]$. Let $z_1, z_2 \in C[0,L]$. Then

$$
\begin{aligned}
Tz_2(x) - Tz_1(x) &= b\Big(g(x) + \int_0^x k(x,y)z_2(y)dy\Big)^2 - b\Big(g(x) + \int_0^x k(x,y)z_1(y)dy\Big)^2 \\
&= b\Big[\Big(g(x) + \int_0^x k(x,y)z_2(y)dy\Big)^2 - \Big(g(x) + \int_0^x k(x,y)z_1(y)dy\Big)^2\Big] \\
&= b\Big[\Big(g(x) + \int_0^x k(x,y)z_2(y)dy - g(x) - \int_0^x k(x,y)z_1(y)dy\Big) \\
&\quad \cdot \sum_{i=0}^1 \Big(g(x) + \int_0^x k(x,y)z_2(y)dy\Big)^i \cdot \Big(g(x) + \int_0^x k(x,y)z_1(y)dy\Big)^{1-i}\Big] \\
&\quad bF(x,z_1,z_2)\int_0^x k(x,y)\big(z_2(y) - z_1(y)\big)dy.
\end{aligned}
\tag{4}
$$

Therefore,

$$
\|Tz_2 - Tz_1\|_\infty \le b \sup F(x,z_1,z_2) \cdot K\|z_2 - z_1\|_\infty.
\tag{5}
$$

Furthermore,

$$
\|F\|_\infty \le 2\big(\|g\|_\infty + KL\big).
$$

Hence,

$$
\|Tz_2 - Tz_1\|_\infty \le 2b\big(\|g\|_\infty + KL\big)K\|z_2 - z_1\|_\infty.
\tag{6}
$$

Consequently, T is a contraction if

$$
2K|b|\big(\|g\|_\infty + KL\big) < 1.
\tag{7}
$$

We need to show that $T : C[0,L] \to C[0,L]$. Observe that

$$
\left\|\Big(g(x) + \int_0^x k(x,y)z(y)dy\Big)^2\right\|_\infty \le \big(\|g\|_\infty + K\|z\|_\infty\big)^2.
\tag{8}
$$

Therefore

$$
\|Tz\|_\infty \le |b|\big(\|g\|_\infty + K\|z\|_\infty\big)^2
$$

$$
\le |b|\big(\|g\|_\infty + KL\big)^2;
\tag{9}
$$

thus $T : C[0,L] \to C[0,L]$

$$
|b|\big(\|g\|_\infty + KL\big)^2 < L.
$$

Hence T is a contraction and maps $[0,L]$ into itself given (3) holds.

3 Numerical Method

Consider the nonlinear Volterra integral equation (2). Let $\mathcal{I} = \left\{x_i\right\}_{i=0}^n$ be the partition of $[0, L]$ with a uniform mesh h; that is,

$$0 = x_0 < x_1 < x_2, \ldots x_{n-1} < x_n = L,$$

and let S denote the $(n+1)$-dimensional subspace of $C[0, L]$ spanned by $\{\phi_k\}_{k=0}^n$. We seek an approximate solution $u_h \in S$ for $u(x)$ of the form

$$\begin{aligned}
u_h(x) &= \alpha_0\phi_0(x) + \alpha_1\phi_1(x) + \alpha_2\phi_2(x) + \cdots + \alpha_n\phi_n(x) \\
&= \sum_{k=0}^n \alpha_k\phi_k(x) \approx u(x),
\end{aligned} \tag{10}$$

where $\left\{\alpha_k\right\}_{k=0}^n$ are the coefficients to be determined.

We take S to be a piecewise linear subspace of $C[0, L]$, that is, we choose

$$\phi_k(x) = \begin{cases} \frac{x - x_{k-1}}{h_k}, & \text{for} \quad x_{k-1} \le x \le x_k, \\ \frac{x_{k+1} - x}{h_{k+1}}, & \text{for} \quad x_k \le x \le x_{k+1}, \\ 0, & \text{otherwise}, \end{cases} \tag{11}$$

where $h_k = x_k - x_{k-1}$ is the length of the subinterval (element) k and the derivative of the basis functions is

$$\phi_k'(x) = \begin{cases} \frac{1}{h_k}, & \text{for} \quad x_{k-1} \le x \le x_k, \\ \frac{-1}{h_{k+1}}, & \text{for} \quad x_k \le x \le x_{k+1}, \\ 0, & \text{otherwise}. \end{cases}$$

Each basis function ϕ_k satisfies the following properties, see [12].

1. The interpolation property

$$\phi_k(x_j) = \begin{cases} 1, & \text{if } k = j, \\ 0, & \text{if } k \ne j. \end{cases}$$

2. The partition of unity

$$\sum_{k=0}^n \phi_k(x) = 1, \qquad k, j = 0, 1, 2, \cdots n.$$

Substituting (10) into (2) and rearranging give

$$\sum_{k=0}^n \alpha_k\phi_k(x) - b\left(g(x) + \int_0^x k(x, y)\sum_{k=0}^n \alpha_k\phi_k(y)dy\right)^2 := R(x), \tag{12}$$

where $R(x)$ represents the residual.

We want to determine the values of α_k such that the residuals over the elements are minimized in a weighted average sense.

$$\int_{x_i}^{x_{i+1}} w(x)R(x)dx = 0, \tag{13}$$

where $w(x)$ is the weight function. Here we use the Galerkin criterion, in which the residual $R(x)$ is orthogonal to the weight function $w(x)$ (see [16]). This follows since $w(x) \in S$ and $R(x)$ is orthogonal to every element $v_h \in S$.

In this study, we chose a weight function which is of the same form as the approximate solution $u_h(x)$ but with arbitrary coefficients. Therefore,

$$w(x) = \beta_0\phi_0(x) + \phi_1(x)\beta_1 + \cdots + \phi_n(x)\beta_n = \sum_{j=0}^{n} \beta_j\phi_j(x). \tag{14}$$

Substituting (12) and (14) in (13) we get the following:

$$\int_{x_i}^{x_{i+1}} w(x)R(x)dx = \int_{x_i}^{x_{i+1}} \sum_{j=0}^{n} \beta_j\phi_j(x) \sum_{k=0}^{n} \alpha_k\phi_k(x)dx$$

$$- \int_{x_i}^{x_{i+1}} \sum_{j=0}^{n} \beta_j\phi_j(x)b\left(g(x) + \int_0^x k(x,y)\sum_{k=0}^{n}\alpha_k\phi_k(y)dy\right)^2 dx = 0.$$

Since the β_j 's are arbitrary, we get the following equation:

$$\sum_{j=0}^{n} \beta_j\left[\int_{x_i}^{x_{i+1}} \phi_j(x)\sum_{k=0}^{n}\alpha_k\phi_k(x)dx - \int_{x_i}^{x_{i+1}}\phi_j(x)b\left(g(x)+\right.\right.$$

$$\left.\left. \int_0^x k(x,y)\sum_{k=0}^{n}\alpha_k\phi_k(y)dy\right)^2 dx\right] = 0.$$

Thus

$$\sum_{k=0}^{n} \alpha_k \int_{x_i}^{x_{i+1}} \phi_j(x)\phi_k(x)dx - \int_{x_i}^{x_{i+1}}\phi_j(x)b\left(g(x) + \sum_{k=0}^{n}\alpha_k\int_0^x k(x,y)\phi_k(y)dy\right)^2 dx = 0.$$

Therefore

$$\sum_{k=0}^{n} \alpha_k \int_{x_i}^{x_{i+1}} \phi_k(x)\phi_j(x)dx - \int_{x_i}^{x_{i+1}}\phi_j(x)b\left(g(x) + \sum_{k=0}^{n}\alpha_k\int_0^x k(x,y)\phi_k(y)dy\right)^2 dx = 0, \tag{15}$$

which is a nonlinear system of equations which must be solved for $\{\alpha_k\}_{k=0}^{n}$.

4 Convergence Analysis

We now analyze the error, to start the analysis we first define the norm

$$\|e(x)\|_\infty = \|u(x) - u_h(x)\|_\infty$$
$$= \max_{0 \le k \le n} \|u(x_k) - u_h(x_k)\|$$
$$= \max_{0 \le k \le n} \|u(x_k) - \alpha_k\|. \tag{16}$$

Consider the Volterra integral equation (2). Then substitute (10) into (2), we get

$$u_h(x) = b\left(g(x) + \int_0^x k(x,y)u_h(y)dy\right)^2, \quad x \in [0,L]. \tag{17}$$

The following theorem gives the upper bound of $\|e(x)\|_\infty$.

Theorem 4.1 *Assume that $b \in \mathbb{R}$, $g : [0,L] \to \mathbb{R}$ and $k : [0,L] \times [0,L] \to \mathbb{R}$ are continuous functions. $u(x)$ is the exact solution of (2) and $u_h(x)$ is the approximate solution. Then*

$$\|e(x)\|_\infty = \|u(x) - u_h(x)\|_\infty$$
$$\leqslant D_1\frac{h^{q+1}}{4(q+1)} + \left(D_3\frac{h^{q+1}}{4(q+1)}\right)\left(D_5\frac{h^{q+1}}{4(q+1)} + D_7\max_{0\leq k\leq n}|\alpha_k|\right),$$

where D_1, D_3, D_5 and D_7 are appropriately defined constants.

Proof. Note that

$$e(x) = u(x) - u_h(x). \tag{18}$$

Let $x = x_i$ in (18). Therefore,

$$e_i = u(x_i) - u_h(x_i) = b\left(g(x_i) + \int_0^{x_i} k(x_i,y)u(y)dy\right)^2 - b\left(g(x_i) + \right. \tag{19}$$
$$\left. \int_0^{x_i} k(x_i,y)u_h(y)dy\right)^2$$
$$= b\left[2g(x_i)\int_0^{x_i} k(x_i,y)\left[R + \Lambda_n(y) - u_h(y)\right]dy + \right.$$
$$\left(\int_0^{x_i} k(x_i,y)\left[R + \Lambda_n(y) - u_h(y)\right]dy\right)\cdot\left(\int_0^{x_i} k(x_i,y)\left[R + \Lambda_n(y) - u_h(y)\right]dy + \right.$$
$$\left.\left. 2\int_0^{x_i} k(x_i,y)u_h(y)dy\right)\right], \tag{20}$$

where $u(y)$ is as in (10),

$$\Lambda_n(y) = \sum_{k=0}^n u(y_k)\phi_k(y), \tag{21}$$

and $R = u(y) - \Lambda_n(y)$ is the remainder of interpolation corresponding to the finite element and $\Lambda_n(y)$ is the N-order Lagrange finite element solution. By the use of interpolation polynomial error estimation, we have the following:

$$|R| \leqslant \frac{h^{q+1}}{4(q+1)}\max_{\xi\in[0,L]}|u(\xi)^{q+1}| = \frac{h^{q+1}}{4(q+1)}M, \tag{22}$$

where $M = \max_{\xi\in[0,L]}|u(\xi)^{q+1}|$ and q is the degree of the piecewise Lagrange polynomials.

Substitute equations (21) and (10) into (19), we then get the following equation:

$$e = b\Bigg[\int_0^{x_i} 2g(x_i)k(x_i,y)\left[R + \sum_{k=0}^{n}\left(u(y_k) - \alpha_k\right)\phi_k(y)\right]ds$$

$$+ \left(\int_0^{x_i} k(x_i,y)\left[R + \sum_{k=0}^{n}\left(u(y_k) - \alpha_k\right)\phi_k(y)\right]dy\right)\cdot\left(\int_0^{x_i} k(x_i,y)\Big[R+$$

$$\sum_{k=0}^{n}\left(u(y_k) - \alpha_k\right)\phi_k(y)\Big]dy + 2\int_0^{x_i} k(x_i,y)\left(\sum_{k=0}^{n}\alpha_k\phi_k(y)\right)dy\right)\Bigg]. \qquad (23)$$

Then

$$|e| = \Bigg|b\Bigg[\int_0^{x_i} 2g(x_i)k(x_i,y)\left[R + \sum_{k=0}^{n}\left(u(y_k) - \alpha_k\right)\phi_k(y)\right]dy$$

$$+ \left(\int_0^{x_i} k(x_i,y)\left[R + \sum_{k=0}^{n}\left(u(y_k) - \alpha_k\right)\phi_k(y)\right]dy\right)\cdot\left(\int_0^{x_i} k(x_i,y)\Big[R+$$

$$\sum_{k=0}^{n}\left(u(y_k) - \alpha_k\right)\phi_k(y)\Big]dy + 2\int_0^{x_i} k(x_i,y)\left(\sum_{k=0}^{n}\alpha_k\phi_k(y)\right)dy\right)\Bigg]\Bigg|$$

$$|e| = |b|\Bigg|\Bigg[\int_0^{x_i} 2g(x_i)k(x_i,y)\left[R + \sum_{k=0}^{n}\left(u(y_k) - \alpha_k\right)\phi_k(y)\right]dy$$

$$+ \left(\int_0^{x_i} k(x_i,y)\left[R + \sum_{k=0}^{n}\left(u(y_k) - \alpha_k\right)\phi_k(y)\right]dy\right)\cdot\left(\int_0^{x_i} k(x_i,y)\Big[R+$$

$$\sum_{k=0}^{n}\left(u(y_k) - \alpha_k\right)\phi_k(y)\Big]dy + 2\int_0^{x_i} k(x_i,y)\left(\sum_{k=0}^{n}\alpha_k\phi_k(y)\right)dy\right)\Bigg]\Bigg|$$

$$|e| \leq |b|\Bigg[\Bigg|\int_0^{x_i} 2g(x_i)k(x_i,y)\left[R + \sum_{k=0}^{n}\left(u(y_k) - \alpha_k\right)\phi_k(y)\right]ds\Bigg|$$

$$+ \Bigg|\left(\int_0^{x_i} k(x_i,y)\left[R + \sum_{k=0}^{n}\left(u(y_k) - \alpha_k\right)\phi_k(y)\right]dy\right)\Bigg|\cdot\Bigg|\left(\int_0^{x_i} k(x_i,y)\Big[R+$$

$$\sum_{k=0}^{n}\left(u(y_k) - \alpha_k\right)\phi_k(y)\Big]dy + 2\int_0^{x_i} k(x_i,y)\left(\sum_{k=0}^{n}\alpha_k\phi_k(y)\right)dy\right)\Bigg|\Bigg]$$

$$\leq |b|\Bigg[\int_0^{x_i}|2g(x_i)||k(x_i,y)|\left[|R| + \Bigg|\sum_{k=0}^{n}\left(u(y_k) - \alpha_k\right)\phi_k(y)\Bigg|\right]dy$$

$$+ \left(\int_0^{x_i}|k(x_i,y)|\left[|R| + \Bigg|\sum_{k=0}^{n}\left(u(y_k) - \alpha_k\right)\phi_k(y)\Bigg|\right]dy\right)\cdot\left(\int_0^{x_i}|k(x_i,y)|\Big[|R|+$$

$$\Bigg|\sum_{k=0}^{n}\left(u(y_k) - \alpha_k\right)\phi_k(y)\Bigg|\Big]dy + 2\int_0^{x_i}|k(x_i,y)||u_h(y)|dy\right)\Bigg].$$

Now set

$$\delta = [e(y_0), e(y_1) \ldots e(y_k), \ldots e(y_n)]^T, \qquad \Phi = [\phi_0(y), \phi_1(y), \ldots \phi_k(y), \ldots, \phi_n(y)]^T,$$

and

$$\Gamma = [\alpha_0, \alpha_1, \ldots \alpha_k, \ldots, \alpha_n]^T,$$

where $e(y_k) = u(y_k) - u_h(y_k) = u(y_k) - \alpha_k$.

Then

$$| \Lambda_n(y) - u_h(y) | = \left| \sum_{k=0}^{n} (\alpha(y_k) - \alpha_k) \phi_k(y) \right| = | \delta \cdot \Phi | \leqslant \|\delta\|_\infty \cdot \|\Phi\|_\infty \leqslant C\|\delta\|_\infty. \quad (24)$$

Since $e(y_k)$ for $k = 0, 1, 2, ..., n$ represents the interpolation error, we have

$$e(y_0) = e(y_1) = \cdots = e(y_n) = 0, \qquad (25)$$

$$\left| \sum_{k=0}^{n} \alpha_k \phi_k(y) \right| = | \Gamma \cdot \Phi | \leqslant \|\Gamma\|_\infty \cdot \|\Phi\|_\infty \leqslant C\|\Gamma\|_\infty. \qquad (26)$$

Using equation (22), (24), (25) and (26) we then obtain the following:

$$\begin{aligned}
\|e\|_\infty \leqslant{}& D_1 \frac{h^{q+1}}{4(q+1)} + D_2\|\delta\|_\infty \\
&+ \left(D_3 \frac{h^{q+1}}{4(q+1)} + D_4\|\delta\|_\infty \right) \left(D_5 \frac{h^{q+1}}{4(q+1)} + D_6\|\delta\|_\infty + D_7\|\Gamma\|_\infty \right) \\
={}& D_1 \frac{h^{q+1}}{4(q+1)} + D_2 \max_{0 \leq y_k \leq n} | e(y_k) | \\
&+ \left(D_3 \frac{h^{q+1}}{4(q+1)} + D_4 \max_{0 \leq y_k \leq n} | e(y_k) | \right) \\
&\cdot \left(D_5 \frac{h^{q+1}}{4(q+1)} + D_6 \max_{0 \leq y_k \leq n} | e(y_k) | + D_7 \max_{0 \leq k \leq n} | \alpha_k | \right) \\
={}& D_1 \frac{h^{q+1}}{4(q+1)} + \left(D_3 \frac{h^{q+1}}{4(q+1)} \right) \left(D_5 \frac{h^{q+1}}{4(q+1)} + D_7 \max_{0 \leq k \leq n} | \alpha_k | \right),
\end{aligned}$$

where $G = \max\limits_{0 \leq x_i \leq L} | g(x_i) |$, $K = \max\limits_{\substack{0 \leq x_i \leq L \\ 0 \leq y \leq L}} | k(x_i, y) |$, $L = \max\limits_{0 \leq i \leq n} | x_i |$ $D_1 = 2| b |GKLM$,

$D_2 = 2| b |CGKL$, $D_3 = | b |KL$, $D_4 = | b |CKL$, $D_5 = KLM$, $D_6 = CKL$, $D_7 = 2CKL$.

Corollary 4.1 *Let q be the degree of the piece-wise Lagrange polynomials. If $q = 1$, by using the interpolation polynomial error estimation (22) we get*

$$| R | \leqslant \frac{h^2}{8} M. \qquad (27)$$

Therefore

$$\|e(x)\|_\infty = \|u(x) - u_h(x)\|_\infty \leqslant D_1 \frac{h^2}{8} + \left(D_3 \frac{h^2}{8} \right) \left(D_5 \frac{h^2}{8} + D_7 \max_{0 \leq k \leq n} | \alpha_k | \right).$$

5 Numerical Computation

We now consider a specific example and implement the finite element method to illustrate the procedure.

Example 5.1 Consider the following nonlinear(nonstandard) Volterra integral equations:

$$u(x) = 2 \left(1 + \int_0^x (x - y)u(y)dy \right)^2, \qquad x \in [0, 1], \tag{28}$$

whose exact solution is unavailable. To simplify the numerical computation for the above example, we linearize the problem and implement the finite element method. The algebraic equations obtained from the implementation of the finite element method can be written in a vector form as follows:

$$\mathbf{K}\alpha = \mathbf{F}, \tag{29}$$

where $\mathbf{K}$ is the stiffness (coefficient) matrix and $\mathbf{F}$ is the source(force) vector. We now choose the number of elements n. Let $n = 10$, the algebraic equations obtained from the implementation of the finite element method for ten elements in a vector form are written as:

$$\mathbf{A}\alpha = \mathbf{d}, \tag{30}$$

where

$$\mathbf{A} = \begin{bmatrix} \frac{83}{2500} & \frac{499}{30000} & 0 & 0 & 0 & 0 & 0 & 0 & 0 & 0 & 0 \\ \frac{163}{10000} & \frac{239}{3750} & \frac{529}{30000} & 0 & 0 & 0 & 0 & 0 & 0 & 0 & 0 \\ 0 & \frac{379}{30000} & \frac{209}{3750} & \frac{233}{10000} & 0 & 0 & 0 & 0 & 0 & 0 & 0 \\ 0 & 0 & \frac{49}{30000} & \frac{53}{1250} & \frac{1129}{30000} & 0 & 0 & 0 & 0 & 0 & 0 \\ 0 & 0 & 0 & \frac{-207}{10000} & \frac{89}{3750} & \frac{1939}{30000} & 0 & 0 & 0 & 0 & 0 \\ 0 & 0 & 0 & 0 & \frac{-1751}{30000} & \frac{-1}{3750} & \frac{1083}{10000} & 0 & 0 & 0 & 0 \\ 0 & 0 & 0 & 0 & 0 & \frac{-3461}{30000} & \frac{-37}{1250} & \frac{5179}{30000} & 0 & 0 & 0 \\ 0 & 0 & 0 & 0 & 0 & 0 & \frac{-1957}{10000} & \frac{-241}{3750} & \frac{7849}{30000} & 0 & 0 \\ 0 & 0 & 0 & 0 & 0 & 0 & 0 & \frac{-9101}{30000} & \frac{-391}{3750} & \frac{3793}{10000} & 0 \\ 0 & 0 & 0 & 0 & 0 & 0 & 0 & 0 & \frac{-13271}{30000} & \frac{-187}{1250} & \frac{15889}{30000} \\ 0 & 0 & 0 & 0 & 0 & 0 & 0 & 0 & 0 & \frac{-6167}{10000} & \frac{1433}{2500} \end{bmatrix},$$

$$
\alpha = \begin{bmatrix} \alpha_0 \\ \alpha_1 \\ \alpha_2 \\ \alpha_3 \\ \alpha_4 \\ \alpha_5 \\ \alpha_6 \\ \alpha_7 \\ \alpha_8 \\ \alpha_9 \\ \alpha_{10} \end{bmatrix} ; \qquad \mathbf{d} = \begin{bmatrix} \frac{1}{10} \\ \frac{1}{5} \\ \frac{1}{5} \\ \frac{1}{5} \\ \frac{1}{5} \\ \frac{1}{5} \\ \frac{1}{5} \\ \frac{1}{5} \\ \frac{1}{5} \\ \frac{1}{5} \\ \frac{1}{10} \end{bmatrix}.
$$

After solving the above system of equations, we consider the graphical representation of the solution for $n = 5$, $n = 10$, $n = 20$ and $n = 40$.

Since the exact solution of (28) is unavailable, the graphical representation in Figure 1 of the approximate solution is found to resemble those obtained in [9]. We now estimate the rate of convergence using the numerical results obtained from implementing the finite element method on (28). To estimate the rate of convergence we use the following:

$$
p = \frac{\log \left| \dfrac{u^{\frac{h}{2}} - u^h}{u^{\frac{h}{4}} - u^{\frac{h}{2}}} \right|}{\log 2},
$$

where u^h, $u^{\frac{h}{2}}$ and $u^{\frac{h}{4}}$ are the approximate solution to $u(x)$ for the step size h, $\frac{h}{2}$ and $\frac{h}{4}$, respectively .

Table 1: The rate of convergence for different values of h using (28).

h	$\mathbf{u}_h(x)$	p
$\frac{1}{5}$	1.961133515140453	3.044666782640548
$\frac{1}{10}$	1.994338539181266	1.720724066245102
$\frac{1}{20}$	1.998362629972080	1.966888879806644
$\frac{1}{40}$	1.999583524683324	1.999142447697078
$\frac{1}{80}$	1.999895834518747	
$\frac{1}{160}$	1.999973958401418	

The results in Table 1 indicate a second-order rate of convergence. Hence we can conclude that the finite element method is better compared to the one-point collocation methods and quadrature methods presented in [9], since the methods in [9] indicate the first-order rate of convergence.
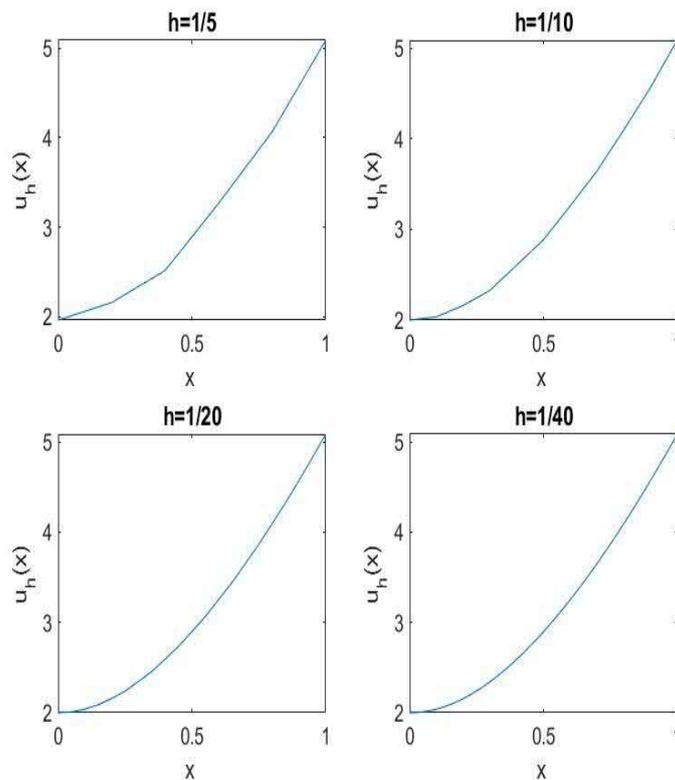
Figure 1: The graphical representation of the solutions for different values of h.

6 Conclusion

In this paper, we solved the nonlinear (nonstandard) Volterra integral equation on a uniform mesh and used the Lagrange polynomials as basis functions together with the Galerkin finite element method, where the weight function is chosen in such a way that it takes the form of the approximate solution but with arbitrary coefficients. We implemented the finite element method to the nonlinear (nonstandard) Volterra integral equations. We proved the error analysis of the approximate solution. We implemented the finite element method to a specific nonlinear (nonstandard) Volterra integral equation. We looked at the graphical representation of the approximate solution for $n = 5$, $n = 10$, $n = 20$ and $n = 40$. Since the exact solution of (28) is unavailable, we compared the graphical representation in Figure 1 with the graphical representation of the approximate solution obtained by using the one-point collocation and quadrature methods in the paper presented by Malindzisa and Khumalo [9], from which we observed that the graphs in Figure 1 are similar to the ones obtained [9]. We also consider the estimate for the rate of convergence for different values of h using (28) from which we obtained the results in Table 1 which indicates a second-order rate of convergence. From the results obtained in Table 1 we conclude that the finite element method is better compared to

the one-point collocation methods and quadrature methods presented by Malindzisa and Khumalo in [9] for this example since the methods in [9] indicate the first-order rate of convergence.

References

[1] M. Aigo. On the numerical approximation of volterra integral equations of the second kind using quadrature rules. *International Journal of Advanced Scientific and Technological Research* **1** (2013) 558–564.

[2] R. Benitez and V. Bolos. Blow-up collocation solutions of nonlinear homogeneous Volterra integral equations. *Applied Mathematics and Computation* **26** (C) (2015) 754–768.

[3] J. Blom and H. Brunner. The numerical solution of nonlinear volterra integral equations of the second kind by collocation and iterated collocation methods. *SIAM journal on scientific and statistical computing* **8** (5) (1987) 806–830.

[4] H. Brunner. Iterated collocation methods for Volterra integral equations with delay arguments. *Mathematics of Computation* **62** (206) (1994) 581–599.

[5] T. Diogo. Collocation and iterated collocation methods for a class of weakly singular Volterra integral equations. *Journal of computational and applied mathematics* **229** (2) (2009) 363–372.

[6] T. Diogo and P. Lima. Collocation solutions of a weakly singular Volterra integral equation. *Trends in Applied and Computational Mathematics* **8** (2) (2007) 229–238.

[7] V. Horvat. On collocation methods for Volterra integral equations with delay arguments, *Mathematical Communications* **4**(1) (1999) 93–109.

[8] R. Katani and S. Shahmorad. Block by block method for the systems of nonlinear Volterra integral equations. *Applied Mathematical Modelling* **34** (2) (2010) 400–406.

[9] H. Malindzisa and M. Khumalo. Numerical solutions of a class of nonlinear Volterra integral equations. *Abstract and Applied Analysis* **2014**, Article ID 652631(2014). https://doi.org/10.1155/2014/652631.

[10] H. Mamba and M. Khumalo. On the analysis of numerical methods for nonstandard Volterra integral equation. *Abstract and Applied Analysis* **2014**, Article ID 763160(2014). https://doi.org/10.1155/2014/763160.

[11] F. Mirzaee. A computational method for solving linear Volterra integral equations. *Applied Mathematical Sciences* **6** (17) (2012) 807–814.

[12] J. N. Reddy. *An Introduction to Nonlinear Finite Element Analysis: With Applications to Heat Transfer, Fluid Mechanics, and Solid Mechanics*, OUP, Oxford, 2014.

[13] J. Saberi-Nadjafi and M. Heidari. A quadrature method with variable step for solving linear Volterra integral equations of the second kind. *Applied mathematics and computation* **188** (1) (2007) 549–554.

[14] D. Saveljeva, et al. *Quadratic and Cubic Spline Collocation for Volterra Integral Equations.* Tartu University Press, Tartu, 2006.

[15] B. G. Sloss and W. Blyth. Corrington's Walsh function method applied to a nonlinear integral equation. *The Journal of Integral Equations and Applications* **6** (2) (1994) 239–256.

[16] O. C. Zienkiewicz, R. L. Taylor, P. Nithiarasu and J. Zhu. *The Finite Element Method.* Vol. 3, McGraw-hill, London, 1977.

Control of a Novel Class of Uncertain Fractional-Order Hyperchaotic Systems with External Disturbances via Sliding Mode Controller

B. Labed [1,2*], S. Kaouache [1,2] and M. S. Abdelouahab [2]

[1] *Departement of Mathematics. University of Mentouri Brothers, Constantine 25017, Algeria*
[2] *Laboratory of Mathematics and their interactions, Abdelhafid Boussouf University Center, Mila 43000, Algeria*

Abstract: In this paper, a novel class of fractional-order hyperchaotic systems is proposed. In order to control hyperchaos in these systems, an appropriate sliding mode controller is also designed. Based on the Lyapunov stability theory, the control scheme guarantes the asymptotic stability of the fractional-order hyperchaotic systems in the presence of uncertainty and external disturbance. Simulation results of control design of fractional-order Liu and Lorenz hyperchaotic systems are presented to show the effectiveness of the proposed scheme and stabilization of the systems on the sliding surface.

Keywords: *hyperchaotic systems; fractional-order system; sliding mode control; Lyapunov stability.*

Mathematics Subject Classification (2010): 34A34, 37B25, 37B55, 93C55, 37C25, 93D05.

1 Introduction

The concepts of derivation and fractional integration are often associated with the names of Riemann and Liouville, while the question about the generalization of the notion of fractional-order derivative is older. Indeed, the history of fractional calculus goes back more than three centuries. Recently, fractional calculus has attracted the increasing attention of physicists as well as engineers in several fields of engineering science [1].

---

* Corresponding author: `mailto:labed.math@yahoo.fr`

On the other hand, the chaos theory as a very interesting nonlinear phenomenon has been intensively investigated due to its great importance for applications in several areas of science and technology [2]. It is well known that chaotic systems are defined as nonlinear dynamical systems which are very sensitive to initial conditions. The principal feature used to identify a chaotic behaviour is the well-known Lyapunov exponent criteria. In fact, a system that has one positive Lyapunov exponent is known as a chaotic system. However, a hyperchaotic system is defined as a chaotic system with more than one positive Lyapunov exponent. It is worth mentioning that hyperchaotic systems can show more complex dynamical behaviors than a chaotic system. Thus, the behavior of a hyperchaotic system has the characteristics of high security and it is widely used in secure communication [3], encryption [4] and so on.

The chaos control is an important research problem in the chaos theory. Many control strategies have been developed in the literature for the stabilization of nonlinear fractional-order chaotic and hyperchaotic systems such as the active control [5, 6], the adaptive control [7], the backstepping control [8], the fuzzy adaptive control [9], and the sliding mode control (SMC) [10].

A SMC is a robust nonlinear control. The main feature of the SMC is that it can switch the control law very quickly to drive the states of the system from any initial states onto some predefined sliding surface.

Recently, the SMC has been considered as a challenging research topic for the control and synchronization of fractional-order chaotic systems. For example, in [11], Roopaei et al. have introduced a class of integer-order chaotic systems covering about half of the recently published integer-order chaotic models. In [12], Yin et al. have presented a SMC law for a novel class of three different fractional-order nonlinear systems to realize the chaos control.
Motivated by the above two contributions, in this paper, we first introduce a novel class of fractional-order hyperchaotic systems. Then, we propose a SMC law to control hyperchaos in such fractional-order systems. The controller is used to stabilize the novel fractional-order hyperchaotic systems, even the fractional-order systems with uncertainty and external disturbance. Numerical simulations show that the proposed method can easily stabilize the system on the sliding surface.

The present manuscript is organized as follows. In Section 2 we present our novel class of fractional-order hyperchaotic systems. Section 3 presents the employment of the sliding mode control design of fractional hyperchaotic systems. Numerical simulations are presented to show the viability and efficiency of the proposed method in Section 4. Finally, the paper is concluded in Section 5.

2   Description of a Novel Class of Hyperchaotic Systems

Our proposed class of the fractional-order hyperchaotic systems is described as

$$\begin{cases} D^{\alpha_1} x_1 = x_2 f(x) - \xi_1(x), \\ D^{\alpha_2} x_2 = g(x) - \beta x_2, \\ D^{\alpha_3} x_3 = x_2 h(x) - \xi_2(x), \\ D^{\alpha_4} x_4 = x_2 k(x) - \xi_3(x), \end{cases} \tag{1}$$

where $x = (x_1, x_2, x_3, x_4)^T \in \mathbb{R}^4$ is the state variable, f, g, k, h, ξ_j, $j = 1, 2, 3$ are considered as a continuation of the nonlinear vector functions, which belong to $\mathbb{R}^4 \mapsto \mathbb{R}$ space,

β is the known parameter for any negative or non-negative value, $\alpha_i \in]0,1[$, $i = 1,2,3,4$, are the fractional orders, and D^α is the Caputo derivative which is defined as

$$D^\alpha x(t) = J^{n-\alpha} x^{(n)}(t), \quad \alpha \in (0,1), \tag{2}$$

where $n = \lceil \alpha \rceil$, i.e., n is the first integer which is not less than α; $x^{(n)}$ is the general n-order derivative and J^γ is the γ-order Riemann–Liouville integral operator expressed as follows:

$$J^\gamma y = \frac{1}{\Gamma(\gamma)} \int_0^t (t-\tau)^{\gamma-1} y(\tau) d\tau, \tag{3}$$

where $\Gamma(.)$ is the gamma function.

Remark 2.1 The major advantage of the Caputo definition is that the initial conditions for fractional-order differential equations take the same form as for integer-order differential equations.

Remark 2.2 In system (1), the fractional-order system is called a commensurate fractional-order system if $\alpha_1 = \alpha_2 = \alpha_3 = \alpha_4$, otherwise the system is called an incommensurate fractional-order system.

Remark 2.3 Note that many hyperchaotic systems can be described by the proposed class (1). Table 1 details this class of fractional-order hyperchaotic systems.

3 Sliding Mode Control of a Fractional-Order Hyperchaotic System and Stability Analysis

In the following context, we shall design a sliding mode controller to establish the asymptotic stability of the fractional-order hyperchaotic system in question.

3.1 Control design via the sliding mode methodology

Let us consider the fractional-order hyperchaotic system (1), which is perturbed by the uncertainty $\Delta g(x)$ of $g(x)$ and the external disturbance $d(t)$.
Now, the control technique will be employed as

$$\begin{cases} D^{\alpha_1} x_1 = x_2 f(x) - \xi_1(x), \\ D^{\alpha_2} x_2 = g(x) - \beta x_2 + \Delta g(x) + d(t) + u, \\ D^{\alpha_3} x_3 = x_2 h(x) - \xi_2(x), \\ D^{\alpha_4} x_4 = x_2 k(x) - \xi_3(x). \end{cases} \tag{4}$$

In the sequel, the following assumptions are required.
Assumptions.
* Suppose that f, g, k, h and ξ_j, $j = 1,2,3$ are required to ensure the existence and uniques of the system (4) in the presence of the uncertainty $\Delta g(x)$ and the external disturbance $d(t)$ under the controller u in the interval $[t_0, +\infty[$, $t_0 > 0$ for any given initial condition.
* The uncertainties $\Delta g(x)$ and the external perturbation $d(t)$ are always bounded. Suppose that m_1, m_2 are the upper bound of $\Delta g(x)$ and $d(t)$, respectively, i.e.,

$$\begin{cases} \|\Delta g(x)\| \le m_1, \\ \|d(t)\| \le m_2. \end{cases} \tag{5}$$

Name and Mode	$f(.), g(.), h(.)$ and $k(.)$	$\xi_1(.), \xi_2(.)$ and $\xi_3(.)$
Lorenz's system [14] $\begin{cases} D^{\alpha_1}x_1 = a(x_2 - x_1) + x_4, \\ D^{\alpha_2}x_2 = cx_1 - x_1x_3 - x_2, \\ D^{\alpha_3}x_3 = x_1x_2 - bx_3, \\ D^{\alpha_4}x_4 = -x_2x_3 + rx_4 \end{cases}$	$\begin{cases} f(x) = a, \\ g(x) = cx_1 - x_1x_3, \\ h(x) = x_1, \\ k(x) = -x_3 \end{cases}$	$\begin{cases} \xi_1(x) = -ax_1 + x_4, \\ \xi_2(x) = -bx_3, \\ \xi_3(x) = rx_4 \end{cases}$
Chen's system [15] $\begin{cases} D^{\alpha_1}x_1 = a(x_2 - x_1) + x_4, \\ D^{\alpha_2}x_2 = dx_1 + cx_2 - x_1x_3, \\ D^{\alpha_3}x_3 = x_1x_2 - bx_3, \\ D^{\alpha_4}x_4 = x_2x_3 + kx_4. \end{cases}$	$\begin{cases} f(x) = a, \\ g(x) = cx_1 - x_1x_3, \\ h(x) = x_1, \\ k(x) = -x_3 \end{cases}$	$\begin{cases} \xi_1(x) = -ax_1 + x_4, \\ \xi_2(x) = -bx_3, \\ \xi_3(x) = rx_4 \end{cases}$
Liu's system [16] $\begin{cases} D^{\alpha_1}x_1 = a(x_2 - x_1), \\ D^{\alpha_2}x_2 = bx_1 - x_4 + x_1x_3, \\ D^{\alpha_3}x_3 = -x_1x_2 - cx_3 + x_4, \\ D^{\alpha_4}x_4 = x_2 + dx_1. \end{cases}$	$\begin{cases} f(x) = a, \\ g(x) = bx_1 - x_4 + x_1x_3, \\ h(x) = -x_1, \\ k(x) = 1 \end{cases}$	$\begin{cases} \xi_1(x) = -ax_1, \\ \xi_2(x) = -cx_3 + x_4, \\ \xi_3(x) = dx_1 \end{cases}$
Finance's system [17] $\begin{cases} D^{\alpha_1}x_1 = x_3 + (x_2 - a)x_1 + x_4, \\ D^{\alpha_2}x_2 = 1 - bx_2 - x_2^2, \\ D^{\alpha_3}x_3 = -x_1 - cx_3, \\ D^{\alpha_4}x_4 = -dx_1x_2 - kx_4. \end{cases}$	$\begin{cases} f(x) = x_1, \\ g(x) = 1 - x_1^2, \\ h(x) = 0, \\ k(x) = -dx_1 \end{cases}$	$\begin{cases} \xi_1(x) = x_3 - ax_1 + x_4, \\ \xi_2(x) = -x_1 - cx_3, \\ \xi_3(x) = -kx_4 \end{cases}$
Lü's system [18] $\begin{cases} D^{\alpha_1}x_1 = a(x_2 - x_1) + x_4, \\ D^{\alpha_2}x_2 = cx_2 - x_1x_3, \\ D^{\alpha_3}x_3 = x_1x_2 - bx_3, \\ D^{\alpha_4}x_4 = x_1x_3 + dx_4. \end{cases}$	$\begin{cases} f(x) = a, \\ g(x) = -x_1x_3, \\ h(x) = x_1, \\ k(x) = 0 \end{cases}$	$\begin{cases} \xi_1(x) = -ax_1 + x_4, \\ \xi_2(x) = -bx_3, \\ \xi_3(x) = x_1x_3 + dx_4 \end{cases}$

Table 1: The class of fractional-order hyperchaotic systems characterized by the class (1).

To ensure the asymptotic stability of the dynamical system (4) on the switching surface, the fractional integral-type sliding mode surface s is selected as

$$s(t) = D^{\alpha_1 - 1}x_2 + \int_0^t \lambda x_2(\tau) + \Psi(\tau)d\tau, \tag{6}$$

where $\Psi(.)$ is a function selected as

$$\Psi(t) = x_1 f(x) + x_3 h(x) + x_4 k(x). \tag{7}$$

The controller gain λ has been introduced in the sliding mode surface s to confirm that the dynamics of the system will be stabilized quickly.

It is well known that for the sliding mode technique, the sliding surface and its derivative must satisfy

$$s(t) = 0, \quad \dot{s}(t) = D^{\alpha_1}x_2 + \lambda x_2 + x_1 f(x) + x_3 h(x) + x_4 k(x) = 0. \tag{8}$$

Therefore, the equivalent control law is obtained by

$$\begin{aligned} u_{eq} &= D^{\alpha_2}x_2 - g(x) - \Delta g(x) - d(t) + \beta x_2 \tag{9} \\ &= -g(x) - \Delta g(x) - d(t) - x_1 f(x) - x_3 h(x) - x_4 k(x) + (\beta - \lambda)x_2. \tag{10} \end{aligned}$$

In the real world applications, $\Delta g(x)$ and $d(t)$ are unknown. Therefore the equivalent control input is modified to

$$u_{eq} = -g(x) - x_1 f(x) - x_3 h(x) - x_4 k(x) + (\beta - \lambda)x_2. \tag{11}$$

To design the reaching mode control scheme, which drives the states onto the sliding surface, the reaching law can be selected as

$$u_{ad} = -\eta sign(s), \tag{12}$$

where

$$sgn(s) = \begin{cases} 1, & s > 0, \\ 0, & s = 0, \\ -1, & s < 0 \end{cases} \tag{13}$$

represents the sign function, and η is the reach gain of the controller, which is a positive constant. In this way, the total control law is constructed as

$$\begin{aligned} u &= u_{eq} + u_{ad} \\ &= -x_1 f(x) - x_3 h(x) - x_4 k(x) - g(x) + (\beta - \lambda)x_2 - \eta sign(s). \end{aligned} \tag{14}$$

3.2 Stability analysis

Theorem 3.1 *If the controller u is selected as in the equation(14), then the trajectories of the fractional-order dynamics (4) converge to the sliding surface $s(t) = 0$ for $m_1 + m_2 < \eta$.*

Proof. Define the following Lyapunov functional candidate:

$$V = \frac{1}{2}s^2. \tag{15}$$

The time derivative of V is given by

$$\begin{aligned} \dot{V} &= \dot{s}s = \left\{ D^{\alpha 2}x_2 + \lambda x_2 + x_1 f(x) + x_3 h(x) + x_4 k(x) \right\} s \\ &= \left\{ g(x) - \beta x_2 + \Delta g(x) + d(t) + u + \lambda x_2 + x_1 f(x) + x_3 h(x) + x_4 k(x) \right\} s \\ &= \left\{ \Delta g(x) + d(t) - \eta sign(s) \right\} s \\ &\leq (m_1 + m_2 - \eta)\,|s|\,. \end{aligned} \tag{16}$$

Equation (16) implies that as long as suitable m_1, m_2 and η, which satisfy $m_1 + m_2 < \eta$, are selected, one obtains $\dot{V} < 0$.

In view of Barbalat's lemma [19], it can be concluded that $s, \dot{s} \in L_\infty$. As $t \to \infty$, s approaches zero, which shows that all trajectories of the proposed system will converge to the sliding surface $s(t) = 0$. This completes the proof.

Remark 3.1 In the case when the system uncertainty and external disturbance are ignored and if the controller u is selected as in equation(14), the trajectories of the fractional-order systems (4) converge to the sliding surface $s(t) = 0$ for all $\eta > 0$.

Proof. Define the following Lyapunov functional candidate:

$$V = \frac{1}{2}s^2. \tag{17}$$

The time derivative of V is given by

$$
\begin{aligned}
\dot{V} &= \dot{s}s = \left\{ D^{\alpha 2}x_2 + \lambda x_2 + x_1 f(x) + x_3 h(x) + x_4 k(x) \right\} s \\
&= \left\{ g(x) - \beta x_2 + \Delta g(x) + d(t) + u + \lambda x_2 + x_1 f(x) + x_3 h(x) + x_4 k(x) \right\} s \\
&= -\eta sign(s)s \\
&= -\eta \left| s \right| < 0.
\end{aligned}
\tag{18}
$$

In view of Barbalat's lemma [19], it can be concluded that $s, \dot{s} \in L_\infty$. As $t \to \infty$, s approaches zero, which shows that all trajectories of the proposed system will converge to the sliding surface $s(t) = 0$, for all $\eta > 0$.

4   Simulation Results

To illustrate the performance of the proposed control approach, we present two examples, namely, fractional-order hyperchaotic Liu's system and fractional-order hyperchaotic Lorenz's system. Numerical simulations are implemented using the MATLAB software.

4.1   Sliding mode control design of hyperchaotic Liu's system

Here, we will firstly consider a case when the system uncertainty and external disturbance are ignored. By introducing the control input to the second state equation of fractional-order hyperchaotic Liu's system, the controlled system is derived as

$$
\begin{cases}
D^{\alpha_1}x_1 = a(x_2 - x_1), \\
D^{\alpha_2}x_2 = bx_1 - x_4 + x_1 x_3 + u, \\
D^{\alpha_3}x_3 = -x_1 x_2 - cx_3 + x_4, \\
D^{\alpha_4}x_4 = x_2 + dx_1.
\end{cases}
\tag{19}
$$

For the fractional order values $\alpha_1 = 0.98$, $\alpha_2 = 0.97$, $\alpha_3 = 0.97$ and $\alpha_4 = 0.98$, the system (19) without the controller u exhibits a hyperchaotic behavior, as shown in Figure 1, when the parameters are given by

$$
(a, b, c, d, k) = (10, 35, 1.4, 5),
\tag{20}
$$

and the initial value is taken as

$$
(x_1(0), x_2(0), x_3(0), x_4(0))^T = (10, 15, 1, 1)^T.
\tag{21}
$$

The sliding surface is given by

$$
S(t) = D^{\alpha_1 - 1}x_2 + \int_0^t \lambda x_2(\tau) + \Psi(\tau)d\tau,
\tag{22}
$$

where

$$
\Psi(t) = ax_1 - x_1 x_3 + x_4.
\tag{23}
$$

According to the general control law given by equation(14), the vector controller u can be designed as

$$
u = -(a + b)x_1 - \lambda)x_2 - \eta sign(s).
\tag{24}
$$
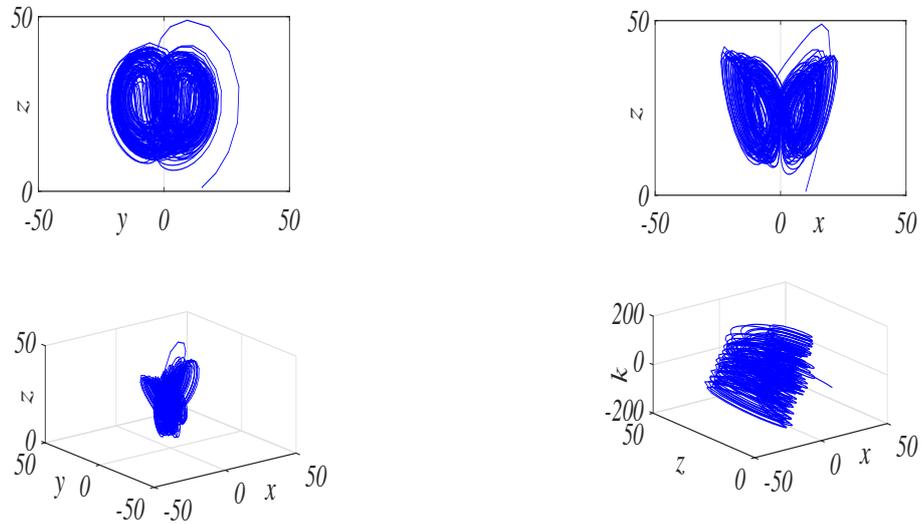
Figure 1: Hyperchaotic attractors of Liu's system (19).
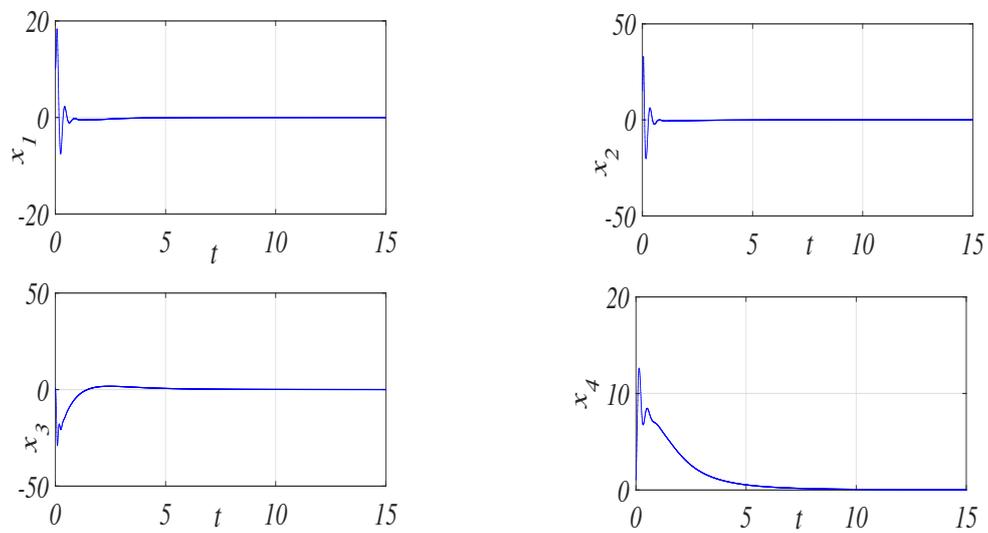
Figure 2: Time-history of the controlled states of equation(19).

With the gain of control law $\eta = 0.02$ and the parameter $\lambda = 0.01$, the states x_1, x_2, x_3 and x_4 of the system (19) with the sliding surface (22) in the presence of the controller (24) are illustrated in Figure 2.

From Figure 2, it is clear that the control law (24) is efficient for controlling fractional-

order hyperchaotic Liu's system.

4.2   Sliding mode control design of uncertain hyperchaotic Lorenz's system

In this part, we consider the fractional-order version of hyperchaotic Lorenz's system in the presence of uncertainty and external disturbance, which is expressed as

$$\begin{cases} D^{\alpha_1} x_1 = a(x_2 - x_1) + x_4, \\ D^{\alpha_2} x_2 = cx_1 - x_1 x_3 - x_2 + \Delta g(x) + d(t) + u, \\ D^{\alpha_3} x_3 = x_1 x_2 - bx_3, \\ D^{\alpha_4} x_4 = -x_2 x_3 + rx_4. \end{cases} \tag{25}$$

For the fractional order values $\alpha_1 = 0.95$, $\alpha_2 = 0.96$, $\alpha_3 = 0.96$ and $\alpha_3 = 0.97$, the system
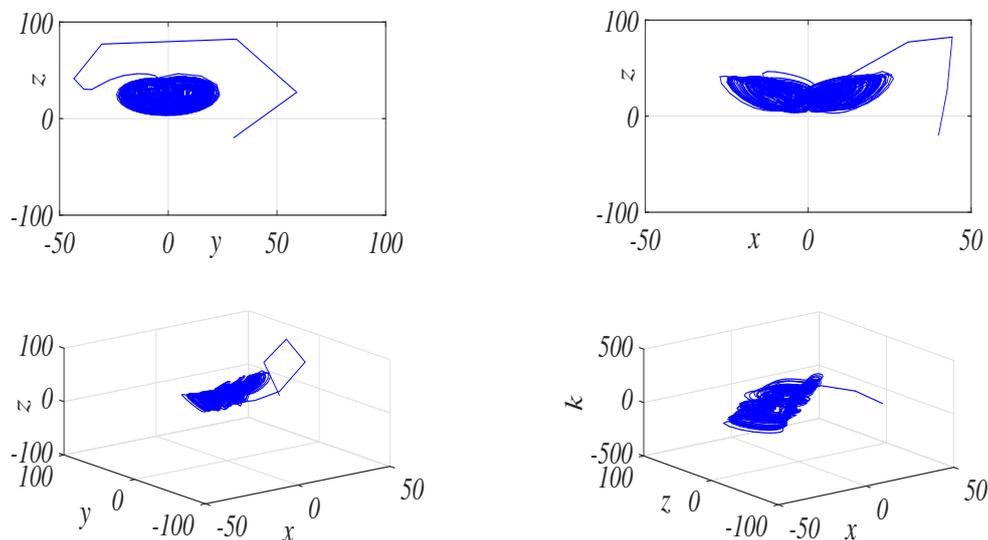
Figure 3: Hyperchaotic attractors of the Lorenz's System (25).

(25) without the uncertainty $\Delta g(x)$, the external disturbance $d(t)$ and the controller u, exhibits a hyperchaotic behavior, as shown in Figure 3, when the parameters of the system are given by

$$(a, b, c, r) = (10, \frac{8}{3}, 28, -1), \tag{26}$$

and the initial value

$$(x_1(0), x_2(0), x_3(0), x_4(0))^T = (40, 30, -20, -50)^T. \tag{27}$$

The uncertainty $\Delta f(x)$ applied to the system is given by

$$\Delta g(x) = 0.05 \cos(2x_2). \tag{28}$$

The external disturbances $d(t)$ are defined as

$$d(t) = 0.02 \sin(2t). \tag{29}$$
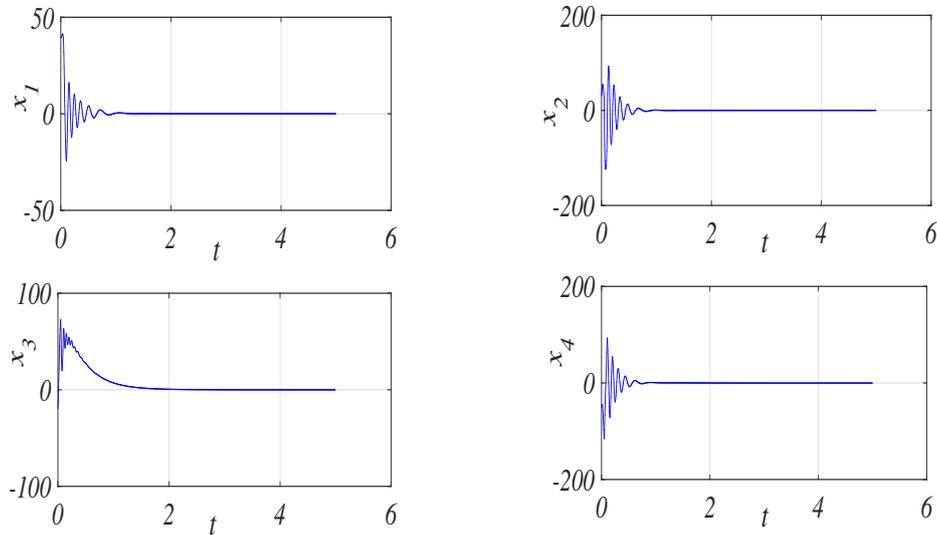
Figure 4: Time-history of the controlled states of equation (25).

The sliding surface is given by

$$s(t) = D^{\alpha_1 - 1}x_2 + \int_0^t \lambda x_2(\tau) + \Psi(\tau)d\tau, \tag{30}$$

where

$$\Psi(t) = ax_1 + x_1x_3 - x_3x_4. \tag{31}$$

According to the general control law given by equation(14), the vector controller u can be designed as:

$$u = -(a+c)x_1 + x_3x_4 + (1-\lambda)x_2 - \eta sign(s). \tag{32}$$

With the gain of control law $\eta = 0.02$ and the positive parameter $\lambda = 1$, the states x_1, x_2, x_3 and x_4 of the system (25) with the sliding surface (30) in the presence of the controller (32) are illustrated in Figure 4. From Figure 4, the control law (32) is capable of controlling fractional-order hyperchaotic Lorenz's system in the presence of uncertainty and external disturbance.

5   Conclusion

In this paper, a novel class of fractional-order hyperchaotic systems with uncertainty and external disturbance has been proposed. Based on the Lyapunov stability theorem, a sliding mode control law has been designed to control hyperchaos in such fractional-order systems. The sliding mode controller has been shown to guarantee the asymptotic stability of the proposed fractional-order hyperchaotic systems in the presence of uncertainty and external disturbance. From the numerical examples for the class of fractional-order Liu and Lorenz systems, it is obvious that a satisfying control performance can be realised by using the proposed scheme.

Acknowledgements

References

[1] S. Sutha, P. Lakshmi and S. Sankaranarayanan. Fractional-order sliding mode controller design for a modified quadruple tank process via multi-level switching. *Comput. Electr. Eng.* **45** (2015) 10–21.

[2] T. T. Hartley, C. F. Lorenzo and H. K. Qammar. Chaos in a fractional order Chua system. *IEEE Trans. Circuits Syst. I.* **42** (8) (1996) 485–490.

[3] I. M. Olga, A. K. Alexey, and E. H. Alexander. Generalized synchronization of chaos for secure communication: remarkable stability to noise. *Physics Letters A* **374** (29) (2010) 2925–2931.

[4] E. Inzunza-Gonzalez and C. Cruz-Hernandez. Double hyperchaotic encryption for security in biometric systems. *Nonlinear Dynamics and Systems Theory* **13** (1) (2013) 55–68.

[5] S. Kaouache and M. S. Abdelouahab. Generalized synchronization between two chaotic fractional non-commensurate order systems with different dimensions. *Nonlinear Dynamics and Systems Theory* **18** (3) (2018) 273–284.

[6] S. Kaouache and M. S. Abdelouahab. Modified projective synchronization between integer order and fractional order hyperchaotic systems *Jour. of Adv. Research in Dynamical and Control Systems* **10** (5) (2018) 96–104.

[7] J. H. Park. Adaptive control for modified projective synchronization of a four-dimensional chaotic system with uncertain parameters. *J. Comput. Appl. Math.* **213** (1) (208) 288–293.

[8] K. S. Ojo, A. N. Njah, S. T. Ogunjo and O. I. Olusola. Reduced Order Function Projective Combination Synchronization of Three Josephson Junctions Using Backstepping Technique. *Nonlinear Dynamics and Systems Theory* **14** (2) (2014) 119–133.

[9] A. Poursamad and A. H. Davaie-Markazi. Robust adaptive fuzzy control of unknown chaotic systems. *Appl. Soft. Comput.* **9** (3) (2009) 970–976.

[10] M. Tavazoei and M. Haeri. Synchronization of chaotic fractional-order systems via active sliding mode controller. *Physica A: Statistical Mechanics and its Applications* **387** (2008) 57–70.

[11] M. Roopaei, B. R. Sahraei and T. C. Lin. Adaptive sliding mode control in a novel class of chaotic systems. *Communications in Nonlinear Science and Numerical Simulation* **15** (12) (2010) 4158–4170.

[12] C. Yin, S. M. Zhong and W. F. Chen. Design of sliding mode controller for a class of fractional-order chaotic systems. *Communications in Nonlinear Science and Numerical Simulation* **17** (1) (2012) 356–366.

[13] I. Podlubny. *Fractional Differential Equations.* Academic Press, San Diego, 1999.

[14] X. Y. Wang and J. M. Song. Synchronization of the fractional order hyperchaos Lorenz systems with activation feedback control. *Commun. Nonlinear Sci. Numer. Simul.* **14** (8) (2009) 3351–3357.

[15] X. Li. Modified projective synchronization of a new hyperchaotic system via nonlinear control. *Chin. Phys. B* **52** (2009) 274–278.

[16] L. Liu, C. Liu and Y. Zhang. Analysis of a novel four-dimensional hyperchaotic system. *Chin. J. Phys.* **46** (2008) 386–393.

[17] H. Yu, G. Cai and Y. Li. Dynamic analysis and control of a new hyperchaotic finance system. *Nonlinear Dyn.* **67** (2012) 2171–2181.

[18] A. Chen, J. Lu, J. Lű and S. Yu. Generating hyperchaotic Lu attractor via state feedback control. *Physica A* **364** (2006) 103–110.

[19] H. K. Khalil. *Nonlinear Systems.* 2nd ed., Prentice Hall, New Jersey, USA, 2001.

Stochastic Dengue Mathematical Model in the Presence of *Wolbachia*: Exploring the Disease Extinction

M. Z. Ndii [1*] and A. K. Supriatna [2]

[1] *Department of Mathematics, University of Nusa Cendana, Kupang-NTT, Indonesia*
[2] *Department of Mathematics, Padjadjaran University, Jawa Barat, Indonesia*

Abstract: A new strategy against dengue is proposed by the use of the *Wolbachia* bacterium. In this paper, we analyse the effects of *Wolbachia* on dengue transmission dynamics using deterministic and stochastic epidemic models. The reduction in the reproduction number is measured and the probability of disease extinction is determined. We found that *Wolbachia* can reduce the reproduction number by up to 64%. We also found that the probability of extinction is around 90%, although the reproduction number is slightly above one. However, if the reproduction number is too high, which indicates a higher transmission level, the probability of disease extinction is smaller. Consequently, an outbreak is likely to take off. The results suggest that *Wolbachia* can be effective to reduce dengue transmission, particularly in areas with low to moderate transmission level.

Keywords: *Wolbachia; mathematical model; dengue; stochastic; probability; extinction.*

Mathematics Subject Classification (2010): 93E03, 92B05, 37N25.

1 Introduction

Dengue is a vector-borne disease transmitted via the bite of mosquitoes. Over half of the world's population is at risk of dengue, particularly in tropical and subtropical areas. Around 390 million cases happen annually [1] and can result in a higher fatality rate when no proper treatment is conducted [2].

The traditional strategies such as insecticide have been found less effective and hence an innovative biological strategy by the use of the *Wolbachia* bacterium has been proposed [3–6]. *Wolbachia* reduces the level of dengue virus in salivary glands, which lower

---

* Corresponding author: mailto:meksianis.ndii@staf.undana.ac.id

214

the transmission probability [3, 7]. It also reduces the mosquito's lifespan, and hence mosquitoes have less time to transmit dengue. Furthermore, *Wolbachia* reduces the reproductive rate [3] and causes an effect called the bendy proboscis which leads to a reduced biting rate [8]. Additionally, there is a reproductive advantage for female mosquitoes since *Wolbachia* gives the so-called cytoplasmic incompatibility (CI) [9, 10]. The CI causes the *Wolbachia*-carrying females to reproduce when mating with the non-*Wolbachia* or *Wolbachia*-carrying males. On the other hand, non-*Wolbachia* females can only reproduce when mating with non-*Wolbachia* males.

The field trials of releasing *Wolbachia*-carrying mosquitoes have been conducted in several places including Indonesia. The results show that *Wolbachia*-carrying mosquitoes can persist in the population [11]. This is align with the results from mathematical analysis [12, 13]. The next crucial step is to determine the effectiveness of the *Wolbachia* intervention when it is implemented in the field.

Mathematical models have been widely used to understand the life sciences and technology-related problems [14–17]. A number of mathematical models have been developed to measure the effectiveness of *Wolbachia* to reduce dengue transmission [18–22]. They showed that *Wolbachia* can reduce dengue transmission by up to 80% and is highly effective in areas with low to moderate transmission level. However, these models are deterministic and do not take into account the effects of stochasticity. For a small population size, a stochastic approach is more appropriate. In this paper, stochastic epidemic models in the absence and presence of *Wolbachia* have been developed to measure the effectiveness of the *Wolbachia* intervention. The models are based on the deterministic mathematical models formulated by Ndii *et al.* [19, 21]. Furthermore, the reproduction number and the probability of extinction are determined. This paper is organised as follows. Section 2 presents the deterministic and stochastic model in the absence of *Wolbachia* and derivation of the probability generating function. Section 3 presents deterministic and stochastic models in the presence of *Wolbachia* and considers the derivation of the probability generating function. Results are presented in Section 4. The discussion and conclusions are presented at the end of the paper.

2   Mathematical Model in the Absence of *Wolbachia*

The determinsitic and stochastic epidemic models in the absence of *Wolbachia* are presented. A deterministic model serves as a basis for the development of a stochastic epidemic model [23, 24].

2.1   Deterministic model

In this section, a deterministic model in the presence of *Wolbachia* is presented. The model is in the form of a system of differential equations which has been formulated by Ndii *et al.* [21]. The human population is divided into four subpopulations, namely, Susceptible (S_H), Exposed (E_H), Infectious (I_H) and Recovered (R_H). Furthermore, a constant human population size is assumed, and hence the human birth and death rates are assumed to be equal, that is, $B = \mu_H$ and $N_H = S_H + E_H + I_H + R_H$.

The mosquito population is divided into subpopulations of Aquatic (A_N) which consists of eggs, larvae and pupae, Susceptible (S_N), Exposed (E_N) and Infectious (I_N) mosquitoes. The total adult female mosquito population is $F_N = S_N + E_N + I_N$. The subscript N is used to denote the non-*Wolbachia* mosquitoes. We use this subscript here for consistency and to differentiate from the *Wolbachia*-carrying mosquitoes included in

the models in the later sections. We group eggs, larvae and pupae into one compartment as they are not involved in the transmission of dengue. No recovered class is required for mosquitoes as they remain infected for the rest of their lives.

The deterministic mathematical model for dengue in the absence of *Wolbachia* is governed by the following system of differential equations:

$$\frac{dS_H}{dt} = BN_H - \frac{b_N T_N I_N}{N_H} S_H - \mu_H S_H, \tag{1}$$

$$\frac{dE_H}{dt} = \frac{b_N T_N I_N}{N_H} S_H - \gamma_H E_H - \mu_H E_H, \tag{2}$$

$$\frac{dI_H}{dt} = \gamma_H E_H - \sigma I_H - \mu_H I_H, \tag{3}$$

$$\frac{dR_H}{dt} = \sigma I_H - \mu_H R_H, \tag{4}$$

$$\frac{dA_N}{dt} = \rho_N \frac{F_N}{2} \left(1 - \frac{A_N}{K} \right) - (\tau_N + \mu_{NA}) A_N, \tag{5}$$

$$\frac{dS_N}{dt} = \tau_N \frac{A_N}{2} - \left(\frac{b_N T_N I_H}{N_H} + \mu_N(t) \right) S_N, \tag{6}$$

$$\frac{dE_N}{dt} = \left(\frac{b_N T_N I_H}{N_H} \right) S_N - (\gamma_N + \mu_N(t)) E_N, \tag{7}$$

$$\frac{dI_N}{dt} = \gamma_N E_N - \mu_N(t) I_N. \tag{8}$$

The description of parameters is given in Table 2.

When bitten by the infectious mosquitoes, humans have a chance to be exposed to dengue at rate of $b_N T_N I_N / N_H$ (equations (1) and (2)). The parameter b_N is the successful biting rate and T_N is the transmission probability from non-*Wolbachia* mosquitoes to humans and reverse. The exposed humans move to an infectious class at rate of γ_H and recover from dengue at rate of σ.

The aquatic population increases as the male and female mosquitoes mate and breed, but the population growth is limited by the carrying capacity K through a logistic term

$$\rho_N \frac{F_N M_N}{M_N + F_N} \left(1 - \frac{A_N}{K} \right).$$

Since there are equal numbers of male and female mosquitoes, $M_N = F_N$, this becomes $\rho_N F_N (1 - A_N/K)/2$ (equation (5)). The aquatic mosquito population dies at rate of μ_{NA} and mature into susceptible female mosquitoes at rate of τ_N, where only half of the maturing aquatics are female. Susceptible mosquitoes progress to the exposed class after biting infectious humans at rate of $b_N T_N I_H / N_H$. They then become infectious at rate of γ_N (equation (8)), where $1/\gamma_N$ is the extrinsic incubation period.

The reproduction number is obtained by creating the next generation matrix and finding the maximum eigenvalues of that matrix. The reproduction number of that model is given by

$$\mathcal{R}_0^2 = \frac{b_N^2 T_N^2 \gamma_H \gamma_N S_N}{N_H \mu_N \left(\gamma_H + \mu_H\right)\left(\sigma + \mu_H\right)\left(\gamma_N + \mu_N\right)}. \tag{9}$$

2.2 Stochastic model

We developed a stochastic version of deterministic model using a continous-time Markov chain (CTMC) model, where time is continous and the states are discrete. Let

$$X(t) = (S_H(t), E_H(t), I_H(t), A_N(t), S_N(t), E_N(t), I_N(t))$$

denote the discrete-valued random variables. It is assumed that the number of infections produced by an individual type i is independent of the number of infections produced by any other type. The individuals of type i have the same probability generating function (pgf). Let $\{X_{ji}\}_{j=1}^n$ be the offspring random variables for type i, where X_{ji} is the number of infected individuals of type j produced by the individuals of type i. The probability that one individual of type i produces x_j infected individuals of type j is given by

$$P_i(x_1, x_2, ..., x_n) = Prob\left\{X_{1i} = x_1, ..., X_{ni} = x_n\right\}. \tag{10}$$

The corresponding transition probabilities for the model in the absence of *Wolbachia* are

$$\text{Prob}\{\Delta S_H = 1|X)\} = BN_H\Delta t + \mathcal{O}(\Delta t),$$
$$\text{Prob}\{(\Delta S_H, \Delta E_H) = (-1, +1)\} = b_N T_N S_H I_N / N_H \Delta t + \mathcal{O}(\Delta t),$$
$$\text{Prob}\{(\Delta E_H, \Delta I_H) = (-1, +1)\} = \gamma_H E_H \Delta t + \mathcal{O}(\Delta t),$$
$$\text{Prob}\{(\Delta I_H, \Delta R_H) = (-1, +1)\} = \sigma I_H \Delta t + \mathcal{O}(\Delta t),$$
$$\text{Prob}\{(\Delta S_H) = -1\} = \mu_H S_H \Delta t + \mathcal{O}(\Delta t),$$
$$\text{Prob}\{(\Delta E_H) = -1\} = \mu_H E_H \Delta t + \mathcal{O}(\Delta t),$$
$$\text{Prob}\{(\Delta I_H) = -1\} = \mu_H I_H \Delta t + \mathcal{O}(\Delta t),$$
$$\text{Prob}\{(\Delta R_H) = -1\} = \mu_H R_H \Delta t + \mathcal{O}(\Delta t),$$
$$\text{Prob}\{(\Delta E_N) = -1\} = \mu_N E_N \Delta t + \mathcal{O}(\Delta t),$$
$$\text{Prob}\{(\Delta I_N) = -1\} = \mu_N I_N \Delta t + \mathcal{O}(\Delta t), \tag{11}$$
$$\text{Prob}\{(\Delta A_N) = 1\} = (\rho_N F_N/2)(1 - A_N/K)\Delta t + \mathcal{O}(\Delta t),$$
$$\text{Prob}\{(\Delta A_N, \Delta S_N) = (-1, +1)\} = \tau_N/2 A_N \Delta t + \mathcal{O}(\Delta t),$$
$$\text{Prob}\{(\Delta S_N, \Delta E_N) = (-1, +1)\} = b_N T_N S_N I_H / N_H \Delta t + \mathcal{O}(\Delta t),$$
$$\text{Prob}\{(\Delta E_N, \Delta I_N) = (-1, +1)\} = \gamma_N E_N \Delta t + \mathcal{O}(\Delta t),$$
$$\text{Prob}\{(\Delta S_N) = -1\} = \mu_N S_N \Delta t + \mathcal{O}(\Delta t),$$
$$\text{Prob}\{(\Delta E_N) = -1\} = \mu_N E_N \Delta t + \mathcal{O}(\Delta t),$$
$$\text{Prob}\{(\Delta I_N) = -1\} = \mu_N I_N \Delta t + \mathcal{O}(\Delta t).$$

2.3 Continous-time branching processes

We construct the branching process and probability of extinction. The offspring pgf for E_H, given $E_H(0) = 1$ and $I_H(0) = 0$, $E_N(0) = 0$, $I_N(0) = 0$, is

$$f_1(u_1, u_2, u_3, u_4) = \frac{\gamma_H u_2 + \mu_H}{\gamma_H + \mu_H}, \quad u_1, u_2, u_3, u_4 \in [0, 1].$$

The expression $\gamma_H/(\gamma_H + \mu_H)$ means the probability that an exposed individual becomes infectious. The expression $\mu_H/(\gamma_H + \mu_H)$ means the probability that an exposed individual leaves compartment due to death.

The offspring pgf for I_H, given $I_H(0) = 1, E_H(0) = E_N(0) = I_N(0) = 0$, is

$$f_2(u_1, u_2, u_3, u_4) = \frac{(b_N T_N S_N/N_H)u_2 u_3 + \sigma + \mu_H}{(b_N T_N S_N/N_H) + \sigma + \mu_H}, \quad u_1, u_2, u_3, u_4 \in [0, 1].$$

The expression $b_N T_N S_N/N_H/(b_N T_N S_N/N_H + \sigma + \mu_H)$ means the probability that an infectious individual results in a new exposed mosquito. The expression $(\sigma + \mu_H)/(b_N T_N S_N/N_H + \sigma + \mu_H)$ means the probability that an infectious individual leaves the compartment due to recovery or death.

The offspring pgf for E_N, given $E_N(0) = 1, E_H(0) = I_H(0) = I_N(0) = 0$, is

$$f_3(u_1, u_2, u_3, u_4) = \frac{\gamma_N u_4 + \mu_N}{\gamma_N + \mu_N}, \quad u_1, u_2, u_3, u_4 \in [0, 1].$$

The expression $\gamma_N/(\gamma_N + \mu_N)$ means the probability that an exposed mosquito becomes infectious. The expression $\mu_N/(\gamma_N + \mu_N)$ means the probability that an exposed individual leaves compartment due to death.

The probability generating function for I_N, given $I_N(0) = 1, E_N(0) = 0, E_H(0) = 0, I_H(0) = 0$, is

$$f_4(u_1, u_2, u_3, u_4) = \frac{b_N T_N u_1 u_4 + \mu_N}{b_N T_N + \mu_N}, \quad u_1, u_2, u_3, u_4 \in [0, 1].$$

The expression $b_N T_N/(b_N T_N + \mu_N)$ is the probability that an infectious mosquito results in a new exposed individual. The expression $\mu_N/(b_N T_N + \mu_N)$ is the probability that an infectious mosquito leaves the compartment due to death.

The expectation matrix $M_c = [M_{ji}]$ of the pgf is an $n \times n$ non-negative matrix where the elements of that matrix (m_{ij}) are the expected number of offsprings of group j produced by an individual in group i:

$$m_{ji} = \frac{df_i}{du_j}\Big|_{u_1 = \ldots = u_n = 1} < \infty. \tag{12}$$

The extinction threshold is the spectral radius of the expectation matrix, denoted by $\rho(M)$. The elements of the expectation matrix are found using (12).

The expectation matrix of the model is as follows:

$$\mathbb{M} = \begin{bmatrix} 0 & 0 & 0 & \frac{b_N T_N}{b_N T_N + \mu_N} \\ \frac{\gamma_H}{\gamma_H + \mu_H} & \frac{b_N T_N S_N/N_H}{b_N T_N S_N/N_H + \sigma + \mu_H} & 0 & 0 \\ 0 & \frac{b_N T_N S_N/N_H}{b_N T_N S_N/N_H + \sigma + \mu_H} & 0 & 0 \\ 0 & 0 & \frac{\gamma_N}{\gamma_N + \mu_N} & \frac{b_N T_N}{b_N T_N + \mu_N} \end{bmatrix}.$$

The eigenvalues of the expectation matrix are the roots of the characteristic equations

$$\lambda^4 + (A+C)\lambda^3 + CA\lambda^2 - ABCD = 0, \tag{13}$$

where

$$A = \frac{b_N T_N}{b_N T_N + \mu_N}, \quad B = \frac{\gamma_N}{\gamma_N + \mu_N}, \quad C = \frac{b_N T_N S_N / N_H}{b_N T_N S_N / N_H + \sigma + \mu_N}, \quad D = \frac{\gamma_N}{\gamma_N + \mu_N}.$$

Allen and Driessche [25] showed the general relationship between $\mathcal{R}_0$ and $\rho(\mathbb{M})$ as follows:

$$\mathcal{R}_0 < 1(=1, >1) \quad \text{if and only if} \quad \rho(\mathbb{M}) < 1(=1, >1).$$

3 Mathematical Model in the Presence of *Wolbachia*

This section presents a dengue mathematical model in the presence of *Wolbachia*. The model has been formulated by Ndii *et al.* [19, 21]. The model serves as a basis for the development of a stochastic model in the presence of *Wolbachia*.

3.1 Deterministic model

A deterministic model in the presence of *Wolbachia* is governed by the following system of differential equations. We include the model for *Wolbachia*-carrying mosquitoes. The population is divided into Susceptible (S), Exposed (E), Infectious (I) and Recovered (R) compartments. For the mosquito population, there is an aquatic compartment (A). The subscripts H, N, and W represent the human, non-*Wolbachia* and *Wolbachia*-carrying mosquitoes.

In this model, the exposed rate is different to that in the absence of *Wolbachia*. In this model, a susceptible human has been exposed to dengue after being bitten by non-*Wolbachia* or *Wolbachia*-carrying infectious mosquitoes at rate of $b_N T_N I_N / N_H$ or $b_W T_{HW} I_W / N_H$, respectively (see equations (17) and (18)). Here b_W is the biting rate for *Wolbachia*-carrying mosquitoes and T_{HW} is the transmission probability from *Wolbachia*-carrying mosquitoes to humans. Note that the transmission probability from humans to *Wolbachia*-carrying mosquitoes is assumed to be equal to that from humans to non-*Wolbachia* mosquitoes, so $T_{WH} = T_N$. By contrast, there are differences in the transmission probabilities of dengue from mosquitoes to humans for *Wolbachia* and non-*Wolbachia* mosquitoes.

The effects of the cytoplasmic incompatibility and imperfect maternal transmission on the mosquito populations are included in this model. The effect of the CI is incorporated by differences in the mating functions. The non-*Wolbachia* female mosquitoes reproduce when mating with the *Wolbachia* male mosquitoes, and hence it gives

$$\frac{\rho_N F_N M_N}{P}, \tag{14}$$

where $P = F_N + M_N + F_W + M_W$. It is assumed that the ratio of male to female mosquitoes is 1:1, and therefore the equation is reduced to $\rho_N F_N^2 / (2(F_N + F_W))$ (see equation (21)). The aquatic *Wolbachia* mosquitoes are produced when *Wolbachia*-carrying female mosquitoes mate with either non-*Wolbachia* or *Wolbachia* males, giving the term

$$\frac{\rho_W F_W (M_N + M_W)}{P}, \tag{15}$$

where $P = F_N + M_N + F_W + M_W$, which simplifies to $\rho_W F_W/2$ (equation (25)). The growth of aquatic mosquitoes is limited by the carrying capacity K, so that each mating function is multiplied by

$$\frac{A_N + A_W}{K}. \tag{16}$$

The *Wolbachia*-carrying aquatic mosquitoes mature to be the *Wolbachia*-carrying adult mosquitoes at rate of τ_W. To capture the imperfect maternal transmission of *Wolbachia* [3, 26], it is assumed that a proportion α of them become *Wolbachia*-carrying adults and the rest $(1 - \alpha)$ become non-*Wolbachia* adults (see equations (22) and (26)).

The mathematical model in the presence of *Wolbachia* is governed by the following system of differential equations:

$$\frac{dS_H}{dt} = BN_H - \frac{b_N T_N I_N}{N_H} S_H - \frac{b_W T_{HW} I_W}{N_H} S_H - \mu_H S_H, \tag{17}$$

$$\frac{dE_H}{dt} = \frac{b_N T_N I_N}{N_H} S_H + \frac{b_W T_{HW} I_W}{N_H} S_H - \gamma_H E_H - \mu_H E_H, \tag{18}$$

$$\frac{dI_H}{dt} = \gamma_H E_H - \sigma I_H - \mu_H I_H, \tag{19}$$

$$\frac{dR_H}{dt} = \sigma I_H - \mu_H R_H, \tag{20}$$

$$\frac{dA_N}{dt} = \rho_N \frac{F_N^2}{2(F_N + F_W)} \left(1 - \frac{(A_N + A_W)}{K}\right) - (\tau_N + \mu_{NA}) A_N, \tag{21}$$

$$\frac{dS_N}{dt} = \tau_N \frac{A_N}{2} + (1 - \alpha) \tau_W \frac{A_W}{2} - \left(\frac{b_N T_N I_H}{N_H} + \mu_N(t)\right) S_N, \tag{22}$$

$$\frac{dE_N}{dt} = \frac{b_N T_N I_H}{N_H} S_N - (\gamma_N + \mu_N(t)) E_N, \tag{23}$$

$$\frac{dI_N}{dt} = \gamma_N E_N - \mu_N(t) I_N, \tag{24}$$

$$\frac{dA_W}{dt} = \rho_W \frac{F_W}{2} \left(1 - \frac{(A_N + A_W)}{K}\right) - (\tau_W + \mu_{WA}) A_W, \tag{25}$$

$$\frac{dS_W}{dt} = \tau_W \alpha \frac{A_W}{2} - \left(\frac{b_W T_N I_H}{N_H} + \mu_W(t)\right) S_W, \tag{26}$$

$$\frac{dE_W}{dt} = \frac{b_W T_N I_H}{N_H} S_W - (\gamma_W + \mu_W(t)) E_W, \tag{27}$$

$$\frac{dI_W}{dt} = \gamma_W E_W - \mu_W(t) I_W. \tag{28}$$

By using the concept of the next generation matrix, we obtain the reproduction number of the model in the presence of *Wolbachia* as

$$\mathbb{R}_0 = \frac{b_N^2 T_N^2 \gamma_N \gamma_H S_N}{(\gamma_N + \mu_N)\mu_N(\gamma_H + \mu_H)(\sigma + \mu_H)N_H} + \frac{b_W^2 T_{HW} \gamma_W T_N \gamma_H S_W}{(\gamma_W + \mu_W)\mu_W(\sigma + \mu_H)(\gamma_H + \mu_H)N_H}. \tag{29}$$

3.2   Stochastic model

A stochastic model in the presence of *Wolbachia* is presented. The model is a corresponding model of the deterministic model as presented in Ndii *et al.* [19].

Let $X(t) = (S_H(t), E_H(t), I_H(t), R_H(t), S_N(t), E_N(t), I_N(t), S_W(t), E_W(t), I_W(t))$. The corresponding transition probabilities are

$$\text{Prob}\{\Delta S_H = 1|X)\} = BN_H\Delta t + \mathcal{O}(\Delta t),$$
$$\text{Prob}\{(\Delta S_H, \Delta E_H) = (-1, +1)\} = b_N T_N S_H I_N / N_H \Delta t + b_W T_{HW} S_H I_W / N_H \Delta t + \mathcal{O}(\Delta t),$$
$$\text{Prob}\{(\Delta E_H, \Delta I_H) = (-1, +1)\} = \gamma_H E_H \Delta t + \mathcal{O}(\Delta t),$$
$$\text{Prob}\{(\Delta I_H, \Delta R_H) = (-1, +1)\} = \sigma I_H \Delta t + \mathcal{O}(\Delta t),$$
$$\text{Prob}\{(\Delta S_H) = -1\} = \mu_H S_H \Delta t + \mathcal{O}(\Delta t),$$
$$\text{Prob}\{(\Delta E_H) = -1\} = \mu_H E_H \Delta t + \mathcal{O}(\Delta t),$$
$$\text{Prob}\{(\Delta I_H) = -1\} = \mu_H I_H \Delta t + \mathcal{O}(\Delta t),$$
$$\text{Prob}\{(\Delta R_H) = -1\} = \mu_H R_H \Delta t + \mathcal{O}(\Delta t),$$
$$\text{Prob}\{(\Delta A_N) = 1\} = (\rho_N F_N^2 / 2(F_N + F_W))(1 - (A_N + A_W)/K)\Delta t + \mathcal{O}(\Delta t),$$
$$\text{Prob}\{(\Delta A_N, \Delta S_N) = (-1, +1)\} = \tau_N / 2 A_N \Delta t + (1 - \alpha)\tau_W A_W / 2 \Delta t + \mathcal{O}(\Delta t),$$
$$\text{Prob}\{(\Delta S_N, \Delta E_N) = (-1, +1)\} = b_N T_N S_N I_H / N_H \Delta t + \mathcal{O}(\Delta t),$$
$$\text{Prob}\{(\Delta E_N, \Delta I_N) = (-1, +1)\} = \gamma_N E_N \Delta t + \mathcal{O}(\Delta t),$$
$$\text{Prob}\{(\Delta S_N) = -1\} = \mu_N S_N \Delta t + \mathcal{O}(\Delta t),$$
$$\text{Prob}\{(\Delta E_N) = -1\} = \mu_N E_N \Delta t + \mathcal{O}(\Delta t),$$
$$\text{Prob}\{(\Delta I_N) = -1\} = \mu_N I_N \Delta t + \mathcal{O}(\Delta t),$$
$$\text{Prob}\{(\Delta A_W) = 1\} = (\rho_W F_W / 2)(1 - (A_N + A_W)/K)\Delta t + \mathcal{O}(\Delta t),$$
$$\text{Prob}\{(\Delta A_W, \Delta S_W) = (-1, +1)\} = \tau_W \alpha / 2 A_W \Delta t + \mathcal{O}(\Delta t),$$
$$\text{Prob}\{(\Delta S_W, \Delta E_W) = (-1, +1)\} = b_W T_N S_W I_H / N_H \Delta t + \mathcal{O}(\Delta t),$$
$$\text{Prob}\{(\Delta E_W, \Delta I_W) = (-1, +1)\} = \gamma_W E_W \Delta t + \mathcal{O}(\Delta t),$$
$$\text{Prob}\{(\Delta A_W) = -1\} = \mu_{WA} A_W \Delta t + \mathcal{O}(\Delta t),$$
$$\text{Prob}\{(\Delta S_W) = -1\} = \mu_W S_W \Delta t + \mathcal{O}(\Delta t),$$
$$\text{Prob}\{(\Delta E_W) = -1\} = \mu_W E_W \Delta t + \mathcal{O}(\Delta t),$$
$$\text{Prob}\{(\Delta I_W) = -1\} = \mu_N I_N \Delta t + \mathcal{O}(\Delta t).$$

$$(30)$$

3.3   Continous-time branching processes

This section presents the probability generating function (pgf) of the model in the presence of *Wolbachia*. The probability generating function for E_H, given $E_H(0) = 1$, $E_N(0) = E_W(0) = I_H(0) = I_N(0) = I_W(0) = 0$, is

$$\phi_1(u_1, u_2, u_3, u_4, u_5, u_6) = \frac{\gamma_H u_2 + \mu_H}{\gamma_H + \mu_H}, \quad u_1, ..., u_6 \in [0, 1].$$

The offspring probability generating function for I_H, given $I_H(0) = 1$, $E_N(0) = E_W(0) = E_H(0) = I_N(0) = I_W(0) = 0$, is

$$\phi_2(u_1, u_2, u_3, u_4, u_5, u_6) = \frac{b_N T_N S_N / N_H u_2 u_3 + b_W T_N S_W / N_H u_2 u_5 + \sigma + \mu_H}{b_N T_N S_N / N_H + b_W T_N S_W / N_H + \sigma + \mu_H},$$

where $u_1, ..., u_6 \in [0, 1]$. The offspring probability generating function for E_N, given $E_N(0) = 1$, $E_H(0) = E_W(0) = I_H(0) = I_N(0) = I_W(0) = 0$, is

$$\phi_3(u_1, u_2, u_3, u_4, u_5, u_6) = \frac{\gamma_N u_4 + \mu_N}{\gamma_N + \mu_N}, \quad u_1, ..., u_6 \in [0, 1].$$

The probability generating function for I_N, given $I_N(0) = 1$, $E_H(0) = E_W(0) = E_N(0) = I_H(0) = I_W(0) = 0$, is

$$\phi_4(u_1, u_2, u_3, u_4, u_5, u_6) = \frac{b_N T_N u_1 u_4 + \mu_N}{b_N T_N + \mu_N}, \quad u_1, ..., u_6 \in [0, 1].$$

The probability generating function for E_W , given $E_W(0) = 1$, $E_H(0) = E_N(0) = I_N(0) = I_H(0) = I_W(0) = 0$, is

$$\phi_5(u_1, u_2, u_3, u_4, u_5, u_6) = \frac{\gamma_W u_6 + \mu_W}{\gamma_W + \mu_W}, \quad u_1, ..., u_6 \in [0, 1].$$

The probability generating function for I_W, given $I_W(0) = 1$, $E_H(0) = E_W(0) = E_N(0) = I_N(0) = I_H(0)$, is

$$\phi_6(u_1, u_2, u_3, u_4, u_5, u_6) = \frac{b_W T_{HW} u_1 u_6 + \mu_W}{b_W T_{HW} + \mu_W}, \quad u_1, ..., u_6 \in [0, 1].$$

Using the procedure given in equation (12), we obtain the expectation matrix. The expectation matrix is

$\mathbb{M} =$

$$\begin{bmatrix} 0 & 0 & 0 & \frac{b_N T_N}{b_N T_N + \mu_N} & 0 & \frac{b_W T_{HW}}{b_W T_{HW} + \mu_W} \\ \frac{\gamma_H}{\gamma_H + \mu_H} & \frac{b_N T_N S_N / N_H + b_W T_N S_W / N_H}{b_N T_N S_N / N_H + b_W T_N S_W / N_H + \sigma + \mu_H} & 0 & 0 & 0 & 0 \\ 0 & \frac{b_N T_N S_N / N_H}{b_N T_N S_N / N_H + b_W T_N S_W / N_H + \sigma + \mu_H} & 0 & 0 & 0 & \\ 0 & 0 & \frac{\gamma_N}{\gamma_N + \mu_N} & \frac{b_N T_N}{b_N T_N + \mu_N} & 0 & 0 \\ 0 & \frac{b_W T_N S_W / N_H}{b_N T_N S_N / N_H + b_W T_N S_W / N_H + \sigma + \mu_H} & 0 & 0 & 0 & 0 \\ 0 & 0 & 0 & 0 & \frac{\gamma_W}{\gamma_W + \mu_W} & \frac{b_W T_{HW}}{b_W T_{HW} + \mu_W} \end{bmatrix}.$$

The spectral radius of the matrix $\mathbb{M}$ determines whether the system is sub critical, critical or supercritical.

4   Results

This section presents the reproduction number and the probability of disease extinction.

4.1   Reproduction number

We compare the reproduction number of the model in the absence and presence of *Wolbachia*. Therefore, the aims to assess the reduction in the reproduction number and hence the effectiveness of the *Wolbachia* intervention can be determined. The expressions for the reproduction number in the absence and presence of *Wolbachia* are given in equations (9) and (29), respectively. The parameter values for the models are given in Table 2.

The reproduction number for the model in the absence and presence of *Wolbachia* is 3.31 and 1.17, respectively. This shows that there is around 64.65% reduction in the reproduction number. An epidemic would not take off when $\mathcal{R}_0 < 1$, otherwise it will take off. The result implies that the *Wolbachia* intervention can stop dengue transmission in areas with the reproduction number being at most around 3, which indicates a moderate transmission level. This is because the *Wolbachia* intervention can reduce the basic reproduction number below one. When the reproduction number is higher than three, *Wolbachia* can still reduce dengue transmission though the epidemic still takes off. The numerical simulation is presented in Figure 1.
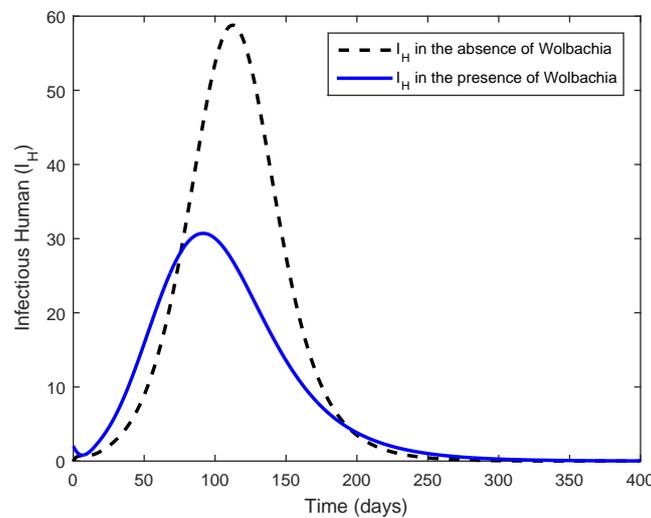
Figure 1: The number of infectious individuals in the absence and presence of *Wolbachia*.

Figure 1 shows that the peak of an outbreak is reduced in the presence of *Wolbachia*. An epidemic peak happens on around the 100th day. Furthermore, the number of infectious individuals at the peak time is around 60. It declines when the *Wolbachia* intervention is implemented. Nevertheless, the end time of epidemic is relatively similar. This indicates that the *Wolbachia* intervention is effective in reducing dengue transmission.

4.2   Probability of extinction

This section presents the probability of extinction ($\mathbb{P}_0$) in the absence and presence of *Wolbachia*. This aims to measure the performance of *Wolbachia* in reducing dengue transmission. When the basic reproduction number is less than one, the probability of extinction is one. Therefore, we investigate the scenario where the reproduction number is greater than one and determine the probability of disease extinction.

The fixed point of the probability generating function is used to determine the probability of extinction

$$\mathbb{P}_0 = \lim_{t \to \infty} \text{Prop}\{I(t) = P(t) = 0\} = \begin{cases} 1, & \text{if } \rho(M) \leq 1, \\ q_k^{i_0^k}, & \text{if } \rho(M) > 1, \end{cases}$$

where q_k is the fixed point of the probability generating function and i_0^k denotes the initial conditions of the infectious individuals of type k.

Table 1: The initial conditions and the probability of extinction in the absence and presence of *Wolbachia*. The initial conditions are for E_H, I_H, E_N, I_N, E_W, I_W. Here W stands for *Wolbachia*.

Initial conditions						$\mathbb{P}_0$ non-W	$\mathbb{P}_0$ with-W
1	0	0	0	0	0	0.6622	0.9470
1	1	0	0	0	0	0.4384	0.8969
2	0	0	0	0	0	0.4385	0.8969
0	2	0	0	0	0	0.4385	0.8969
5	5	0	0	0	0	0.0162	0.5803

The results show that the probability of extinction for the model in the presence of *Wolbachia* is higher than that in the absence of *Wolbachia*. Furthermore, it is found that the probability of extinction declines when the initial number of infected individuals increases. In the absence of *Wolbachia*, the probability of extinction is around 0.6622. It becomes 0.9470 when *Wolbachia*-carrying mosquitoes are introduced into the population. Furthermore, the probability of extinction is close to 60% when there are 10 initially infected individuals in the population. However, the probability of extinction is close to zero for the same initial condition without the *Wolbachia* intervention.

5   Discussion and Conclusion

In this paper, we formulated stochastic models for dengue in the presence of *Wolbachia*. This research aims to measure the effectiveness of the *Wolbachia* intervention to reduce dengue transmission. We determine the proportion of reduction in the basic reproduction number and also the probability of extinction. The result shows that there is around 64% reduction in the basic reproduction number in the presence of *Wolbachia*. This is relatively similar to the result found by Ferguson *et al.* [18]. They found a reduction of 65-75% in the basic reproduction number when the *Wolbachia* intervention is implemented. Furthermore, when the reproduction number is significantly high, the reduction in the reproduction number is not sufficient to end dengue transmission. This is similar to the result obtained by Hughes and Britton [27]. The results imply that the *Wolbachia* intervention may be effective in regions with moderate transmission level.

The mathematical expression of the probability of extinction is derived. We found that the probability of extinction is higher in the presence of *Wolbachia*-carrying mosquitoes than that in the absence of *Wolbachia*. A 90% chance of disease extinction is obtained when the *Wolbachia* intervention is implemented. Around 60% chance of disease extinction is still obtained, although the number of the initially infected individuals is around ten. This implies that a *Wolbachia* intervention can be effective in reducing dengue transmission.

It can be concluded that the use of the *Wolbachia* bacterium can be an alternative strategy against dengue where the probability of disease extinction can reach 90%. Additionally, the use of the *Wolbachia* bacterium would be effective in reducing dengue transmission, particularly in areas with moderate transmission level. Therefore, the combination of the *Wolbachia* bacterium and the other strategy such as vaccination may be needed to optimise the delivery of the intervention.

References

[1] S. Bhatt, P. W. Gething, O. J. Brady, J. P. Messina, A. W. Farlow, et al. The global distribution and burden of dengue. *Nature* **496** (2013) 1476–4687.

[2] World Health Organisation. Dengue and severe dengue Fact sheet No.117, http://www.who.int/mediacentre/factsheets/fs117/en/, [Online; accessed 03 March 2015] (February 2015).

[3] T. Walker, P. H. Johnson, L. A. Moreira, I. Iturbe-Ormaetxe, F. D. Frentiu, et al. The *WMel Wolbachia* strain blocks dengue and invades caged Aedes aegypti populations. *Nature* **476** (2011) 450–453.

[4] A. A. Hoffmann, B. L. Montgomery, J. Popovici, I. Iturbe-Ormaetxe, P. H. Johnson, et al. Successful establishment of *Wolbachia* in *Aedes* populations to suppress dengue transmission. *Nature* **476** (2011) 454–457.

[5] L. Lambrechts, N. M. Ferguson, E. Harris, E. C. Holmes, E. A. McGraw, S. L. O'Neill, E. E. Ooi, S. A. Ritchie, P. A. Ryan, T. W. Scott, C. P. Simmons, S. C. Weaver. Assessing the epidemiological effect of *Wolbachia* for dengue control. *The Lancet Infectious Diseases* **15** (2015) 862–866.

[6] Y. H. Ye, A. M. Carrasco, F. D. Frentiu, S. F. Chenoweth, N. W. Beebe, A. F. van den Hurk, C. P. Simmons, S. L. O'Neill, and E. A. McGraw. *Wolbachia* reduces the transmission potential of dengue-infected *Aedes aegypti. PLoS Neglected Tropical Diseases* **9** (2015) e0003894.

[7] F. D. Frentiu, T. Zakir, T. Walker, J. Popovici, A. T. Pyke, A. van den Hurk, E. A. McGraw, S. L. O'Neill. Limited dengue virus replication in field-collected *Aedes aegypti* mosquitoes infected with *Wolbachia. PLoS Negl Trop Dis.* **8** (2014) e2688.

[8] A. P. Turley, L. A. Moreira, S. L. O'Neill, E. A. McGraw. *Wolbachia* infection reduces blood-feeding success in the dengue fever mosquito, *Aedes aegypti. PLoS Neglected Tropical Diseases.* **3** (2009) e516.

[9] M. Turelli. Cytoplasmic incompatibility in populations with overlapping generations. *Evolution* **64** (2010) 232-241.

[10] H. L. Yeap, P. Mee, T. Walker, A. R. Weeks, S. L. O'Neill, et al., Dynamics of the "Popcorn" *Wolbachia* infection in outbred *Aedes aegypti* informs prospects for mosquito vector control. *Genetics* **187** (2011) 583-595.

[11] A. A. Hoffmann, I. Iturbe-Ormaetxe, A. G. Callahan, B. L. Phillips, K. Billington, J. K. Axford, B. Montgomery, A. P. Turley, and S. L. O'Neill, Stability of the *wMel Wolbachia* infection following invasion into *Aedes aegypti* populations. *PLoS Neglected Tropical Diseases* **8** (2014) e3115.

[12] M. Z. Ndii, R. I. Hickson, and G. N. Mercer, Modelling the introduction of *Wolbachia* into *Aedes aegypti* to reduce dengue transmission. *The ANZIAM Journal* **53** (2012) 213–227.

[13] A. K. Supriatna, N. Anggriani, Melanie, and H. Husniah, The optimal strategy of *Wolbachia*- infected mosquitoes release program: An application of control theory in controlling dengue disease. In: *Proc. International Conference on Instrumentation, Control and Automation (ICA).* Bandung, Indonesia, 2016, 38–43.

[14] M. Z. Ndii, N. Anggriani, and A. K. Supriatna. Application of differential transformation method for solving dengue transmission mathematical model. In: *AIP Conference Proceedings*. Bandung, Indonesia, 2018, 020012.

[15] S. A. Alharbi, A. S. Rambely and A. O. Almatroud. Dynamic modelling of boosting the immune system and its functions by vitamins intervention. *Nonlinear Dynamics and System Theory* **19** (2) (2019) 263–273.

[16] B. Benaid, H. Bouzahir, C. Imzegouan, and F. E. Guezar. Stability analysis for stochastic neural networks with markovian switching and infinite delay in a phase space. *Nonlinear Dynamics and System Theory* **19** (3) (2019) 372–385.

[17] S. Boudiar, A. Ouannas, S. Bendoukha, and A. Zarair. Coexistence of different types of chaos synchronization between non-identical and different dimensional dynamical systems. *Nonlinear Dynamics and System Theory* **18** (2) (2018) 253–258.

[18] N. M. Ferguson, D. T. Hue Kien, H. Clapham, R. Aguas, V. T. Trung, T. N. Bich Chau, J. Popovici, P. A. Ryan, S. L. O'Neill, E. A. McGraw, V. T. Long, L. T. Dui, H. L. Nguyen, N. V. Vinh Chau, B. Wills, and C. P. Simmons. Modeling the impact on virus transmission of *Wolbachia*-mediated blocking of dengue virus infection of *Aedes aegypti*. *Science Translational Medicine* **7** (2015) 279ra37.

[19] M. Z. Ndii, R. I. Hickson, D. Allingham, and G. N. Mercer, Modelling the transmission dynamics of dengue in the presence of *Wolbachia*. *Mathematical Biosciences* **262** (2015) 157–166.

[20] M. Z. Ndii, D. Allingham, R. I. Hickson, and K. Glass. The effect of *Wolbachia* on dengue dynamics in the presence of two serotypes of dengue: symmetric and asymmetric epidemiological characteristics. *Epidemiology and Infection* **144** (2016) 2874–2882.

[21] M. Z. Ndii, D. Allingham, R. Hickson, and K. Glass. The effect of *Wolbachia* on dengue outbreaks when dengue is repeatedly introduced. *Theoretical Population Biology* **111** (2016) 9–15.

[22] N. Anggriani, A. K. Supriatna, The effect of *Wolbachia* introduction and predatory in dengue disease transmission. *Advanced Science, Engineering and Medicine* **7** (2015) 864–868.

[23] L. J. S. Allen and L. Jr. Extinction thresholds in deterministic and stochastic epidemic models. *Journal of Biological Dynamics* **6** (2012) 590–611.

[24] M. Z. Ndii and A. Supriatna. Stochastic mathematical models in epidemiology. *Information* **20** (2017) 6185–6196.

[25] L. Allen and P. van den Driessche. Relations between deterministic and stochastic thresholds for disease extinction in continuous and discrete time infectious disease models. *Mathematical Biosciences* **243** (2013) 99–108.

[26] A. A. Hoffmann, M. Turelli, and L. G. Harshman. Factors affecting the distribution of cytoplasmic incompatibility in Drosophila simulans. *Genetics* **126** (1990) 933–948.

[27] H. Hughes and N. Britton. Modelling the use of *Wolbachia* to control dengue fever transmission. *Bulletin of Mathematical Biology* **75** (2013) 796-818.

[28] T. W. Scott, P. H. Amerasinghe, A. C. Morrison, L. H. Lorenz, G. G. Clark, D. Strickman, P. Kittayapong, and J. D. Edman. Longitudinal studies of *Aedes aegypti (Diptera: Culicidae)* in Thailand and Puerto Rico: Blood feeding frequency. *Journal of Medical Entomology* **37** (2000) 89–101.

[29] G. Bian, Y. Xu, P. L., Y. Xie, and Z. Xi. The endosymbiotic bacterium *Wolbachia* induces resistance to dengue virus in *Aedes aegypti*. *PLoS Pathogen* **6** (2010) e1000833.

[30] D. J. Gubler. Dengue and dengue hemorrhagic fever. *Clinical Microbiology Reviews* **11** (1998) 480–496.

[31] G. Chowel, P. Diaz-Duenas, J. C. Miller, A. A. Velazco, J. M. Hyman, P. W. Fenimore, and C. Castillo-Chaves. Estimation of the reproduction number of dengue fever from spatial epidemic data. *Mathematical Biosciences* **208** (2007) 571–589.

[32] H. M. Yang, M. L. G. Macoris, K. C. Galvani, M. T. M. Andrighetti, and D. M. V. Wanderley. Assessing the effects of temperature on the population of *Aedes aegypti*, the vector of dengue. *Epidemiology and Infection* **137** (2009) 1188–1202.

Appendix

Parameter Descriptions

The following table presents the parameter descriptions and values of the models.

Table 2: The description, values, units, and references of the parameters for the mathematical model. The letter W is to denote *Wolbachia*.

Symbol	Description	Value	Unit	Source
α	Maternal transmission	0.9	N/A	[3, 12, 26]
b_N	Biting rate	0.63	day^{-1}	[28]
ρ_W	Reproductive rate of *Wolbachia*-carrying mosquitoes	$0.95\rho_N$	N/A	[3]
T_{HW}	Transmission probability from *Wolbachia*-carrying mosquitoes to human	$0.5T_N$	N/A	[29]
μ_W	Death rate of *Wolbachia*	1.1 μ_N	N/A	[3, 10]
b_W	Biting rates of *Wolbachia*-carrying mosquitoes	0.95 b_N	N/A	[8]
γ_H	Progression rate from exposed to infectious human	1/5.5	day^{-1}	[30]
γ_N	Progression from exposed to infectious non-W	1/10	day^{-1}	[31]
γ_W	Progression rate from exposed to infectious	1/10	day^{-1}	[31]
μ_N	Adult mosquito death rate (non-W)	1/14	day^{-1}	[32]
μ_{NA}	Death rate of aquatic non-W	1/14	day^{-1}	[32]
μ_{WA}	Aquatic death rate	1/14	day^{-1}	[32]
ρ_N	Reproductive rate of non-W	1.25	day^{-1}	[12]
σ	Recovery rate	1/5	day^{-1}	[30]
T_N	Transmission probability	0.2614	N/A	[19]
τ_N	Maturation rate of non-W	1/10	day^{-1}	[32]
τ_W	Maturation rate of W	1/10	day^{-1}	[32]

CAMBRIDGE SCIENTIFIC PUBLISHERS

Lyapunov Exponents and Stability Theory
Stability, Oscillations and Optimization of Systems: Volume 6,
317 pp, 2012   ISBN   £55/$100/€80

N.A. Izobov

Institute of Mathematics, National Academy of Sciences of Belarus,
Minsk, Belarus

This monograph deals with one of two basic methods of stability investigation of solutions to differential systems – the method of characteristic Lyapunov indices. It provides necessary knowledge from modern theory of Lyapunov indices and presents results of the author who is a leading expert in this field. Main attention is focused on the following areas:

- the theory of low Perrone indices, general Bole indices, central Vinograd indices and the author's exponential indices
- the freezing method
- investigation of effect of exponentially decreasing perturbations on characteristic indices of linear differential systems
- stability of characteristic indices of linear systems with respect to small perturbations
- Lyapunov problem on investigation of asymptotic stability with respect to linear approximation
- Millionschikov method of turnings and its methodical application in modern theory of Lyapunov indices

Requiring only a fundamental knowledge of general stability theory, this book serves as an excellent text for graduate students studying ordinary differential equations and stability theory as well as a useful reference for analysts interested in applied mathematics.

CONTENTS